AN EXPERIMENTAL INVESTIGATION OF LUMINESCENCE AND PHOTOCONDUCTIVITY IN SINGLE CRYSTALS OF SPINEL AND SAPPHIRE AND A STUDY OF IONIC MOTION IN NaCl:Cu

By

PRADIP KUMAR BANDYOPADHYAY

Bachelor of Science
Jadavpur University
Calcutta, India
1973

Master of Science
Jadavpur University
Calcutta, India
1976

Submitted to the Faculty of the Graduate College
of the Oklahoma State University
in partial fulfillment of the requirements
for the Degree of
DOCTOR OF PHILOSOPHY
December, 1985

TO

MY PARENTS

Thesis
I985D
B214e
cop. 2

OKLAHOMA STATE UNIVERSITY LIBRARY

AN EXPERIMENTAL INVESTIGATION OF LUMINESCENCE AND PHOTOCONDUCTIVITY IN SINGLE CRYSTALS OF SPINEL AND SAPPHIRE AND A STUDY OF IONIC MOTION IN NaCl:Cu

Thesis Approved:

Thesis Adviser

Dean of the Graduate College

1248602

ACKNOWLEDGEMENTS

The author wishes to express his appreciation to his major adviser, Dr. Geoffrey P. Summers, for his guidance and assistance throughout this study. I am deeply grateful for his constant encouragement and patience. It has been a real privilage working with him.

Appreciation is also expressed to the other committee members, Dr. Timothy M. Wilson, Dr. Joel J. Martin, Dr. Elton E. Kohnke, and Dr. William D. Warde, for their assistance in the preparation of the final manuscript. Special mention must be given to Dr. Timothy M. Wilson for many valuable discussions concerning the theoretical aspects of one of the thesis projects.

Thanks are also extended to Dr. Stephen W.S. McKeever for the loan of equipment used for some of the thermoluminescence measurements. Appreciation must be given to Mr. Heinz Hall and the other members of the Physics-Chemistry Machine Shop Staff for their help throughout this research project. Sincere thanks are also extended to Ms. Audrey Brigham for her excellent assistance in typing both the final draft and the final copy of the manuscript.

Special thanks are also extended to all members of the Physics Faculty for their availability and willingness to be of assistance and for providing an atmosphere of interest and constant encouragement. Thanks are also given to Dr. Bryce Jeffries and Dr. Kishalaya Chakrabarti for their friendship and help.

Special gratitude is expressed to my Mother and family, and to all

my friends who have continuously supported me with their sacrifices and encouragement. Appreciation is also expressed to my wife, Aditi, for her understanding and patience.

Finally, appreciation is extended to the Physics Department of Oklahoma State University for the financial support provided during the past five years of my residence at Oklahoma State University.

TABLE OF CONTENTS

LIST OF TABLES

LIST OF FIGURES

Figure Page

CHAPTER I

CRYSTAL DEFECTS

Introduction

The study of crystal defects forms an important aspect of solid-state science. This is largely because many interesting properties of crystalline solids are dominated by effects due to a tiny concentration of imperfections in an otherwise perfect lattice. The physics of such lattice defects plays an important role in a great variety of applications and on the other hand the investigation of defect properties forms an active area of fundamental research in solids. Thus an extensive science of point defects has been constructed during the past years.

One category of numerous types of point defects present in crystalline solids is known as color centers which invloves electrons or holes responsible for the optical bands in the visible, ultraviolet and near infrared region of the spectrum in otherwise transparent crystals. Radiation damage studies have contributed significantly to the understanding of creation of color centers. Radiation damage leading to the formation of color centers in solids can be induced by: i) particle irradiation such as high energy electrons, protons and neutrons; ii) ionizing radiation such as x-rays, γ-rays; iii) additive coloration in which the crystal is heated at a high temperature in an excess of the metallic vapor. Another category of crystal defects is characterized by the presence of foreign atoms or ions in an otherwise

perfect lattice which may be present as impurities or can be deliberately doped during the crystal growth. Such defects are termed as impurity related defects, due to the presence of which optical properties of an otherwise perfect crystal can be changed markedly.

Among the crystalline solids, alkali halides have been investigated in a most extensive manner. More recently the alkaline earth oxides have also been the subject of many studies (1) due to the fact that oxides were new materials to study and the information obtained from simpler systems such as alkali halides could be used to explain the behavior of crystal defects in oxides.

In this dissertation, the optical properties of defects in alkali halides and oxides will be investigated. From an organizational point of view this thesis can be divided into three parts one of which concentrates on an alkali halide system (NaCl) doped with a foreign ion (Cu) while the other two are aimed at investigating the optical properties of some oxides (Al_2O_3 and $MgAl_2O_4$).

Statement of the Problem

NaCl:Cu^-

Optical properties of impurity ions with ns^2 electron configuration have been investigated in detail. The outermost electron configuration of Cu^- is also of ns^2 (n = 4 for Cu^-) type. Cu^- ions can be produced in NaCl by x-irradiation of NaCl crystals doped with Cu^+. Thus there is a change in the charge state of Cu^+ during irradiation. The pre-irradiation state (recovery of Cu^+ ions) can be achieved by thermal annealing of the irradiated crystals (2,3). However, the mechanism of the recovery process through which Cu^- ions are converted to Cu^+ has not

been investigated in a detailed manner. The present work involves a detailed investigation of this recovery process.

$MgAl_2O_4$

$MgAl_2O_4$ is an oxide with complicated crystal structure, its parent oxides being MgO and α-Al_2O_3. An optical absorption band at 5.3 eV has been assigned with some confidence due to absorption by F-centers (two electrons trapped at an oxygen vacancy) in thermochemically reduced samples (4). Though luminescence from F-type centers in similar oxides such as MgO and CaO has been detected, there is no reported evidence of luminescence and photoconductivity from F-centers even in thermochemically reduced $MgAl_2O_4$. The results obtained in this work strongly suggest that F-centers in $MgAl_2O_4$ may luminesce and produce photoconductivity effects.

α-Al_2O_3

Most of the as received samples of α-Al_2O_3 show the presence of anion vacancy (F-type) defects detected through characteristic absorption and luminescence (5,6). F-type defects in α- Al_2O_3 can also be produced by particle irradiation or by thermochemical reduction. Though much is now known about the optical properties and electronic structure of these F-type defects in particle irradiated and thermochemically reduced α- Al_2O_3, annealed samples have received little attention. The purpose of the present work is to investigate the optical properties of annealed Al_2O_3 samples and to explain the possible origin of the observed luminescence and photoconductivity in thermally quenched crystals.

CHAPTER II

THEORETICAL BACKGROUND

Introduction

This dissertation is based upon the study of: i) electronic structure and optical properties of defects in $MgAl_2O_4$ and Al_2O_3, ii) optical properties and ionic motion of Cu^- ions (impurity related defect) in NaCl. Optical absorption, luminescence, photoconductivity and isothermal anneal experiments were performed to gain information about these defects. This chapter builds the necessary theoretical framework in the light of which the results of different experiments (Chapters IV, V, and VI) will be interpreted. For organizational purposes, this chapter is divided into two sections. Section A includes the theory of optical absorption, luminescence and phototconductivity in crystals containing defects. Section B includes the discussion of optical properties of impurity ions with $ns^2(n=2,3,4,...)$ outermost electronic configurations in alkali halides. The background in Section B is related to the present work on Cu^- ions whose outermost electronic configuration is also of ns^2($n=4$ for Cu^-) type.

Section A

Configurational Coordinate Model

The optical absorption and emission of defects in crystals can be

qualitatively understood using the configuration coordinate model which describes in simple terms the interaction between the defect and the host lattice. The essential features of the model will be developed in the beginning before discussing the applicability of this model to the phenomena of optical absorption and luminescence due to defects in a crystal.

The configuration coordinate model, as applied to both the singly and doubly electron occupied anion vacancy defects or to the impurity related defects having two outermost valence electrons as discussed in this section, is a simple model used to represent information about the electronic structure of a defect.

In a crystal containing a defect, the one or two electron ground state eigenfunctions obtained for the defect electrons are more localized than are the single electron orbitals for the perfect crystal. The ground and excited states of the defect electron will differ, however, from those of a free atom or molecule because the wave functions ions have to reflect the symmetry of the surrounding ions and the interaction with neighboring ions spread out over a larger volume. The energy scheme for the crystal containing such defects is represented in Figure 1, where the bound levels below the conduction band are associated with the defect electron and the levels in the filled valence band are associated with the host electrons in the crystal. When the defect electron has been raised to its lowest optically accessible excited state, it may require only a small additional energy (~0.2eV), which can often be supplied by thermal vibrations of the lattice to be freed in the conduction band.

The total energy of a crystal containing a defect is the sum of the

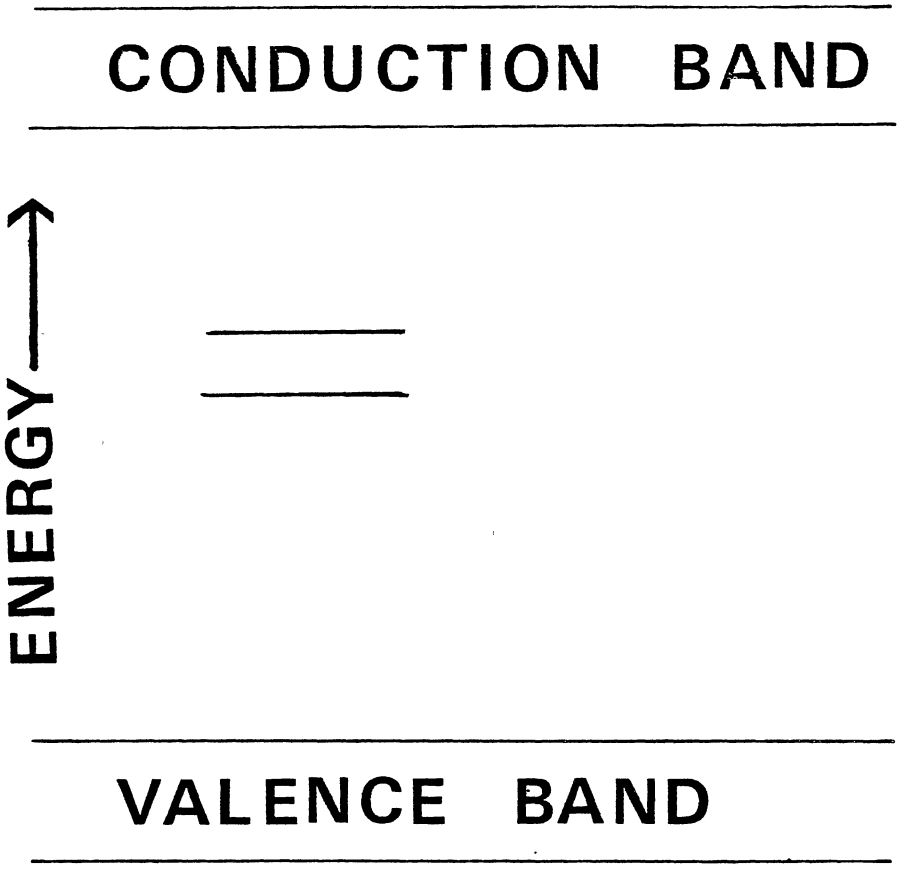

Figure 1. Schematic Diagram Showing the Relative Energies of the Valence and Conduction Band of the Crystal and the Energy Levels for the Defect Electron Trapped at the Anion Vacancy

total electronic energy (defect electron and other electrons in the crystal) and the lattice energy. Figure 2 shows the variation of the total energy of the crystal with the effective configuration coordinate Q, where Q represents in some sense the positions of the nuclei. Each point on the curves, corresponding to the ground state (lower curve) and the first excited state, represents the total energy (U_i) of the crystal corresponding to the nuclei frozen into a particular configuration Q. These curves, though representing the total energy U_i, are given the label corresponding to the state for the defect electron. Curves representing the upper and lower excited states are parabolic in the configuration cooridante Q, indicating the simple harmonic nature of vibration of the nuclei for linear electron-phonon coupling and the typical energy spectrum being given by $(N+1/2)\,\hbar\omega$, where ω is the frequency for a single normal mode of vibration, usually assumed to be a breathing mode of the defect's nearest neighbors. The frequency, ω, is determined by the mass of the vibrating ions and the curvature of the potential energy curve. The eigenvalues $(n+1/2)\,\hbar\omega$ represent the vibronic energy level for a particular state of the defect in the crystal. The energy of a given state-electronic and vibrational - can be represented by a horizontal line on the configuration coorinate diagram. Associated with an electronic energy curve, the vibrational levels differ in energy by $\hbar\omega$. The energy difference between two states or two different curves is the difference between the energy eigenvalues of each represented by the horizontal lines. Since the curvature of the configuration coordinate curves for different electronic states may be different, the vibrational frequency, and hence the vibrational energy spacing within any one states in the configuration coordinate curve can be different

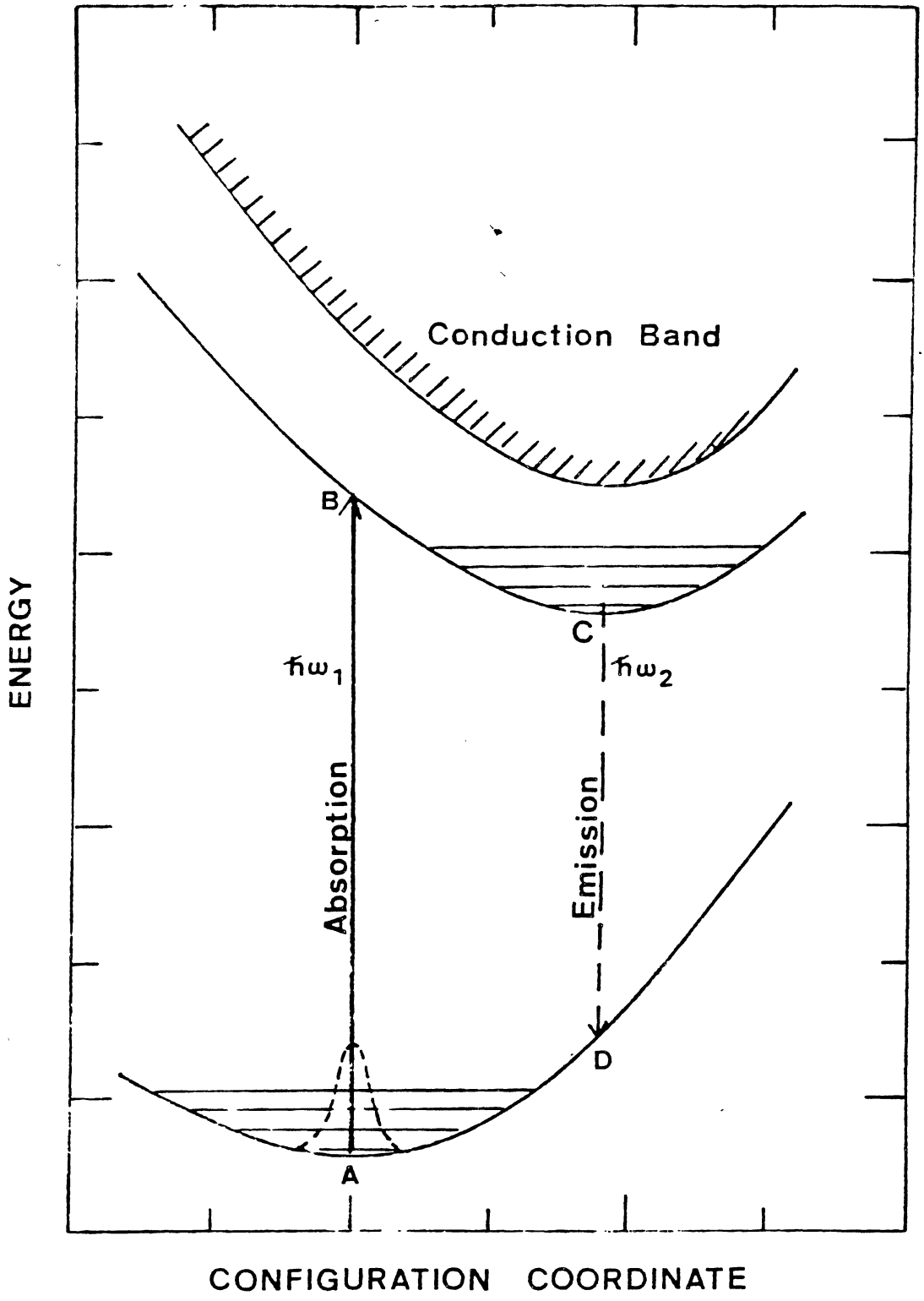

Figure 2. Configuration Coordinate Model

than those corresponding to that of another state.

Optical Absorption

When a crystal containing defects is exposed to photons of the correct energy, electronic excitation of the defect may take place. The defect electron after absorbing a photon is raised to an excited state and may radiatively decay back to the ground state. The probability per unit time that the defect electron will make a transition from state mn to kγ is directly related to the oscillator strength of the transition which is given by:

$$f_{mn,k\gamma} = \left(\frac{2m}{3h}\right) \omega_{mn,k\gamma} |\vec{r}_{mn,k\gamma}|^2, \qquad (1)$$

where the state function of the defect in the ground and the excited state is written as following using Born-Oppenheimer approximation:

$$\Psi_{mn}(\vec{r},\vec{R}) = \phi_{m,R}(\vec{r})\ X_{mn}(\vec{R})$$

and

$$\Psi_{k\gamma}(\vec{r},\vec{R}) = \phi_{k,R}(\vec{r})\ X_{k\gamma}(\vec{R}).$$

In Equation (1), $\vec{r}_{mn,k\gamma}$ is the dipole matrix element sandwiched between the initial and final states of the crystal and is written as

$$\vec{r}_{mn,k\gamma} = \int d\vec{r} \int d\vec{R} X^*_{mn}(\vec{R})\ \phi^*_{mR}(\vec{r}) \vec{r} \phi_{k,R}(\vec{r})\ X_{k\gamma}(\vec{R}). \qquad (2)$$

For convenience, Equation (2) is rewritten as

$$\vec{r}_{mn,r\gamma}=\int d\vec{R}\, X^{*}_{mn}(\vec{R})\ \vec{r}_{mR}(\vec{R})\ X_{r\gamma}(\vec{R}) \tag{3}$$

where

$$\vec{r}_{mk}(\vec{R})\equiv\int d\vec{r}\,\phi^{*}_{mR}(\vec{r})\vec{r}\phi_{k\vec{R}}(\vec{r}). \tag{4}$$

Equation (4) explicitly contains the dependence of the dipole matrix elements on the nuclear coordinates. In fact transitions between such discrete states ($mn\rightarrow k\gamma$) are often not observed for crystals containing defects. What is observed is a broad band representing the sum of many such transitions. One thus considers Equation (1) with a sum over final vibrational states γ and a thermal average over initial vibrational states. The oscillator strength is thus written as

$$\begin{aligned} f_{mk} &\equiv \mathrm{av}_{\eta}\ \Sigma\ f_{m\eta,k\gamma} \\ &= \frac{2m}{3h}\,\mathrm{av}_{\eta}\ \Sigma_{\gamma}\ \omega_{m\eta,k\gamma}\left|\vec{r}_{m\eta,k\gamma}\right|^{2}, \end{aligned} \tag{5}$$

where the dipole matrix element is given by Equation (3).

The Franck-Condon Principle states that during an electronic transition, the electronic state changes so fast that a) atomic nuclei do not move and b) the nuclei do not change their momenta. With this approximation the transition is therefore shown as a vertical line (Figure 2) indicating that the positions of the neighboring nuclei in the lattice do not have time to change appreciably during the electronic transition. The quantum mechanical formulation of the Franck-Condon

Principle rests on the assumption that the variation of the electronic transition moment with $\vec{R}$ is slow, thereby allowing it to be replaced by an average value $\vec{r}_{mk}(\vec{R}_o)$. Using this approximation the expression for oscillator strength becomes

$$f_{mk} = \frac{2m}{3k}\,\omega_{mk}\left|\vec{r}_{mk}(\vec{R}_o)\right|^2. \tag{6}$$

Furthermore it is evident that the integral in Equation (3) involves an overlap integral between two vibrational wave functions. Consequently the most likely transitions will be those between vibrational levels for which the overlap integral is relatively large.

The oscillator strength as expressed in Equation (6) is a useful quantity in determining the absorption and emission transition probabilities of the defect electron. In Equation (5), the strength of the transition is summed and averaged over vibrational states which points to the fact that the absorption or emission spectrum of a defect center is spread out into a broad band due to the proximity of the vibrational levels associated with the various electronic states. To illustrate this, let us consider Figure 2. The dotted curve represents the probability density for the n=0 vibrational level, i.e. the probability of the neighboring nuclei appearing at various distances from the center of the defect, the total energy of the system remaining the same for these different values of Q. For centers, with the neighbouring nuclei displaced from the equilibrium position, the transition will be to points displaced from B on the excited electronic curve. Therefore the lattice vibrations at A lead to a spread in energies due to the steepness of the curve at B thereby giving rise to a

broad absorption band. Immediately after the transition to the excited state, (10^{12} - 10^{-13} sec) the lattice relaxes, emitting phonons, as a new equilibrium position of the nearest neighbor ions is reached.

The oscillator strength is also used on relationships which connect the number of centers involved in an electronic transition with the optical absorption coefficient. It can be shown, that for centers which do not have interactions with each other, the area under the absorption curve is directly proportional to the concentration of the absorbing centers. By measuring the absorption coefficient at the peak of the absorption band and knowing the oscillator strength for that particular transition, it can be shown that the following equation holds,

$$Nf = \frac{9mc}{2e^2} \frac{n}{(n^2+n^2)} \alpha_{max} W = 1.29 \times 10^{17} \frac{n}{(n^2+2)} \alpha_{max} W, \qquad (7)$$

where N = number of centers/cm^3.

f = oscillator strength for a particular electronic transition.

n = refractive index of the crystal for the wavelength at the peak of the absorption.

α_{max} = absorption coefficent (cm^{-1}) at the peak of the absorption band.

W = half-width of the band in electron-volts.

m = mass of the defect electron.

e = charge of the electron.

c = speed of light.

Equation (7) is called Smakula's equation which is used to estimate the concentration of absorbing centers in a crystal.

Another feature of the absorption band is the temperature

dependence of the half-width of the band, which for gaussian bands and linear electron-phonon coupling is given by the following equation:

$$\frac{W^2(T)}{W^2(0)} = \coth\,(h\omega/2k_BT), \tag{8}$$

where ω is the average vibrational frequency in the initial state and W_o is the half-width at T=0K. By measuring W as a function of T, one can derive the effective frequency ω. From this the Huang-Rhys factor which is a dimensionless quantity measuring the strength of the linear coupling of the defect with its nearest neighbors can be estimated. Equation (8) shows that the absorption band should get broader with increasing temperature. This type of behavior is found for the F-center absorption bands in most crystals. The configuration coordinate diagram also predicts the absorption band to be symmetric. The asymmetric absorption bands found in crystals (e.g. F^+ center absorption in CaO and SrO) cannot be explained by the configuration co-ordinate model which takes into account only a single mode of vibration. The dynamic Jahn-Teller effect is the usual explanation for additional structure observed in the absorption bands of some defects in ionic crystals such as the F^+ band in CaO.

Before concluding this section on the absorption of light by crystal defects, let us look at the selection rules which govern the probability that the defect electron will make a transition from the ground state to the excited state. The selection rules may be expressed in group theoretical terms (8). One considers $\vec{R}$ (configuration coordiate) to equal some equilibrium R_o, in a rather symmetric configuration. The functions ϕ_m^* and ϕ_k (Equation 4) and the dipole

operator $\vec{r}$ will each transform as some irreducible representation of the group of the Schrodinger's equation. One forms the direct product of any two of these irreducible representations (e.g., $\Gamma_m^* \times \Gamma_k$). If the result contains the third irreducible representation, the matrix element may be nonzero; if it does not contain the third irreducible representation, the matrix element must be zero and the transition is "forbidden".

This result is illustrated in the case of a cubic center and states Γ_1^+ (s like) and Γ_4^- (p-like). The direct product of $\Gamma_1^+ \times \Gamma_4^-$ is Γ_4^-, and since $\vec{r}$ transforms as Γ_4^-, the transition is allowed. There are other cases in which the selection rules may be determined almost by inspection, but when this is not possible the general theorem just stated may be used.

Generally, if $\vec{r}_{mk}(\vec{R}_o)$ is nonzero, it is not too important to investigate its behavior as a function of $\vec{R}$. In a number of cases, however, $\vec{r}_{mk}(\vec{R}_o)$ will be zero, whereas $\vec{r}_{mk}(\vec{R})$ will be nonzero for certain values of $\vec{R}$. In other words forbidden transitions may be made partially allowed through lattice vibrations and this is indeed the case for some absorptions of Cu^- ions in NaCl. The results of Cu^- absorption in NaCl will be discussed in detail in Chapter IV.

Luminescence

This dissertation investigates in detail the luminescence from α-Al_2O_3 and $MgAl_2O_4$ samples. Temperature dependence of the luminescence originating from these samples have yielded valuable information about defects present in these crystals. Thus it is necessary to build a framework through which the results of luminescence

experiments can be interpreted.

Luminescence originating from crystal defects, usually consists of broad bands. Also the peak energy of emission is usually at a lower energy than that of the corresponding absorption band. These two phenomena can be explained on the basis of configuration coordinate model as shown in Figure 2. The system, in absorbing light, undergoes an electronic transition to an optically accessible excited state (A→B in Figure 2). In the excited electronic state the wavefunction of the defect is often more diffuse and spreads out over the surrounding ions. A polarization effect occurs which gives rise to lattice relaxation. This is indicated by B→C in Figure 2 by a different equilibrium separation of the neighboring ions from the center of the defect in the excited state. At C, the center will again experience thermal vibrations. After some time, the defect may make another transition to the ground state, with the emission of light. This transition is shown going from C to D. Here, too, D is on a sharply varying part of the total energy curve, so that variations in the configuration co-ordinate about C lead to a variation in energy which causes a broad emission band.

At D, the defect will again relax to the starting point A by giving off the excess energy as phonons. As can be seen in Figure 2, the emission energy is less than the energy of absorption by the defect. This effect is often termed as the Stokes shift. The difference in energy is B to C and D to A, which appears in the lattice as phonons during the complete cycle process.

Once the defect electron is in its relaxed excited state as explained above, it has three completing modes of escape: i) radiative

decay to the ground state with the emission occuring at a lower energy than that of the absorption; ii) thermal release into the conduction band across a small energy gap giving rise to photoconductivity; or iii) nonradiative decay to the ground state.

The probability per unit time for spontaneous radiative decay to the ground state is given by $\frac{1}{\tau_R}$ where τ_R is the radiative life time. The transition takes place from an excited electronic state "i'" to a lower electronic state "i" and $\tau_{R_{i'\rightarrow i}}$ is the weighted average of all τ^{-1} over initial vibrational states ν', summed over all final states ν.

$$\frac{1}{\tau_{R_{i'\rightarrow i}}} = \langle \tau^{-1}_{R_{i'\nu'\rightarrow i\nu}} \rangle = \sum_{\nu} \frac{\tau^{-1}_{R_{i'\nu'\rightarrow i\nu}} \exp(-\frac{E_{i'\nu'}}{K_B T})}{\sum_{\nu'} \exp(\frac{-E_{i'\nu'}}{k_B T})} . \tag{9}$$

The second mode of escape for the electron from the relaxed excited state of the center is governed by a temperature dependent probability per unit time for thermal ionization of the electron across an energy gap E_a into the conduction band:

$$\frac{1}{\tau_T} = \frac{1}{\tau_o} \exp\ (-\frac{E_a}{k_B T}). \tag{10}$$

The lifetime of the excited state may be written in terms of a simple model as

$$\frac{1}{\tau} = \frac{1}{\tau_R} + \frac{1}{\tau_o} \exp\ (-\frac{E_a}{k_B T}) + \frac{1}{\tau_Q}, \tag{11}$$

where $\frac{1}{\tau_Q}$ is the probability per unit time of any other process occuring. Assuming a two level model and neglecting other processes

such as nonradiative recombination to the ground state, the lifetime of the excited state is given by

$$\tau = \frac{\tau_R}{1+(\tau_{R/\tau_o}) \exp\left(-\frac{E_a}{k_B T}\right)}. \tag{12}$$

The fraction of optically excited electrons which are thermally assisted into the conduction band is given by

$$\eta_T = \frac{1/\tau_T}{1/\tau} = \frac{1}{1+(\tau_o/\tau_R) \exp\left(\frac{E_a}{k_B T}\right)}, \tag{13}$$

where η_T is the quantum efficiency for thermal ionization or the yield of free electrons. Similarly the quantum efficiency for radiative decay η_R or the fluorescence yield is given by

$$\eta_R = \frac{1/\tau_R}{1/\tau} + \frac{1}{1+(\tau_R/\tau_o) \exp\left(-\frac{E_a}{k_B T}\right)}. \tag{14}$$

In this model,

$$\eta_R + \eta_T = 1. \tag{15}$$

Equations (12) and (14) predict identical temperature dependence for the fluorescence yield and the lifetime of the excited state and such results were obtained by Swank and Brown (10) for the F-centers in KCl (Figure 3a). Equation (12) also shows that the quantum efficiency for fluorescence should decrease and that for photoconductivity increases with increasing temperature. Such results were likewise obtained by

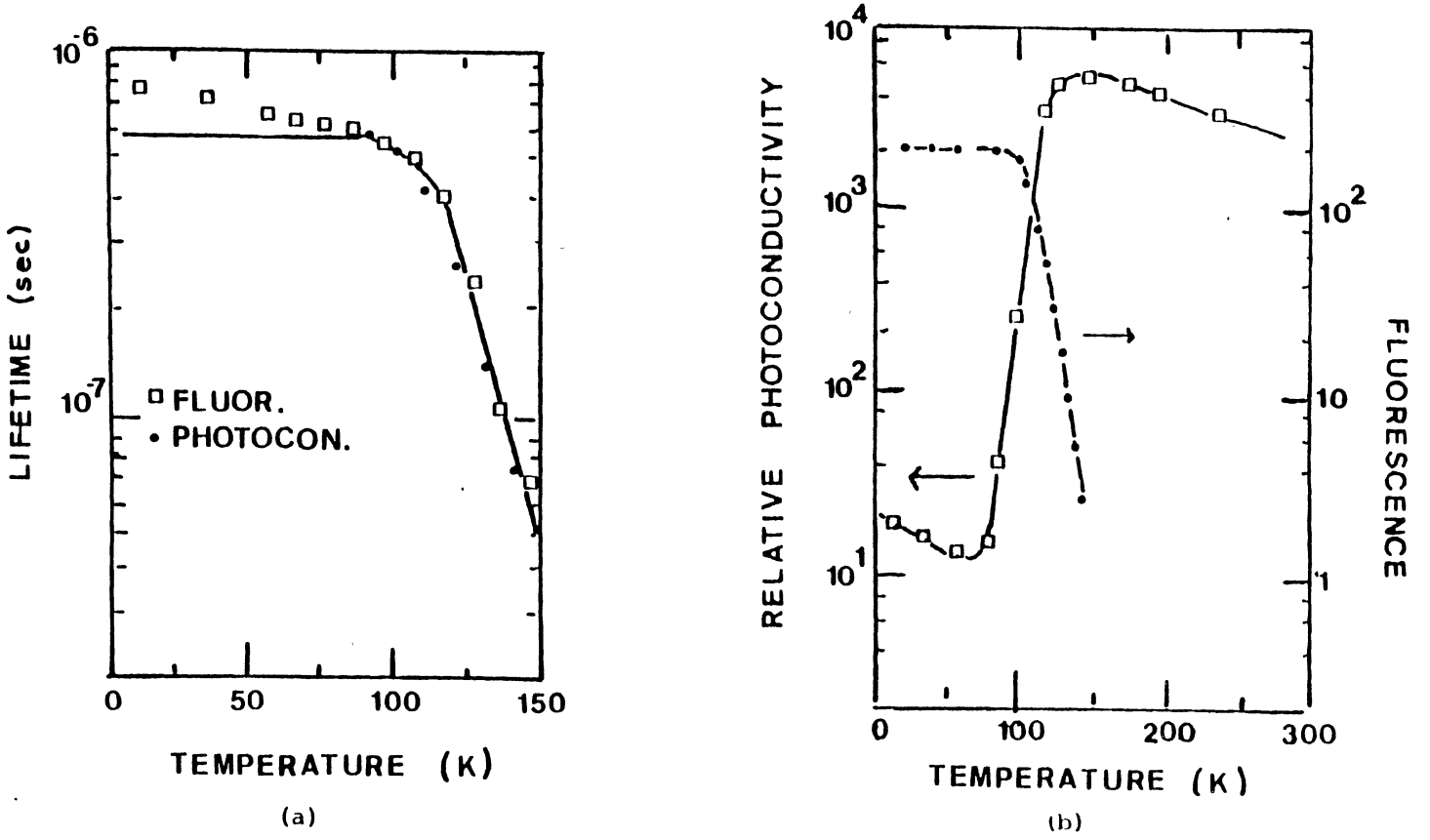

Figure 3. Lifetime of the Excited State From Fluorescence and Photoconductivity Measurements (a); the Relative Fluorescence Yield and Photconductivity Yield for Illumination in the F-Band of KCl (b)
Source: R.F. Swank and F.C. Brown (11)

Swank and Brown for F-center in KCl (Figure 3b). At low temperatures near OK, $\tau \sim \tau_R$. For electric dipole transitions in atoms, τ is of the order 10^{-8} sec. If no allowed transitions can occur, the mean lifetime is much larger. If the probability for thermal ionization is small but the lifetime of the excited state is reasonably long, then the electron has a better chance of getting to the conduction band. The temperature dependence of the luminescence in $MgAl_2O_4$ studied in this dissertation shows the decrease in the luminescence intensity as the temperature is raised from 77K to 300K as indicated by Equation (12). More comments on this aspect will be made in Chapter V.

Photoconductivity

The photoconductivity process involves the absorption of light, the excitation of a charge carrier from a non-conducting ground state to an excited state where it is free to contribute to electric conductivity, and the ultimate trapping of charge carriers from the conduction band. Information about the relaxed excited states of a defect, the carrier mobility, and trapping centers can be obtained from photoconductivity experiments.

In a photoconductivity experiment, the crystal is mounted between plane parallel electrodes and illuminated with light. An electrometer measures the current produced. The photocurrent originating from defects can be classified to two classes, namely primary and secondary. When a crystal is illuminated with light of suitable wavelength, the electrons are raised to the conduction band and drawn towards the anode giving rise to a current. Such a type of current is called primary photocurrent, and this type of current has been measured

in the present work.

The defect electron after making the transition to conduction band are drawn by the field into the unilluminated portion of the crystal where they are trapped after drifting a certain distance. If the applied electric field is zero, the electron will execute a kind of Brownian motion before getting trapped. When the electric field is turned on, the number of electrons trapped at points lying nearer the anode from the point where they were released is greater than the number of electrons which are trapped at points lying towards the cathode. Consequently a current is detected by the electrometer. The detected current is the same as it would be if all the photoelectrons had drifted down the field a certain small distance ω' , the same for all. ω' is known as the mean range of the carriers in the applied field.

The charge measured by the electrometer is given by

$$q = e \frac{x}{d}, \tag{16}$$

where e = electronic charge

x = distance travelled by the photoelectron

d = distance between the electrodes.

Each photoelectron drifts in the applied field with a kind of diffusive motion and constant mobility $\mu=v_d/E$ where v_d is the velocity of the electron and E is the applied field.

Mean range ω' is related to the mobility by the following equation

$$\omega' = \mu E \tau. \tag{17}$$

If n_o electrons are released at time t = 0, as shown in Figure 4, the number remaining at time "t" is given by

$$n = n_o \exp\left(-\frac{t}{\tau}\right). \tag{18}$$

The time 't' and distance x are related by $n=\mu E\tau$ so that Equation (18) can be rewritten as

$$n = n_o \exp\left(-\frac{x}{\omega'}\right). \tag{19}$$

where the definition of ω' as given in Equation (17) has been used.

The number of electrons which end their path in the range dx is given by

$$\frac{dn}{dx}\,dx = \frac{n_o}{\omega} \exp\left(-\frac{x}{\omega'}\right) dx. \tag{20}$$

The total distance drifted by the particles which are trapped before reaching the anode is

$$-\int_o^{x_o} x \frac{dn}{dx}\,dx = \int_o^{x_o} x \frac{n_o}{\omega} \exp\left(-\frac{x}{\omega'}\right) dx$$

$$= \frac{n_o}{\omega}\left[\frac{\exp(-\frac{x}{\omega'})}{(-\frac{1}{\omega'})^2}\left(-\frac{x}{\omega'} - 1\right)\right]\Bigg|_o^{x_o}.$$

Thus,

$$-\int_o^{x_o} x \frac{dn}{dn}\,dx = n_o\left\{\omega'\left(1 - \exp\left(-\frac{x_o}{\omega'}\right)\right) - x_o \exp\left(-\frac{x_o}{\omega'}\right)\right\}. \tag{21}$$

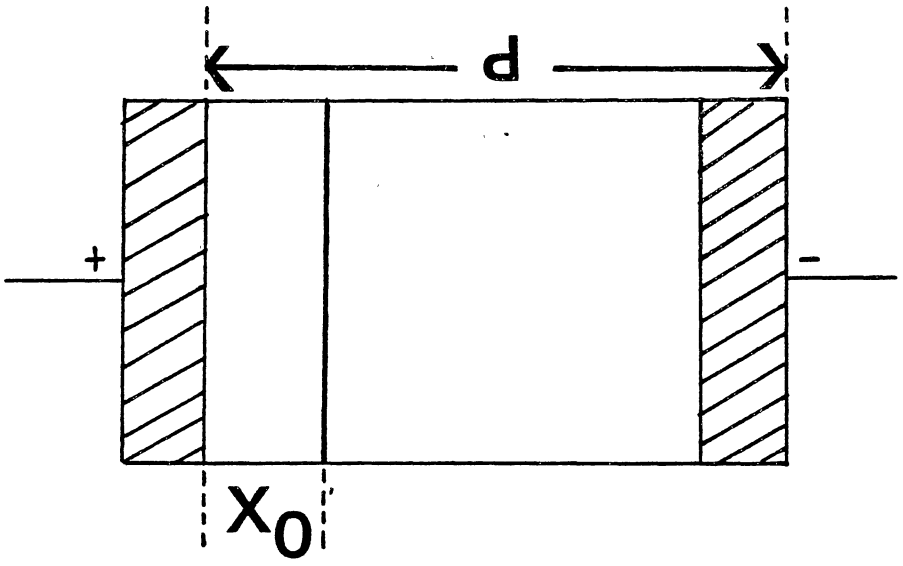

Figure 4. At a Distance X_o from the Anode, η_o Electrons are Released at $t_o = 0$

From Equation (19), the total distance drifted by the $n_o e^{-x_o/\omega'}$ particles which reach the anode is

$$x_o n_o \exp\left(-\frac{x_o}{\omega\tau}\right). \tag{22}$$

From Equations (21) and (22), the mean distance drifted by an electron is given by

$$\bar{x} = \omega\left(1 - \exp\left(-\frac{x_o}{\omega\tau}\right)\right). \tag{23}$$

If d is the length of the crystal, the ratio ψ of the charge passing through the electrometer, $n_o e\,\bar{x}/d$, to the charge released, $n_o e$, is given by

$$\psi = \frac{\omega'}{d}\left(1 - \exp\left(-\frac{x_o}{\omega\tau}\right)\right). \tag{24}$$

This formula has been derived by Hecht (12).

The above equation can be used to derive the net charge flow in the external circuit for the simple case described above. However, in reality the relation between measured charge and the charge released is complicated by the penetration of light into the crystal. The discussion which follows is based on one given by Van Heyningen and Brown (13).

For light pulses of N_o total photons incident upon the crystal, the number actually entering the crystal is $N_o(1-R)$ where R is the reflection coefficient. The light intensity at a depth x can be expressed in terms of the incident intensity and is given by

$$I = I_o \exp(-\alpha x) = N_o(1-R) \exp(-\alpha x), \tag{25}$$

where α = absorption coefficient for a given wavelength. From Equation (25) the number of photons actually absorbed within the crystal in the interval x to x + dx is

$$dN = \alpha N_o(1-R) \exp(-\alpha x)\, dx. \tag{26}$$

The quantum efficiency, n_T, or the number of free electrons, dn, produced per absorbed photon for the interval dx can be written as

$$n_T = \frac{dn}{dN}$$

and

$$dn = n_T \alpha N_o(1-R) \exp(-\alpha x)\, dx. \tag{27}$$

Integrating (27) from o to d, one gets

$$n = n_T N_o(1-R)(1- \exp(-\alpha d), \tag{28}$$

where n is now the number of electrons released within the crystal.

The charge flowing in the external circuit is given by

$$Q = nq = en_T N_o(1-R)(1- \exp(-\alpha d))\, \psi, \tag{29}$$

where ψ is a saturation factor defined as $\bar{x}/d$ such that $\bar{x}$ is the average

electron displacement, equal to the total displacement X of all the electrons divided by n electrons. The factor ψ takes into account the mean range of the electron and the finite depth of the optical absorption.

To derive ψ one proceeds in a manner similar to that used earlier (Equations 19-24) for the simpler case in which n_o electrons were released a distance x_o from the anode. The problem encountered here is somewhat more complicated since the electrons are, in reality, released at all depths throughout the crystal. The total displacement X consists of two parts; X_1 due to electrons trapped in the crystal volume and X_2 due to electrons collected at the anode. Of the Δn electrons released within the interval x to x+dx, a number $d(\Delta n')$ will be trapped in the interval x' to x'+dx' (Figure 5). Following from Equation (20),

$$d(\Delta n') = -\frac{\Delta n}{\omega'} \exp\left[-\frac{(x'-x)}{\omega'}\right] dx';x'>x.$$

Integrating the following expression over all values of x' gives

$$\Delta X_1 = \int_x^d (x'-x)\, d(\Delta n')$$

$$= \int_x^d (x'-x)\, \frac{\Delta n}{\omega'} \exp\left[-\frac{(x'-x)}{\omega'}\right] dx';x'>x$$

$$\Delta X_1 = \omega' \Delta n \left[1 - \frac{d-x+\omega'}{\omega'} \exp\left[-\frac{(d-x)}{\omega'}\right]\right], \qquad (30)$$

the contribution to X_1 coming from electrons released in the interval x to x+dx which are subsequently trapped in the crystal volume. Analogous to Equation (22), for the simple case above, the contribution ΔX_2 to X_2

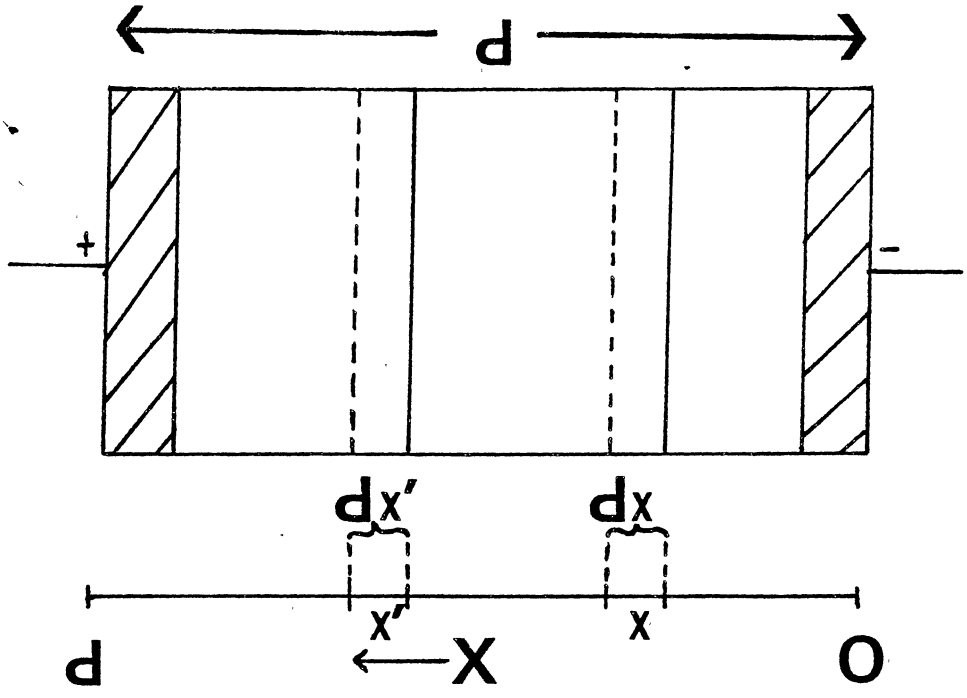

Figure 5. Electrons Released in the Interval from x to x + dx are Trapped Between x' and x' + dx'

which comes from the electrons released between x and x + dx which are collected at the anode is given by

$$\Delta X_2 = \Delta n\ (d-x)\ \exp\ [-\ \frac{(d-x)}{\omega'}]. \tag{31}$$

Equations (30) and (31) were obtained assuming all the electrons (Δn) were released in the interval x to x+dx. However x can take all values between o and d. Replacing the Δ's by differentials, using equation (27) for dn and integrating over $0 \leq x \leq d$ gives

$$X_1 = \int \omega'[1\ -\ \frac{d-x+\omega'}{\omega'} \exp\ [-\ \frac{(d-x)}{\omega'}]\ dn$$

$$= \omega' \eta_T\ \alpha\ N_o(1-R) \int_o^d [\exp(-\alpha x)][1\ -\ \frac{d-x+\omega'}{\omega'} \exp\ [-\ \frac{(d-x)}{\omega'}]]dx. \tag{32}$$

Similarly

$$X_2 = \eta_T \alpha N_o(1-R) \int_o^d \exp(-\alpha x)\ (d-x)\ \exp[-\ \frac{(d-x)}{\omega'}]. \tag{33}$$

The total displacement X is the sum of X_1 and X_2 giving

$$X = \omega' \eta_T \alpha\ N_o(1-R) \int_o^d dx\exp(-\alpha x)\ dx - \omega' \eta_T \alpha N_o \int_o^d \exp(-\alpha x)\ \exp[\frac{(d-x)}{\omega'}]\ dx.$$

So,

$$X = \eta_T N_o(1-R)[\omega'[1-\ \exp(-\alpha d)] - \frac{\omega'^2 \alpha\ \exp(-\alpha d)}{1-\alpha\omega'} + \frac{\omega'^2 \alpha\ \exp\ (-\ \frac{d}{\omega'})}{1-\alpha\omega'}\ ].$$

Dividing X by the total number of electrons released one gets

$$\bar{x} = \frac{X}{n} = \frac{\omega'}{1-\exp(-\alpha d)}\left[(1-\exp(-\alpha d) - \frac{\omega' \alpha \exp(-\alpha d)}{1-\alpha\omega'} + \frac{\omega' \alpha \exp(-\frac{d}{\omega'})}{1-\alpha\omega'}\right]. \quad (34)$$

and consequently,

$$\psi = \frac{\bar{x}}{d} = \frac{1}{1-\exp(-\alpha d)} \left(\frac{\omega'}{d}\right) \left[1 - \frac{\exp(-\alpha d)}{1-\alpha\omega} + \frac{\alpha\omega'\exp(-\frac{d}{\omega'})}{1-\alpha\omega'}\right]. \quad (35)$$

Taking the limit of ψ as $\alpha \to \infty$ which corresponds to all the light being absorbed at X=0 gives

$$\psi = \frac{\omega'}{d}\left[1-\exp\left(-\frac{d}{\omega'}\right)\right], \quad (36)$$

which is in agreement with Equation (24) obtained for the simpler case above.

Taking the limit as $\alpha \to o$ corresponds to uniform absorption. In this limit ψ becomes

$$\psi = \frac{\omega'}{d}\left[1 - \omega'/d \left(1-\exp(-\frac{d}{\omega'})\right)\right]. \quad (37)$$

This case is of particular interest in this study since the experimental measurements were made in the samples having small optical densities and thus correspondingly small absorption coefficients. In addition, for small electric fields, since $\omega << d$, ψ is further approximated by

$$\psi = \frac{\bar{x}}{d} \sim \frac{\omega'}{d}. \quad (38)$$

The photocurrent is therfore given by

$$I = e\eta_T N_o (1-R)\ (1-\exp(-\alpha d))\ \frac{\omega'}{d}, \tag{39}$$

where N_o is the number of photons incident on the crystal per unit time. This can be rearranged to give

$$\eta\omega_o = \frac{I}{N_o}\frac{d^2}{eV}, \tag{40}$$

where

$$\eta = \eta_T(1-R)\ (1-\exp(-\alpha d))$$
$$\omega_o = \omega'\frac{d}{V}.$$

In this form all of the measurable quantities are on one side of the equation and $\eta\omega_o$, the photoresponse of the crystal for a given wavelength, is on the other. It should be noted that the magnitude of the photoresponse from a center is expressed as the product $\eta\omega_o$ where η is the quantum efficiency per incident photon and ω_o is the mean range of the free electron per unit applied electric field.

It should be emphasized that the above analysis is simplified. Even so, it provides a picture in terms of which the photoconductivity observed from F-centers in alkali halides and related materials can be understood. This study is interested principally in the study of photoconductivity originating from F-type centers as a meaningful way to investigate the electronic structure of the defects. For these purposes the above development proves quite satisfactory and is directly related to our present work, viz, the photoresponse from thermochemically reduced $MgAl_2O_4$ as discussed in Chapter V.

Section B

ns^2 Ions in Alkali Halides

A major portion of this dissertation is concerned with the studies of optical properties and ionic motion of Cu^- ions in Sodium Chloride. Optical absorption, isothermal annealing, thermoluminescence and optical bleaching experiments were performed to gain information about this impurity related defect. Cu^- is an ion with two electrons in its outermost 4s shell and thus it is isoelectronic with those ions having ns^2 electron configurations. In this section a survey of different experiments and proposed theories regarding the absorption of ns^2 type of ions in alkali halides will be presented. Such a review is necessary to relate the optical absorption properties of Cu^- in alkali halides with those of other ions having the same outermost electron configuration.

Among the ions with s^2 configuration, $Tl^+(6s^2)$ in alkali halides has been investigated in details. Seitz (14) was the first to present a detailed analysis of Tl^+ absorption in alkali halides. The next section will examine Seitz's model regarding Tl^+ absorption in halides and compare the results with experiments.

Optical Absorption of Tl^+

The absorption spectrum of Tl^+ in KCl is shown in Figure 6. The spectrum consists of two parts, one part characteristic of the pure substance (halide host), and the other part characteristic of the impurity ion Tl^+. The latter component is weaker and lies on the long wavelength side of the former as shown in Table I. The first

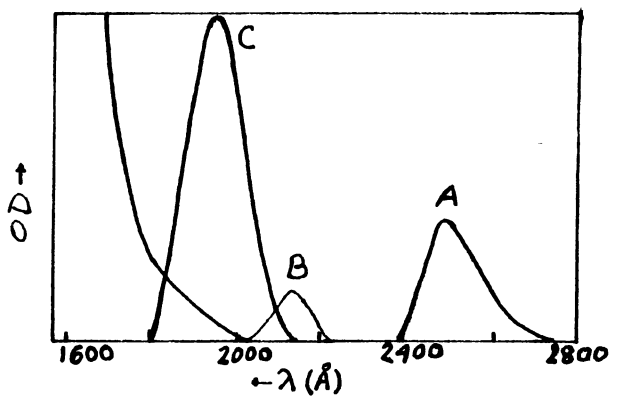

Figure 6. Absorption Spectrum of Tl^{+} in KCL
Source: F. Seitz (14)

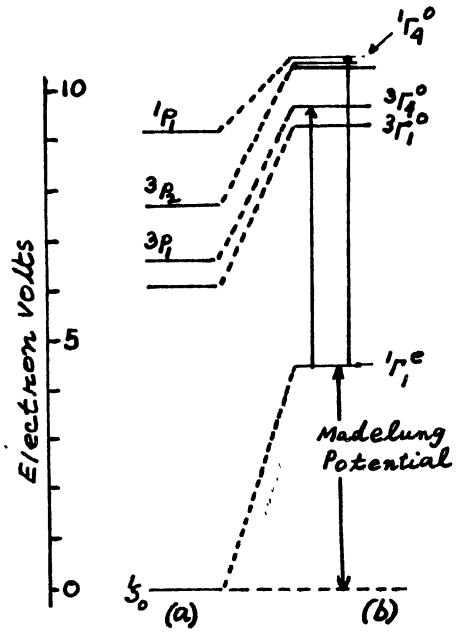

Figure 7. (a) The Energy Level Diagram of Tl^{+} Referred to the Lowest State (b) The Relative Disposition of Levels of the Ion in the Solid
Source: W.B. Fowler (35)

TABLE I

POSITION OF THE ABSORPTION PEAKS IN VARIOUS ALKALI HALIDE-THALLIUM PHOSPHORES IN ELECTRON VOLTS (A, B, and C REFER TO THE PEAK OF FIGURE 6)

	First Fundamental Peak	A	B	C
NaCl	7.82	4.87	5.80	6.20
KCl	7.60	4.92	5.90	6.30
RbCl	7.39	4.98	5.94	6.40
CaCl	7.63	4.90	5.90	6.30
LiBr	6.68			
NaBr	6.49	4.63		5.72
KBr	6.58	4.73		5.88
RbBr	6.43	4.77		5.82
CsBr	6.61	4.69		5.76
LiI	5.59			
NaI	5.39	4.22		5.28
KI	5.63	4.30		5.23
RbI	5.55	4.32		5.15

Source: F. Seitz (14)

fundamental peak corresponds to the excitation of an electron to the excitation levels which lie below the conduction band. The positions of the other three bands named A, B, and C in Figure 6 shift only slightly as the alkali or halogen ions are interchanged. For example, the shift is only about 0.7 eV, toward the red, in passing from chlorides to iodides. In contrast, the fundamental absorption peak shifts by 2.1 eV. This invariance in the peak positions dictates the view that these three peaks correspond to absorption by Tl^+ ion and this was the hypothesis used by Seitz. A possible alternative of the transfer of an electron from a halogen ion to a neighboring Tl^+ ion giving rise to these bands was rejected by Seitz since the peaks show none of the doublet structure associated with the doublet state of a halogen atom.

The analysis of the Tl^+ absorption bands due to Seitz is based upon the positions of the energy levels of the free Tl^+ ion and upon the expected modifications of these levels when the ion is in crystal (see Figure 7).

On the left hand side of Figure 7 are drawn the free ion states, as determined from the spectroscopic measurements. The ground state is ^1S_o, and there exists an excited state multiplet made from a 6s6p configuration. When the Tl^+ ion is placed in the crystal, all of the free Tl^+ states are raised in energy by the Madelung field of the surrounding ions. This raising is more pronounced for the lowest level, and becomes less important as the electron goes to higher levels where it comes more and more into the field of the next nearest positive ions.

In addition to the raising of the levels, splitting of some degenerate levels due to the crystal field also takes place due to the O_h symmetry of Tl^+ in the crystal. States with higher than threefold

degeneracy are split. Thus on the right hand side of Figure 7, $^3P_2$ (j=2) free ion state splits in to a doublet. Symmetries are denoted by the point group notation of the lattice (Γ).

$$^1\Gamma_1^e \rightarrow {}^3\Gamma_4^o \quad \text{(A Band)}$$
$$^1\Gamma_1^e \rightarrow {}^1\Gamma_4^o \quad \text{(C band)}$$
$$^1\Gamma_1^e \rightarrow {}^3\Gamma_3^o,\ {}^3\Gamma_5^o \quad \text{(B band)}$$

Seitz suggested the C and A bands bands are allowed by the spin-orbit coupling and are caused by the transitions from $^1\Gamma_1{}^e$ to $^1\Gamma_4{}^o$ and $^3\Gamma_4{}^o$ respectively. $^3\Gamma_4{}^o$ state will have some residual triplet character, while the $^1\Gamma_4^o$ will be mainly singlet. Since pure singlet-triplet transitions are forbidden, C should be a stronger absorption line than A and this difference in intensity is observed. Seitz assingned the B band as the transition from the ground state to either $^3\Gamma_3{}^o$ or $^3\Gamma_5{}^o$. Transitons to these states are forbidden in the free ion but lattice vibrations may make them weakly allowed in the crystal. This suggestion is consistent with the strong temperature dependence of the B band (15).

After studying the observed transitions of Tl^+ in KCl, let us discuss the essence of several theoretical calculations to predict the energy levels of Tl^+ in the halide host lattice. The situation is complicated because the Tl^+ ion itself has many electrons, and exchange and spin-orbit effects must be considered. For a free Tl^+ ion, the effect of the exchange and the spin orbit coupling in the 6s6p configuration split this level into four states - as pointed out by Knox and Dexter (16). In the case in which both exchange and spin orbit effects are important, neither the LS or jj coupling approximations can be used and the Hamiltonian submatrix must be diagonalized exactly. This procedure yields, in the notation of Condon and Shortley (17), the

following energies relative to the ^1S_o ground state:

$$
\begin{aligned}
W_1 &= W_o - G_1 - \zeta_p \\
W_2 &= W_o - \zeta_p/4 - [(G_1 + 1/4\ \zeta_p)^2 + 1/2\ \lambda^2 \zeta_p{}^2]^{1/2} \\
W_3 &= W_o - G_1 - \zeta_p/2 \\
W_4 &= W_o - \frac{\zeta_p}{4} + [(G_1 + 1/4\ \zeta_p)^2 + 1/2\ \lambda^2 \zeta_p^2]^{1/2}
\end{aligned}
\tag{41}
$$

In the LS limit, the states W_1, W_2, W_3, W_4 will go into the states ^3P_o, $^3P_1$, $^3P_2$, and $^1P_1$ respectively. G_1 and ζ_p are the exchange and spin orbit energies respectively as defined by Condon and Shortly (17). λ is a parameter, introduced by King and Van Vleck (18) which allows for the possiblity that ^1P and ^3P radial functions may differ.

The ratio of the "singlet" and "triplet" oscillator strengths is given by

$$
\frac{^3f}{^1f} = \frac{E_3}{E_1} \frac{\zeta_p^2}{g^2}, \tag{42}
$$

where

$$
2^{-1/2} \lambda g = G_1 + 1/4\ \zeta_p + [(G_1 + 1/4\ \zeta_p)^2 + 1/2\ \lambda^2\ \zeta_p^2]^{1/2} .
$$

Here E_3 and E_1 are the transition energies to $^3P_1$ and $^1P_1$ states (A and C band transition energies) respectively. In the LS limit, $\zeta_p <<< G_1$ and $\frac{^3f}{^1f} \to o$. In the jj limit $\zeta_p >>> G_1$ and $\frac{^3f}{^1f} \to 1/2 \frac{E_3}{E_1}$ if $\lambda = 1$.

Thus the oscillator strength ratio may be a sensitive test of computed wavefunctions. By deriving the values of W_o, G_1, ζ_p and λ as demanded by experiment, comparison of these values yielded by calcula-

tion can be made. Table II shows the computed and experimental values of the parameters for free Tl^+. When the Tl^+ ions is in the crystal the approach to calculate the energy parameters to get the triplet to singlet oscillator strength becomes difficult. Sugano (19) analysed the spectra of s^2 ions in the crystal. He accepted Seitz assignments of the A,B, and C bands and proceeded by means of a molecular orbital model to derive a relation for the ratio of the C-band dipole strength to the A-band dipole strength $[(^1f/3_f)\ ^E3/E_1]$ given by

$$^1f/3_f\ ^E3/E_1 \equiv R = \frac{4-2x+[6-2(2x-1)^2]^{1/2}}{2+2x-[6-2(2x-1)^2]^{1/2}}, \tag{43}$$

where

$$x = \frac{E_B - E_A}{E_C - E_A}. \tag{44}$$

Thus by simply measuring the positions of A,B, and C bands, the dipole strength ratio using the Sugano formula can be predicted. Fakuda (20) and Mabuchi et al.(21) carried out such computations for 14 impurity systems involving In^+, Tl^+, Ga^+, Pb^{++} and Sn^{++}. Their results as shown in Figure 8 are in remarkably good agreement with the experiment. Since Sugano formula is independent of the representation and can be derived directly from the results of Equation (41), the values of W_o, ζ_p, and G_1 can be calculated and compared with those derived from the positions of the A, B, and C bands. In KCl:Tl, W_o = 5.82 eV, G_1 = 0.25 eV and ζ_p = 0.67 eV. From Table II the following points are noted: i) the reduction in W_o can be understood by the effect of the Madelung field which is expected to raise the ground state by more than it does

TABLE II

COMPARISON OF THE ENERGY PARAMETERS FOR FREE Tl^+ WITH THOSE OBTAINED BY SUGANO FORMULA WHEN THE ION IS IN KCl LATTICE

Parameters	Sugano Formula Tl^+:Kcl	Free Tl^+ (experimental)
W_o	5.82 eV	8.19 eV
G_1	0.25 eV	1.05 eV
ζp	0.67 eV	1.015 eV

Source: W.B. Fowler (35)

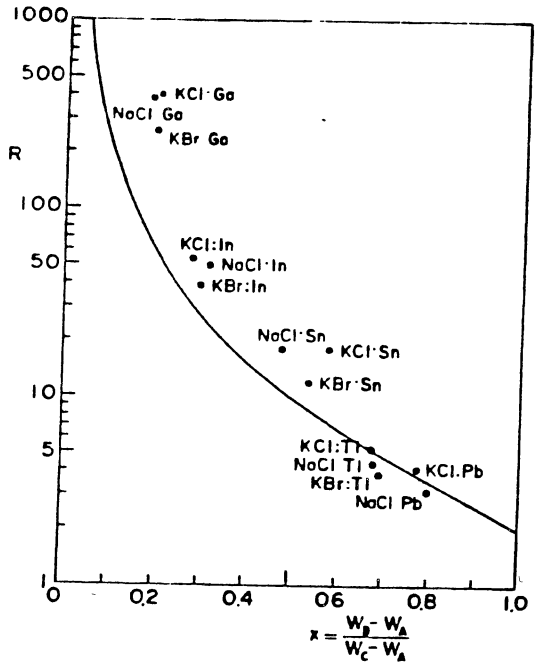

Figure 8. Test of the Sugano Formula for Various s^2 Ions in Alkali Halides. R is the Ratio of the Dipole Strength of the C Band to that of the A Band
Source: W.B. Fowler (35)

the excited states and thus decreases the transition energy; ii) reduction in ζ_p (also found in Ag°, Cu° in alkali halides) is mainly due to the Tl^+ wavefunctions becoming more diffuse probably through configuration interaction or mixing with the state responsible for D band. Knox (22) showed that such a mixing is large; iii) $G = \iint R_s(1)R_p(2) \frac{e^2}{r_{12}} R_s(2) R_p(1) r_1^2 r_2^2 dr_1 dr_2$. G_1 is the exchange integral involving matrix elements of the s and p functions with the coulomb interaction and is sensitive to the overlap of these functions. A sizable reduction in this overlap may be achieved by mixing the atomic p state with more diffuse states.

From the above considerations, it appears that in Tl^+ absorption, exicted state wavefunction of Tl^+ in the crystal are different from those when the ion is free. Knox (22) considers this to be a possible effect of the D band (5.50 eV) on the other three absorption bands discussed so far.

Another feature of interest in Tl^+ absorption is the existence of structure in the A and C bands. For example, Yuster et al. (15) found that C band in KI:Tl has three components. However the absorption spectrum of Cu in alkali halides which will be discussed next, does not show such fine structure.

Sakoda et al. (23) have done molecular orbital calculation of the electronic structure of Tl^+ in KCl. Their calculation is in reasonably satisfactory agreement with experiment for the A, B, and C band energies as shown in Table III.

So far among the s^2 ions, Tl^+ has been discussed. Work on other s^2 ions in alkali halides has been pursued by several investigators (20,21,24). Their work shows that these ions (Ga^+, In^+, Ge^{2+}, Pb^+,

TABLE III

VALUES OF PARAMETERS W_o, G, ζ AND OF ENERGIES OF THE A, B, AND C BANDS IN FREE Tl^+ AND KCl:Tl^+ (IN UNITS OF eV)

Paramters	Experimentally derived free Tl^+	KCl:Tl^+	MO Computation *
W_o	8.180	5.875	5.96
G	1.008	0.28	0.32
ζ	1.015	0.69	0.46
E_A	6.47	5.03	5.30
E_B	7.68	5.94	5.87
E_C	9.38	6.36	6.39

* Obtained from the MO Computation by Sakoda et al. (23).

Source: Sakoda et al. (23).

Sn^{2+}, Sb^{3+}, Bi^{3+}) behave in a way similar to Tl^{+} in alkali halides. Three bands named A, B, and C are observed due to $ns^2 \rightarrow nsnp$ transitions of those ions.

Having discussed the absorption due to ns^2 positive ion impurities in alkali halides, the next section will describe the absorption due to Cu^{-} ions in alkali halides and examine whether Cu^{-} ions in alkali halides behave in a similar way like other ns^2 ions or not.

Section III discusses the different methods of formation of Cu^{-} ions in halides and Section IV will discribe the essential features of Cu^{-} absorption.

Production of Cu^{-} Centers

Cu^{-} centers can be produced in alkali halides by: a) electrolytic coloration (2) b) x-irradiation at room temperature of $NaCl:Cu^{+}$ crystals (3). In electrolytic coloration, $NaCl:Cu^{+}$ crystals can be colored using a pointed cathode with an applied voltage of 450 - 470 V in a furnance at a temperature of 350 -500°C. After coloration, the crystal contains Cu^{-} and F-centers (an F-center is a single electron trapped at a halide ion vancany). The process of Cu^{-} formation involves the movement of copper ions from the cation to the anion sublattice. In electrolytic coloration the crystal is heated at a temperature where appreciable ionic motion can occur. The mechanism of $Cu^{+} \rightarrow Cu^{-}$ conversion has been clarified by Melinkov et al. (25) and by Baranov et al. (26). Melinkov et al. suggested that formation of Cu^{-} center involves a stage in which Cu° or Cu^{+} is in interstitial position. In alkali halides containing Cu^{+}, the presence of interstitial ions has been confirmed experimentally (27). Therefore Cu° atom is also expected to be in an interstitial

position. It is suggested that the interstitial and diffusible Cu° traps an electron forming interstitial Cu^{-} which subsequently replaces the halide ion, the crystal being heated to a high temperature where appreciable ionic motion of the host lattice will occur, for the electrolytic coloration. Cu^{-} centers are formed at anion sublattice in addition to F centers also formed during this process.

Cu^{-} centers can also be produced by x-irradiation of $NaCl:Cu^{+}$ crystals at room temperature, and this method has been applied in this present work. Cu^{-} and F-centers are formed after x-irradiation, but in this case the mechanism of $Cu^{+} \rightarrow Cu^{-}$ conversion appears to be different from that in the case of electrolytic coloration. The mechanism of formation of Cu^{-} centers in x-irradiated $NaCl:Cu^{+}$ crystals has been clarified by Melinkov and Baranov et al. (25,26). It is suggested that Cu^{+} ion in a cation site captures an electron to form Cu° which remains in the same cation sublattice. It is the movement of anion vacancies during irradiation that plays a key role in the formation of Cu^{-} centers. Cu° in the cation site combines with an anion vacancy to form Cu°_{F}-center in which the spin of the unpaired electron in Cu° ($4s^{1}$ electron configuration) is aligned in the direction of the combining anion vancancy as evidenced by esr experiments. The sequence of formation of Cu^{-} can be explained by the following steps:

1. $Cu^{+}_{k} + e^{-} = Cu^{\circ}_{k}$
2. $Cu^{\circ}_{k} + V_{a}^{+} \overset{kT}{=\!=} Cu^{\circ}_{k} V_{a}^{+}$ (Cu°_{F}-center)
3. $Cu^{\circ}F + e^{-} = Cu^{-}_{a} V_{k}$
4. $Cu^{-}_{a} V_{K}^{-} \overset{kT}{=\!=} Cu^{-}_{a} + V_{a}^{-}$,

where the subscripts k and a refer to a cation and anion site respectively. V^{+} and V^{-} refer to anion and cation vacancies. F-centers

are produced by the well established radiolysis mechanism by which interstitial chlorine atoms and F centers are formed in the crystal. The roles of interstitial chlorine and F centers regarding the thermal annealing of Cu^- centers during which the crystal can be brought back to the preirradiation state is the aim of this present study. The intepretation of the experimental results will be made in Chapter IV.

Cu^- Absorption in Alkali Halides

NaCl:Cu^- crystal exhibits three strong absorption bands at 288, 232, 189 nm (2) called S_1,S_2, and S_3 bands and three weak bands at 272, 269 and 259 nm. Figure 9 shows the absorption spectrum of a NaCl:Cu^- crystal at 15K and Table IV shows the peak positions and relative intensities of the Cu^- absorption bands in NaCl, KCl and KI at 15K. When the crystal is γ-irradiated at room temperature, Cu^- absorption bands are at 292 (4.24 eV), 278 (4.46 eV), 258 (4.80 eV), and 234 nm (5.30 eV) in addition to the broad F-band peaking at 460 nm as shown in Figure 10 (3). Each of the two prominent bands at 288 and 232 nm (292 and 234 nm in γ-irradiated crystals) is found to have a symmetric gaussian shape without fine structure. These bands have constant areas for variation with temperature. Oscillator strengths of 292, 234, and 189 nm bands at 300K were estimated to be 0.025, 0.096 and 0.820 respectively (2).

Absorption of other s^2 ions in alkali halides, including Tl^+, have been assigned due to the $ns^2 \rightarrow nsnp$ transition as discussed Section II. The analysis and proposed transitions of the Cu^- absorption bands have been made by Tsuboi (28) and Kleeman (29). It is suggested that the Cu^- absorption bands consist of $3d^{10}4s^2 \rightarrow 3d^{10}4s4p$(s$\rightarrow$p transition as

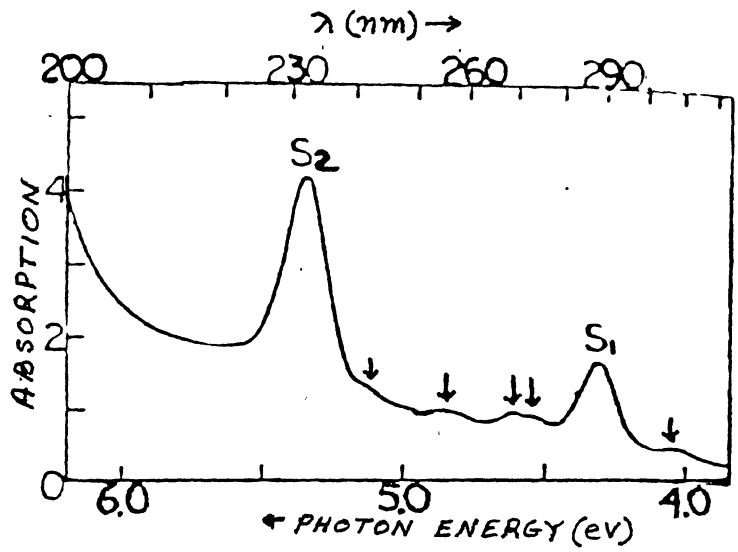

Figure 9. Absorption Spectrum of NaCl:Cu^- Crystal at 15K. Five Weak Bands are Shown by Arrows
Source: T. Tsuboi (2)

TABLE IV

PEAK POSITIONS AND RELATIVE INTENSITIES OF THE Cu^- ABSORPTION BANDS IN NaCl, KCl and KI at 15 K

Band	NaCl Peak Position (nm)	Relative Intensity (nm) (nm)	KCl Peak Position	KI Peak Position
	308	~ 0.01		348
S_1	287.1 (288*)	1	301*	324.4
	271.8 (272*)	0.04	286*	
	268.0 (269*)	0.08	280*	~ 300
	256 (256*)	0.04		
	242	0.03	254*	273
S_2	231.2 (232*)	3.91	242*	263.8
S_3	189*	40	195*	

* Measured at 77K.

Source: T. Tsuboi (2)

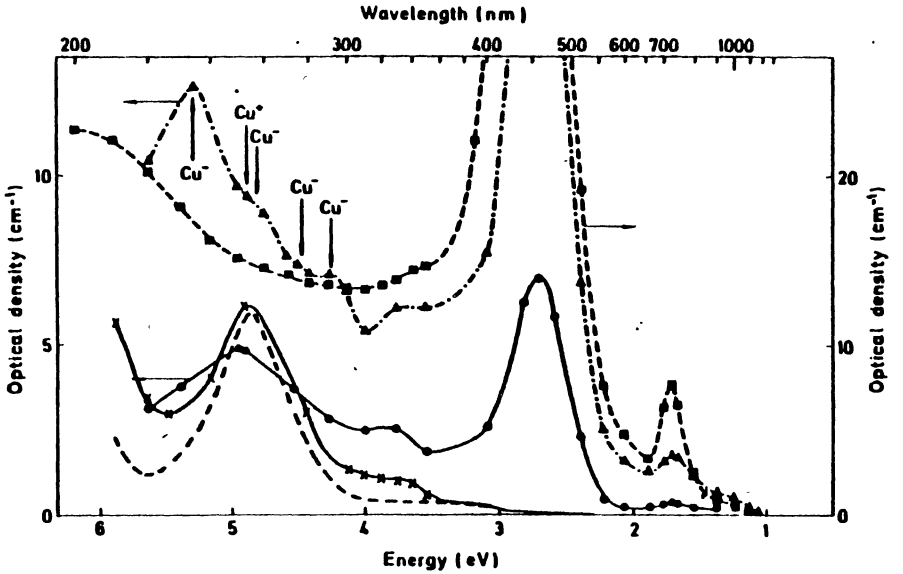

Figure 10. Absorption Spectra of NaCl:Cu^- Irradiated at Different Irradiation Doses
Source: L. Delgado (3)

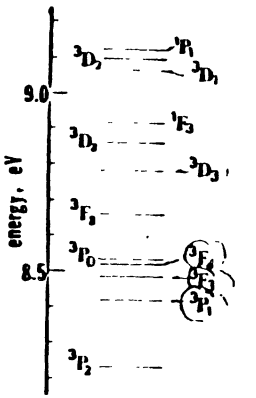

Figure 11. Energy Level Diagram of the $3d^9 4p$ Electron Configuration of a Free Cu^+ Ion
Source: T. Tsuboi (28)

observed for other s^2 ions) and $3d^{10}4s^2 \rightarrow 3d^9 4s^2 4p(d \rightarrow p)$ transitions. According to Tsuboi's assignment, A and B bands as seen in the absorption spectra of ns^2 type of ions in alkali halides are too weak to be observed in NaCl:Cu^-. The band at 288 nm (called S_1 as in Table IV) is assigned to be the C band ($4s^2 \rightarrow 4s4p$) from the observation of 308 nm band at the low energy side of this band. Two other weak bands at 272 nm and 308 nm cannot be assinged to B and A bands since (1A the 272 nm band increases in intensity with increase in temperature but unlike other s^2 ions doped in alkali halides, the energy peak of this band shifts to high energy (ii) the energy separation between the 308 nm and 288 nm bands is much smaller than the energy separation between the C and the A band for other s^2 ions in alkali halides.

Since the spectroscopic data for a free Cu^- ion are not available, it is difficult to estimate the values of the Slater-Condon parameters and spin-orbit coupling parameters as has been done for Tl^+ in Section II. Tsuboi (28) used the weak field approximation to speculate about a feature of the $3d^{10}4s^2 \rightarrow 3d^9 4S\ 4p$ spectrum and thus to explain the origin of other bands. The weak field approximation is better for the Cu^- ion in alkali halides than the strong field approximation, because the 3d inner-core orbital which is under the $4s^2$ shell will not be strongly affected by its ligand ions.

$3d^9 4s^2 4p$ configuration gives multiplets $^3P_{0,1,2}$, $^3D_{1,2,3}$, $^3F_{2,3,4}$, $^1P_1$, $^1D_2$, and $^1F_3$. Band assignments are as follows:

S_2 band (232 nm): $^1S_o \rightarrow {}^1F_3$ (allowed by the cubic crystal field).
S_3 band (189 nm): $^1S_o \rightarrow {}^1P_1$ (dipole allowed, strongest intensity).
[308, 269, 256, 242] nm: $^1S_o \rightarrow {}^3P_1, {}^3D_1, {}^3D_3, {}^3F_3, {}^3F_4$ (spin-orbit allowed).

The remaining band at 272 nm is suggested to arise from the transition to one of the forbidden states such as ^3P_o, $^3P_2$, $^3D_2$, or $^1F_2$. Thus it is suggested that the 234 nm band, the intensity of which was used as a measure of the concentration of Cu^- centers in the isothermal anneal experiments and the strongest 189 nm band arise from the transition to the $^1F_3$ and $^1P_1$ states respectively.

The $3d^9 4s^2 4p$ configuration of a Cu^- ion is qualitatively equal to the $3d^9 4p$ configuration of a Cu^+ ion (28), suggesting that the spectroscopic data of a free Cu^+ ion may be used to speculate the optical properties of a free Cu^- ion. The energy diagram as shown in Figure 11 is qualitatively in agreement with Tsuboi's assignment of Cu^- bands. For example, the $^1P_1$ state is at the highest energy site, whereas the lower spin orbit allowed states are at the low energy side of $^1F_3$ states. However for a free ion, the intensity of d→p transition should be smaller than s→p transition (30,31). The bands at 234 and 189 nm (assigned due to d→p transition) are however bigger in intensity than the 292 nm band (s→p transition). According to Tsuboi (28) such an intensity inversion is caused by the configuration interaction among the $^1P_1$ and $^1F_3$ states of the dp configuration since these states contain the same $^1T_{1u}$ representation in the cubic crystal field. Other support for d→p transition comes from the observation of a large absorption band at the tail of the exciton band in $LiCl:Cu^+$ (32) and $NaCl:Cu^+$ (2). McClure et al. (32) have assigned this band due to $3d^{10} \rightarrow 3d^9 4p$ transition in Cu^+. From a viewpoint of equivalence of the electron configurations between Cu^+ and Cu^- ions, it is believed that the observation of such a 3d→4p bands in alkali halide: Cu^- crystals is plausible. It should be noted that no detailed theoretical calculation has been done to predict

the energy levels of Cu^- ion in halides and thus the band assignments are difficult to make.

The next chapter (Chapter III) discusses the details of the experimental procedures and apparatus used in this dissertation before moving to the presentation and interpretation of experimental results.

CHAPTER III

EXPERIMENTAL APPARATUS AND PROCEDURE

Introduction

This thesis is concerned with three projects. In the first project, the motion of Cu^- ions, their correlations with F-centers and the solid state physics of $Cu^- \rightarrow Cu^+$ conversion process in NaCl was studied. In the second project, photoluminescence and photoconductivity from thermochemically colored $MgAl_2O_4$ (spinel) were examined. The third was concerned with the study of luminescence and photoconductivity of thermochemically reduced Al_2O_3 crystals which were subsequently annealed at high temperatures. In this chapter the details of the experimental equipment and procedures used in these projects are described. The general background of the experimental techniques will be discussed as it pertains to the present work.

Sample Preparation

The NaCl:Cu crystals used were grown in O.S.U's crystal growth laboratory by Mr. Charles Hunt. 0.05 mole percent of CuCl was added to the melt and the crystals were grown by Czochralski technique. Rods of NaCl:Cu were obtained and the samples used in the experimental work were cleaved from these rods. The approximate dimensions of the samples were 1.50 mm by 15.0 mm by 6.50 mm.

The $MgAl_2O_4$ crystal used was obtained from Dr. J.H. Crawford, Jr.

(33) of The University of North Carolina at Chapel Hill. The dimension of the sample was 0.75 mm by 14.0 mm by 9mm. The single crystal of spinel was cut from a boule grown by Union Carbide Corporation and subsequently colored by heating in an atmosphere of Al vapor. Impurity analysis of the sample showed the presence of Chrominum (4ppm), Iron (76 ppm) and Copper (22 ppm). Uncolored samples also grown from Union Carbide Corporation, were used for comparison.

Al_2O_3 crystals used were supplied by Insaco and grown by Adolf Miller Corporation. Three samples of Insaco crystals were used, one of which was unannealed and the other two samples were annealed at 1250°C and 1500°C, for 12 hours respectively. For the sake of convenience the samples will be referred to as Insaco #9 (unannealed), Insaco #9a (annealed) at 1250°C) and Insaco #9b (annealed at 1500°c) respectively.

Optical Absorption

In studying the optical properties of point defects and impurity ions in insulators, optical absorption measurements are valuable since insulators with their large band gaps make the electronic transitions associated with impurities and lattice defects relatively easily observed.Electrons in crystal defects with energy levels in the band gap can be excited by absorbing light analogous to excitations of isolated atoms. The presence of the ions surrounding the defect modifies the electronic transition by introducing phonon interactions and possible splitting of degenerate states by the crystal field, lifting to some extent forbiddenness of selection rules and reducing degeneracy.

The measurements of optical absorption were made using a Perkin-Elmer 330 spectrophotometer in the spectral range from 800 nm to 185

nm. The intensity of the light passing through the crystal is a function of the crystal thickness. One usually measures the optical density which is given by the relation

$$OD = \log_{10} \frac{I_o}{I}, \tag{45}$$

where I_o is the intensity of the reference light and I is the intensity of the light transmitted by the sample. The intensity of transmitted light is given by:

$$I = I_o \exp(-\alpha t), \tag{46}$$

where t = thickness of the crystal and α = absorption coefficient.

From Equations (45) and (46) the relation between absorption coefficient α and optical density 'OD' is given by

$$\alpha = 2.303 \left(\frac{OD}{t}\right) cm.^{-1} \tag{47}$$

By measuring the absorption coefficient, one can estimate the concentration of absorbing defects through Smakula's equation which is given by

$$Nf = 0.87 \times 10^{17} \, n \, \alpha \, w \, (n^2 + 2)^{-2}, \tag{48}$$

where N = concentration of absorbing defects/cm^3, n = index of refraction of the crystal, w = full width at half maximum (FWHM) of the absorption band, and f = oscillator strength of the transition

responsible for the absorption. The factor 0.87 is applicable for a Gaussian line shape. If the band is phonon independent, the shape would be Lorentzian and the corresponding factor in Smakula's equation would then be 1.29.

Thermoluminescence

Thermoluminescence occurs when electrons (holes) are thermally released from a trap and radiatively recombine with holes (electrons) trapped at another site. An example of this process is found in thermoluminescence involving F-centers (oxygen vacancies each of which has trapped two electrons) in α-Al_2O_3 :

$$F + h\nu \rightarrow F^+ + e^- \text{ (conduction band)} \rightarrow F^+ + e^- \text{ (trapped)}$$
$$e^- \text{(trapped)} + \text{phonons (260K)} \rightarrow e^- \text{ (conduction band)}$$
$$e^- \text{ (conduction band)} + F^+ \rightarrow F^* \rightarrow F + h\nu \ (\lambda = 410 \text{ nm})$$

where F^+-centers are oxygen vacancies containing one electron only and thus positively charged with respect to the lattice and F^* is the excited state of an F-center. The energy of emitted light is 3 eV (410 nm) and this is the energy given off when the electron trapped at a different site recombines with F^+ center at 260K.

In TL, the light given off when electron-hole recombination occurs at some site is measured. The transition energy observed will be characteristic of the recombination center whereas the light intensity is proportional to the number of released charge carriers.

Intensity of emitted light is given by

$$I = -\lambda \frac{dN}{dt} = \eta N v a \lambda \,, \tag{49}$$

where λ = proportionality constant, N = number of trapping sites/cm^3, n = number of carriers/cm^3, v = velocity of the carrier, and a = capture cross section. Equation (49) shows that the light intensity, which is directly proportional to the rate of radiative recombination, reflects the concentration of thermally released carriers.

The experimental apparatus for TL experiments utilized a linear heating rate of the sample. In the TL runs from 77K to 300K, the heating rate was ~ 5 K per minute provided by the heater wrapped around an insert for the continuous flow system, while for TL runs above 300K, the heating rate was ~ 20°C per minute. In a typical TL experiment below room temperature the sample was cooled to liquid nitrogen temperature and then illuminated with unfiltered light from a 60 W D_2 lamp and then warmed up with a linear heating rate. The light given off from the sample was measured by a water cooled RCA 31034 photo multiplier. THe horizontal scale of the X-Y recorder monitored the temperature at intervals of 10K. The Y motion of the recorder measured the intensity of the emitted light. Standard thermometric techniques were employed for monitoring temperatures. The cryostats were equipped with copper vs constantan thermocouples attached to the tail piece near the sample. For TL runs above room temperature as was required for NaCl: Cu samples, a computerized set up developed by Dr. S.W.S. McKeever (34) was used. The heating was provided by "Eurotherm" heater. Crystals were placed on the hot plate attached to a heat sink. An EMI photomultiplier tube measured the intensity of the light and the digitized system made it possible to record 200 data points while the smple was heated from room temperature to 500°C, the intensities being recorded at a temperature interval of 0.20°C.

The spectral dependence of the TL intensity was measured by dispersing the emission with a 1/3 m McPherson monochromoter between the sample and C31034 PMT. Another EMI photomultiplier monitored the total increase in TL intensity as the temperature was raised. When the temperature of the samples was close to the TL peak, the light emitted by the sample was quickly scanned by the monochromator at a rate of 200 nm $minute^{-1}$. The sample was heated by a rapid heating rate so that the temperature corresponding to the TL peak could be attained quickly.

Photoluminescence

A block diagram of the photoluminescence apparatus is shown in Figure 12. The exciting light was emitted by a 60W D_2 Lamp and then focused on the sample with a lens. All of the lenses used in these experiments were made from S-1 UV grade quartz because of its flat response from 250 to 2000 nm. Oriel G-522 series interference filters were used to select excitation energies of the luminescence of the sample. After exiting from the cryostat, the emitted light passed through suitable sharp cut filters to eliminate stray light. The emitted light was dispersed by a GCA McPherson 218 0.3 m monochromator with its slits set at 1.5 mm. The monochromator had a linear dispersion of 26.5A /mm and contained a grating blazed at 3000A (other blazes were also available) with 1200 groves/mm. The dispersed light from the monochromator was detected by an RCA C31034 photomultiplier tube cooled to -30°C by a water cooled Pacific photometric Institute Thermoelectric Photomultiplier Housing Model 3463 powered by a power supply/temperature controller model 33. This PMT has a detection range from 200 nm to 900 nm. The current from the photomultiplier was amplified and detected by

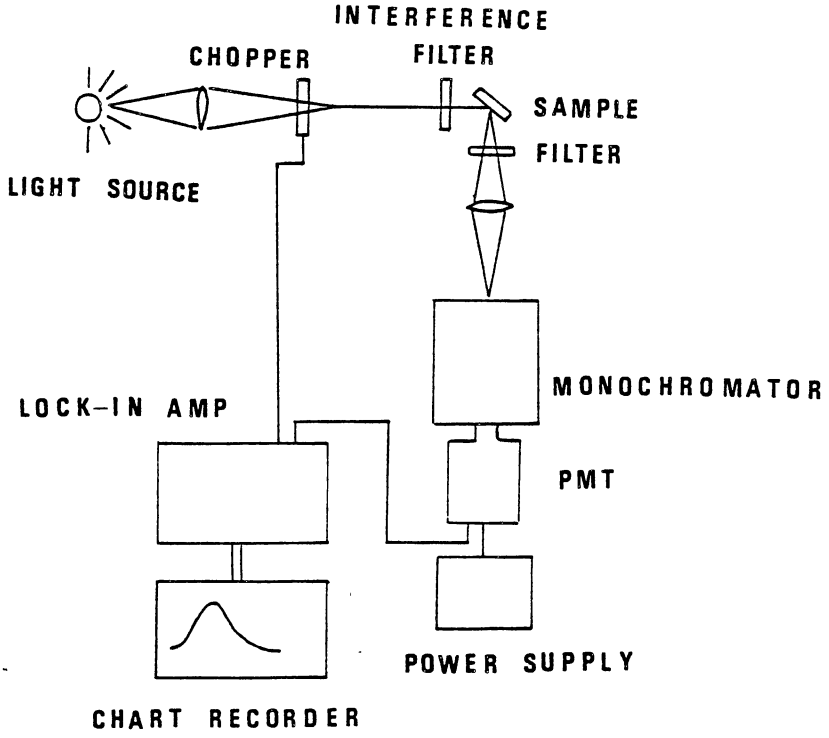

Figure 12. Photoluminescence Apparatus

a Keithley 414S picoammeter. The output was fed into an Omnigraphic (X-Y) chart recorder. The recorder and the McPherson monochromator were synchronized to record signal strength as a function of wavelength. In another set up, the light from the D_2 lamp passed through a Princeton Applied Research (PAR) mechanical light chopper before falling on the interference filter. The current from the photomultiplier tube was amplified by a PAR Model 181 current sensitive preamplifier. This signal was then fed into a PAR Model 128 A Lock-In amplifier. A reference signal from the mechanical chopper was used by the lock-in amplifier to produce a dc output signal proportional to that part of the preamplifier signal which was synchronous with the chopper's signal. This output was fed into the X-Y chart recorder.

In order to analyse the data, the response of the dection system had to be determined as a function of wavelength. The system was set up as in Figure 12 except that a 100 W Tungsten lamp was directed into the McPherson monochromator. The intensity of the light was recorded as a function of wavelength. At 5 nm intervals this resulting curve intensity was divided into the relative number of photons emitted by the lamp. The relative number of photons emitted by the lamp was calculated by approximating the output of a blackbody at the filament. The response of the detection system (photons/sec) as a function of wavelength was determined and the results normalized. One such response curve for the detection system with the monochromator grating blazed at 3000Ψ is shown in Figure 13. The response of the luminescence detection system thus obtained was corrected by multiplying the emission intensity at a given wavelength by the corresponding ratio of $\frac{\text{(number of photons)/sec}}{\text{system response}}$ at that particular wavelength.

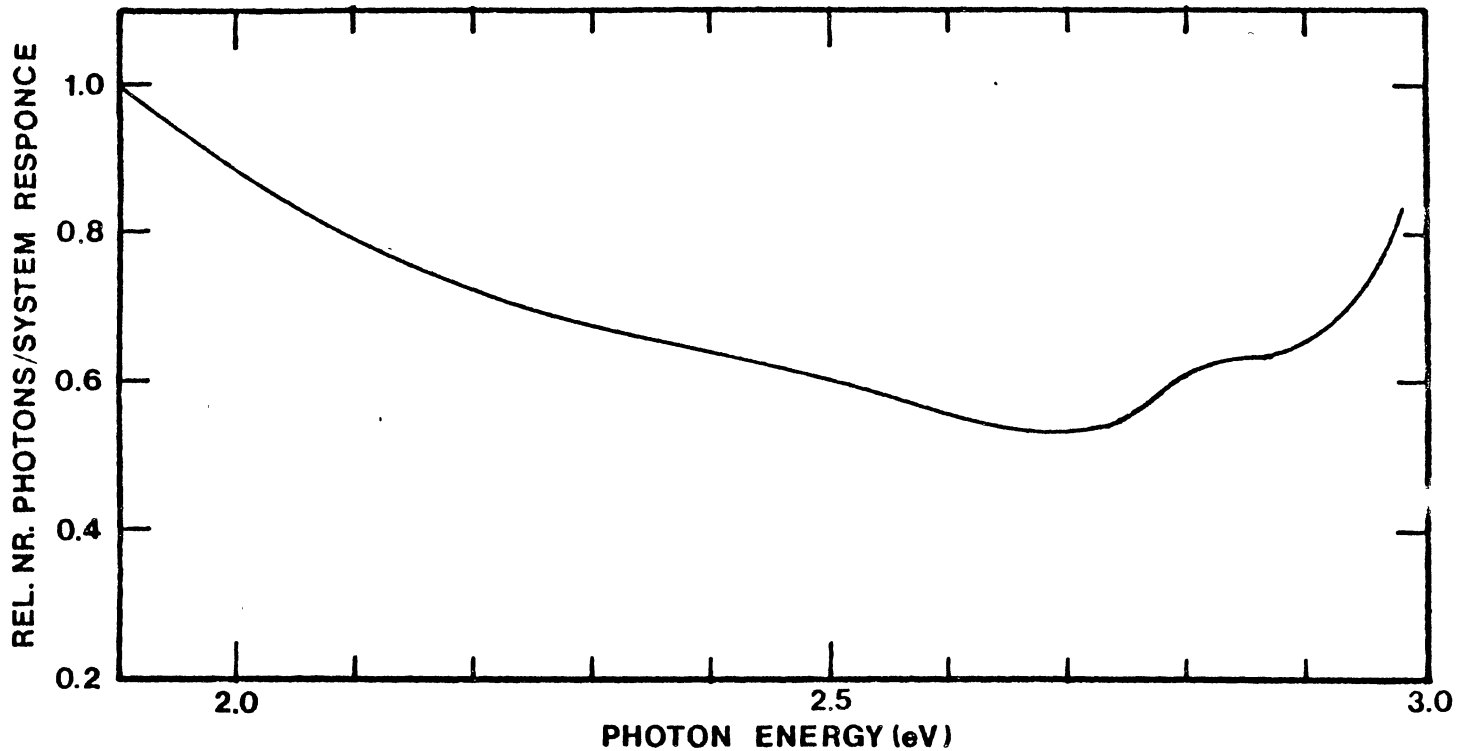

Figure 13. Intensity Normalization Curve. The Monochromator Grating was Blazed at 3000Å

The temperature dependence of the photoluminescence was measured by an Oxford Instrument CF 201 continuous flow helium cryostat. The outer chamber of the cryostat was filled with dry helium gas and temperatures down to 10K could be obtained with the apparatus. Intermediate temperatures between 10K and room temperature were achieved by heating the sample with an automatic temperature controller. The temperature reading in the controller varied within ±0.5 K from the reading of copper vs constantan thermocouple which was attached to the tail piece near the sample. The reference jucntion of the thermocouple was maintained at 0°C. The intermediate temperatures between 10K and 300K were maintained for a few minutes to allow the system to come to thermal equilibrium before the varous measurements were recorded.

In order to study the polarization properties of the luminescence in α Al_2O_3 , the set-up is the same as in Figure 12, except a polariser was inserted between the sample and the monochromator. The transmission axis of the polariser could be set at angles between 0° and 90° with respect to the C-axis of the sample. Polarised luminescence curves for different orientation of the transmission axis of the polariser were corrected for the inherent polarisation effect of the detection system, in which the polariser was placed between the lamp and the entrance slit of the monochromator. Intensity of the dispersed light as a function of wavelength between 300 nm and 530 nm at polariser angles between 0° and 90° (at intervals of 15°) was measured. From the intensity vs. wavelength curves for different orientations of the transmission axis of the polarizer, the correction factors for the inherent polarization of the detection system as a function of the orientation of the polarizer transmission axis were obtained.

Excitation

The excitation spectrum for a corresponding luminescence band was determined as follows: the light from a GOW D_2 lamp was dispersed by the Mcpherson monochromator before falling on the sample. Suitable band pass filters corresponding to the wavelength of the luminescence band were inserted between the sample and EMI photomultiplier tube used for detection. The intensity of the emission at the peak wavelength was then obtained as the wavelength of the exciting light was varied.

Since the intensity of the emission was measured at a set wavelength, the only changing factor was the power and the corresponding number of photons/sec incident upon the sample for a given wavelength of the exciting light. The exciting light from the D_2 lamp was dispersed by the Mcpherson monochromator before entering a sodium salicylate detector whose output was directly proportional to the number of photons. The power of the dispersed light at a particular wavelength was measured by a Molectron radiometer placed at the sample position. From this information, corresponding number of photons/sec incident on the sample was determined. The corrected excitation spectrum was obtained by dividing the excitation intensities by the corresponding number of photons/sec falling on the sample.

The set-up to study the temperature dependence of the excitation was the same as in photoluminescence measurements.

Photoconductivity

A block diagram of the apparatus used in photoconductivity measurements is shown in Figure 14. Incident photon wavelengths were varied from 200 to 350 nm at temperatures ranging from 77K to 295K.

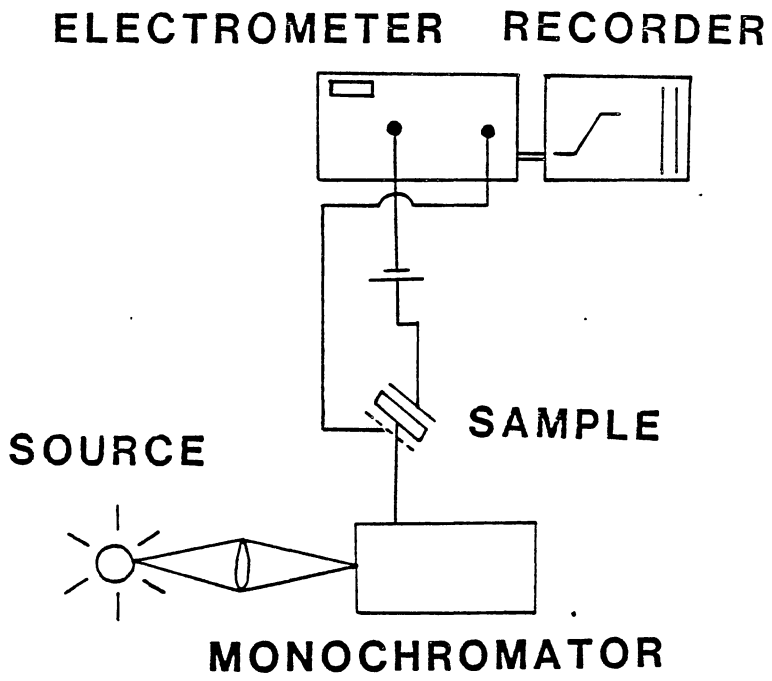

Figure 14. Photoconductivity Set-Up

Light from a 60W D_2 source entered the entrance slit of the monochromator. The dispersed light was focussed on the crystal. The incident light fell on the crystal of thickness d, between plane parallel electrodes. The crystal was placed in the cryostat and an electric field E = v/d, was across the sample in a direction parallel to that of the incident light. A 300 V battery in the external circuit provided the polarizing potential. The signal was detected by Cary 401 vibrating reed electrometer operated in either current or rate of charge mode. The reflection grating of the monochromator was blazed at 2000Å. To maximize transmission, Corning glass filters with sharp optical cut off were used following the light source to eliminate higher orders from the incident light falling on the sample.

60W D_2 source was calibrated in a separate experiment by placing a Molectron 100 pyroelectric radiometer at the sample position. The radiometer was used to determine the power, in microwatts, of the incident light falling on the surface of the sample holder as a function of wavelength. The number of photons striking the front surface of the sample is given by

$$n = \frac{P\lambda}{hc}, \tag{50}$$

where P = power measured in μ watts, h = Planck's constant, and c = speed of light. The number of photons falling on the sample was of the order of 10^{13} sec^{-1} at 300 nm. Knowing the relative number of photons/sec striking the sample as a function of wavelength, the photoconductivity data in an experiment could be corrected according to the spectral dependence of the exciting system.

The photoconductivity measurements were made with the sample holder as shown in Figure 15. The sensitive electrode, g, made of copper foil 0.05 mm thick, 3 mm wide and 3 mm long was connected to the electrometer. This electrode was electrically insulated from the copper tail of the cryostat, a, by a sapphire plate, h, 0.25 mm thick. The incident light passed into the crystal, e, through the front electrode, d, a phosphor-bronze screen of 0.55 mm diameter wire and 100 mesh. The screen was held against the crystal by a quartz plate, c, which was supported by phosphor-bronze springs. Sapphire plates, f, 0.25 mm thick were placed on either side of the crystal and the corresponding electrode to prevent charge from entering or leaving the sample. The sample was located in a copper chamber bolted to the tail of the cryostat. Dry helium exchange gas could be admitted to the chamber to produce good thermal contact.

A shielded lead was connected to the phosphar-bronze screen electrode to a battery in the external circuit which produced an electric field of about 500 v/cm, in a direction parallel to that of the incident light. The direction of the applied electric field was reversed after individual measurements to prevent polarization effects in the crystal.

The sensitive electrode was connected, by a shielded lead, to the input of a Cary 401 vibrating reed electrometer which was used in either the "rate of charge" or "current" mode. For the detection of small photocurrents (~ 10^{-14} amp) , the "rate of charge" method was used. The output of the electrometer was fed to an Omnigraphic 2000 X-Y potentiometric recorder.

In the "rate of charge" method, the photocurrent corresponding to

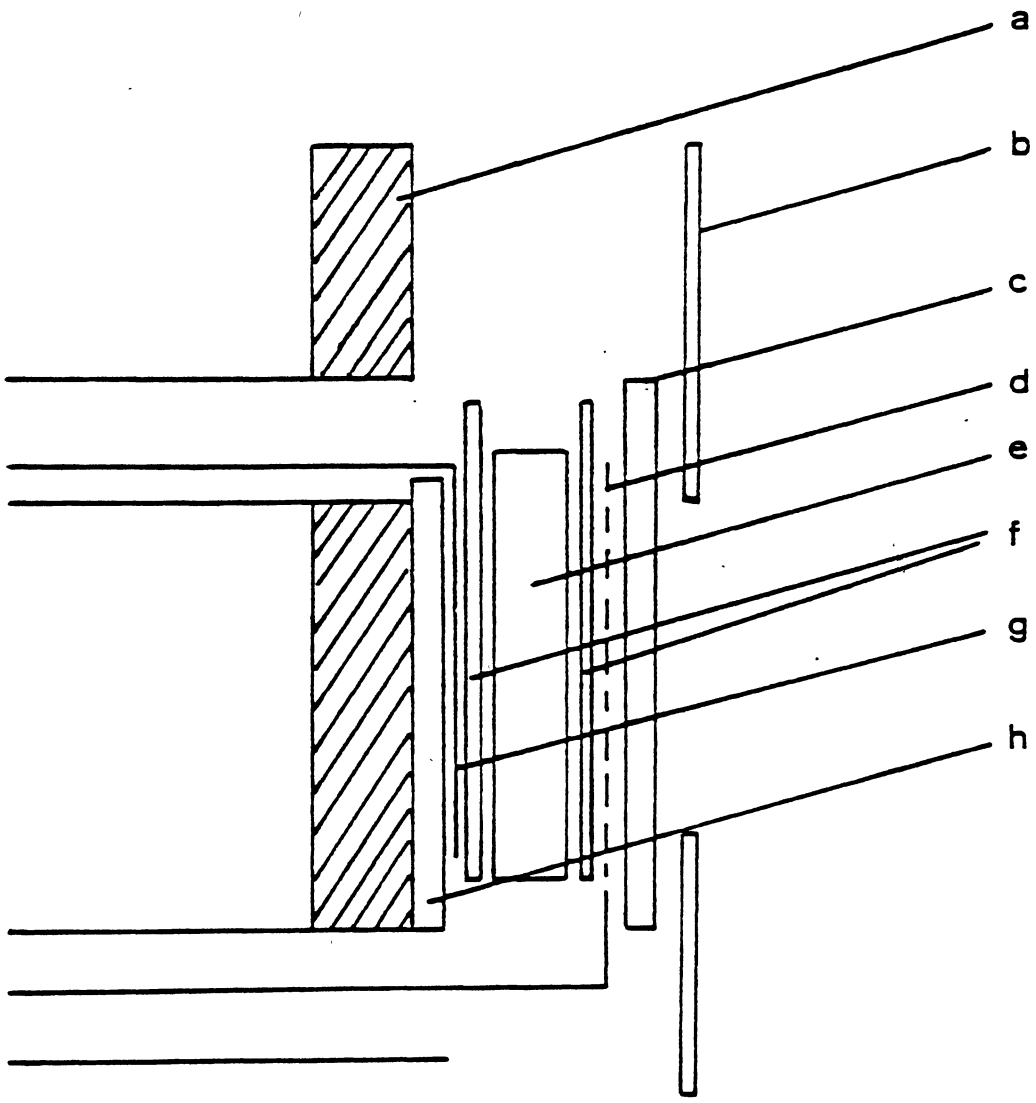

Sample Holder: a. cryostat tail, b. mask, c. quartz, d. phosphor-bronze screen, e. sample, f. sapphire plates, g. copper electrode, h. sapphire plate

Figure 15. Sample Holder used in Photoconductivity Experiments

the incident light of a given wavelength is given by:

$$I_\lambda = \frac{dQ}{dt} = C_c \frac{\Delta E_r}{\Delta t}, \qquad (51)$$

where Q = charge in coulombs, C_c = charge collecting capacitor = 1.9915 x 10^{-11} farad, ΔE_r = change in the recorder reading as a fraction of the full scale times the electrometer range in volts, and Δt = time interval in seconds. Photocurrents measured in the rate of charge method were typically of the order of 10^{-15} amps. In the"current mode" of the electrometer, photocurrents as high as 10^{-12} amps were detected.

The background drift current detectable was of the order of 5 x 10^{-17} amps. The sensitivity of the apparatus fell off as the wavelength of the incident light approached 200 nm due to the fact that the output of the light source fell off rapidly in this region of the spectrum.

X-Irradiation

It was necessary to irradiate NaCl:Cu samples with x-rays at room temperature. 1.5 MeV electrons (current = 10 μA) were deflected by a thick copper target (thickness = 1.5 cm) before falling on the sample. The sample was mounted on a brass sample holder and was placed in air. The geometry of the set up was kept the same during subsequent irradiations to ensure the constancy of the dose. The sample was irradiated for 10 minutes at room temperature in the Van de Graaff set-up. The irradiation dose for 10 minutes exposure was found to be ~ 6 Mrad by comparing the absorption co-efficients at the peak of the F band of two samples of pure NaCl having same dimensions in which one sample was irradiated in the VDG set-up for 10 minutes and the other was

exposed to ^{60}Co source for one hour, the dose from the ^{60}Co source being 21 x 10^3R/hr. The details of the dose calculation in VDG set up will be explained in Chapter IV.

Isothermal Anneal

Isothermal anneal expermients were performed by placing the sample in an optical cryostat. The cryostat was then placed in the sample chamber of Perkin Elmer model 330 spectrophotometer. Heating of the sample was provided by a D.C. Power Supply operating at 1.5A. Once the desired temperature of the sample was obtained, absorption spectrum of the sample was taken by scanning the proper wavelength range. The time interval between subsequent scans was two minutes. Heater voltage was adjusted during the runs and the temperature of the sample was within ± 0.2°C of the desired temperature at which the anneal experiment was performed.

CHAPTER IV

NaCl:Cu

Introduction

This chapter describes the optical properties and ionic motion of Cu^- ions in NaCl. Cu^- is isoelectronic with Tl^+ type ions with ns^2 (n=4, 5, 6) electron configuration. The optical properties of positive ion impurities (e.g. Tl^+) with ns^2 electron configuration which are doped in alakli halides, have been well understood (35) although there are some unknown properties with regard to the absoprtion spectra of the individual s^2 ions. Three absorption bands named A, B, and C have been observed in alkali halides containing Tl^+, In^+, Ga^+, Pb^{2+}, Sn^{2+}, Ag^- or Au^- ions. These bands arise from $ns^2 \rightarrow$ ns np transition of the impurity ion and can be identified in the absorption spectra. Additionally, an absorption band named D has been observed on the low energy tail of the exciton band in alkali halides containing Tl^+, In^+, Ga^+, Pb^+ or Sn^{2+} ions (15,36) whereas two bands named D_1 and D_2 have been observed in alkali halides containing Ag^- or Au^- ions (37,38). The D band has been attributed to a perturbed exciton band, although its theoretical analysis has not been established. In case of Cu^- ions, the band assignment becomes difficult since Cu^- absorption spectra are quite different from the spectra of other s^2 ions. Tsuboi (2) investigated, in details, the absorption of Cu^- in NaCl and suggested that the observed Cu^- spectra consist of the $4s^2 \rightarrow 4s4p$ (s→p) and $3d^{10}4s$

$\rightarrow 3d^9 4s^2 4p$ (d→p) transitions. Lack of theoretical work on Cu^- ions in alkali halide hosts has make the band assignments mainly qualitative in nature. However, the present work is concerned not as much with the assignment of Cu^-- transitions in alkali halides but rather with the behavior of Cu^-- centers on optical and thermal annealing and the mechanism which governs the process of $Cu^- \rightarrow Cu^+$ conversion in NaCl. Optical absorption, isothermal and isochronal annealing and thermoluminescence experiments were carried out but to understand the thermal motion of Cu^- ions in a NaCl host lattice and the process by which the preirradiation state of the crystal is achieved. Before presenting the results of the different experimentations, however, it is necessary to explain how radiation induced defects such as Cu^- ions and F centers are produced in NaCl and how these defects anneal thermally as evidenced from theromluminescence and isothermal anneal experiments performed by earlier workers.

Cu^- is highly unstable in the free state and cannot be doped directly into a halide lattice. In order to produce Cu^-- centers in alkali halides, the host crystal is first doped with Cu^+ ions in small concentrations and subsequent γ or x- irradiation at room temperature or electrolytic coloration of the crystal produces measurable Cu^- concentration of Cu^- ions as evidenced from optical absorption measurements.

Figure 16 shows the crystal structure of NaCl. It can be seen from the figure that each ion is surrounded by six ions of the opposite sign. There is a coulomb interaction between an ion at a particular site and all other ions in the lattice. This interaction gives rise to Madelung energy which is the largest part of the cohesive energy of the

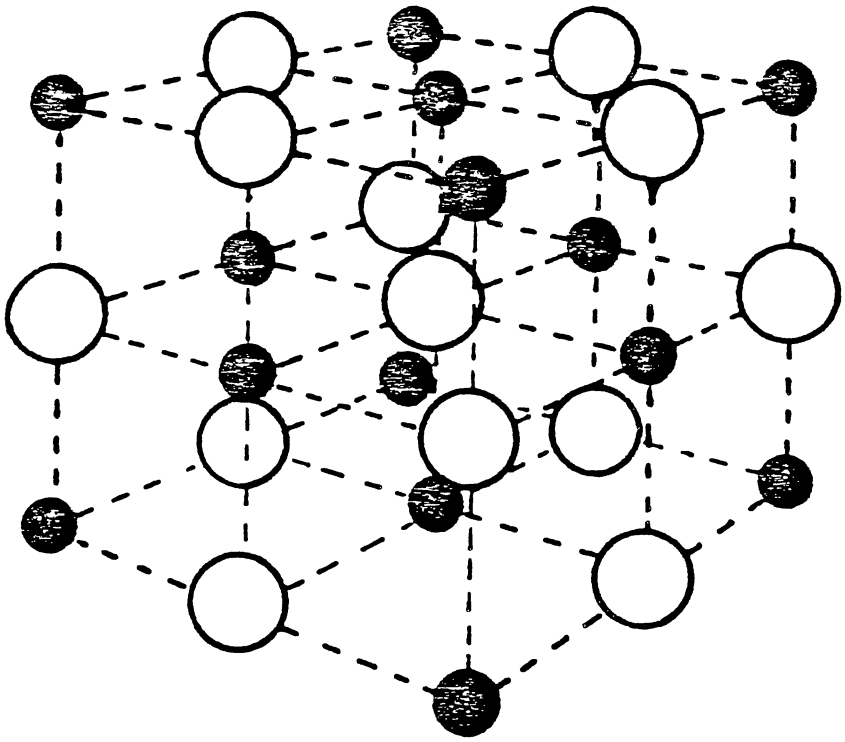

Figure 16. Crystal Structure of NaCl

crystal. The crystal structure of NaCl is face-centered cubic with a basis consisting of an anion (Cl^-) at (0,0,0) and a cation at (1/2a, 1/2a, 1/2a), where a is the length of a cube side. Cu^+ ions are doped into NaCl structure during the growth of the crystal by adding small amount of CuCl in the melt. Cu^+ being monovalent, occupies the substitutional cation site and does not require any charge compensation. The presence of Cu^+ ions in NaCl host is detected by optical absorption measurements which shows a band at 254 nm (4.83 eV). This band has been assigned to the d→p transition of Cu^+ ions in the crystal. Fussgaenger (39) investigated the temperature dependence of the oscillator strength of Cu^+ absorption and using his value Tsuboi (2) obtained the value of 0.020 for the 254 nm Cu^+ band in NaCl at 300K. One feature of interest regarding Cu^+ absorption is that the bands are nearly independent of the halide host and are rather far from the free ion values. In free Cu^+ the $3d^{10}\rightarrow 3d^9 4s$ multiplet spans the energy range of 2.7 to 3.3 eV and $3d^{10}\rightarrow 3d^9 4p$ encloses 8.3 to 9.2 eV (35) but in the crystal, Cu^+ transitions take place over the spectral range from 4.70 to 6.2 eV. Excitation in the 254 nm Cu^+ band produces a single emission band peaking at 351 nm and with a half width of 0.27 eV.

When NaCl: Cu^+ crystals are x or γ- irradiated at room temperature or electrolytically colored, Cu^- ions and F-centers are produced. The absorption spectrum of the x-irradiated or electrolytically colored sample shows the formation of new bands in the visible and ultraviolet region while the 254 nm band is no longer detected in these samples suggesting that Cu^+- centers have been removed by these treatments. In x-irradiated samples, the broad band peaking at 470 nm is assigned to be due to F-centers and the UV bands at 292 (4.24 eV), 278 (4.46

eV), 258 (4.80 eV) and 234 nm (5.30 eV) are assigned to internal transition of the Cu^- ions. The suggested mechanisms of production of Cu^-- and F centers in NaCl need to be discussed at this point. To understand the recovery of the pre-irradiation state of the crystal by which the annealing of radiation induced defects (Cu^-- and F-centers in this case) occur, it is important to know the mechanisms of formation of such defects in the lattice.

The formation of F-centers in irradiated NaCl:Cu crystal is by the well established mechanism of radiolysis. In radiolysis defect production three steps are involved: (i) an electronic excitation resulting in the creation of polarized or charged electronic defect in the lattice, (ii) the conversion of this energy into the kinetic energy of a lattice ion in such a way that the ion moves and, (iii) the motion and stabilization of the displaced ion. The essential idea of the model stems from a characteristic of ionic crystals that may permit the production of directed motion (ionic) from a single ionization of a halide ion. This characteristic is the large amount of ionic relaxation that follows any electronic change and forms the basis of the model proposed by Pooley and Runciman (40) to explain the highly efficient defect production in alkali halides. They concluded that there exists a relation between electron-hole recombination and the production of ionic defects. When a hole is self-trapped, the two halide (Cl^-) nuclei are much closer than are two normal ions. A recombining electron will produce an impulse pushing the two Cl^- ions toward their normal lattice positons. The relaxation of the halides that occurs upon the electron-hole recombination becomes large enough to cause a replacement collision to be propagated by halide ions along a close packed <110> direction and

efficient production of Frenkel pairs consisting of F and H (interstitial Cl^{o}) center is achieved.

The mechanism of production of Cu^{-}-centers is more complex in x-irradiated alkali halides at room temperature. Melinkov et al.(25) and Baranov et al.(26) investigated the production mechanism of Cu^{-} and Ag^{-}-centers in irradiated halides. Melinkov et al.(25) performed electron paramagnetic resonance and optical absorption experiments to study the formation of various silver centers which were produced during the radiation induced coloring of KCl:Ag crystals. Their investigations (25) were mainly concerned with the processes leading to the formation of Ag^{-}_{a} ions ('a' refers to an anion site) which replaced the anions in the KCl lattice (B centers). A four-stage formation mechanism of B centers (Ag^{-} in an anion site) was proposed namely: i) formation of cation silver atoms Ag^{o}_{k} through electron capture by Ag^{+}_{K} ions, where K refers to a cation site; ii) migration of anion vacancies to Ag^{o}_{k} atoms and formation of Ag^{o}_{F}-centers; iii) formation of Ag^{-} ions through electron capture by Ag^{o}_{F} centers; and iv) migration of cation vacancy from the Ag^{-} center and formation of a B-center. Ag^{o}_{F}-centers are an intermediate stage in the formation fof Ag^{-}- centers. EPR and linear dichroism experiments were performed to establish the structure of Ag^{o}_{F}-centers and to obtain information on the distribution of the spin densities. More particularly, it was shown that the degree to which the unpaired electron of the silver atom is shifted toward the anion vacancy amounts to about 30%. By capturing an electron, the Ag^{o}_{F}-centers are transformed into Ag^{-} ions, for which the anion site is most appropriate from the viewpoint of the Madelung energies involved. When this transformation process takes place at high temperatures the cation

vacancies neighboring the Ag^- ions disappear and B-centers are formed. At low temperatures, at which the cation vacancies are immobilized, a B_M-center which has a cation vacancy in its neighborhood can be formed upon capture of an electron by Ag_F^0 centers; such B_M- centers have been observed experimentally (40). These B_M-centers transform to B-centers upon heating. In this model of the formation of Ag^- centers (B-centers), great importance is attributed to the cation Ag^0 atoms and to the Ag_F^0 (on a cation site). Ag_F^0-centers have been detected experimentally (25,26,42).

The formation mechamism of Cu^- centers in alkali halides appears to be similar to the one described above for Ag^-- centers. Cu_F^0-centers are also formed in an intermediate stage in the production of Cu^-- centers in irradiated alkali halides. Optical absorption and emission bands of Cu_F^0-centers in KCl were identified by means of correlated EPR and optical investigations. Baranov et al. (26) observed four optical bands (between 2.50 and 3.50 eV) due to Cu_F^0-centers and two absorption bands (between 2.40 and 2.80 eV) due to Cu_k^0-centers. They reasoned that the appearence of an anion vacancy near a Cu^0 atom results in the splitting of each of the Cu_k^0 absorption bands into two. A similar effect has been found for the Ag_F^0-centers (25). In the case of Cu_F^0-centers, 40% of the unpaired spin density is delocalised to an anion vacancy in the C_4 direction. During x-irradiation at room temperature a Cu_F^0-center is able to trap an electron by means of which Cu^-- centers are produced in the anion sublattice.

After Cu^-- and F-centers are formed in x-irradiated crystals, the following questions may be addressed; (i) what is the decay kinetics that governs the thermal decay of Cu^-- centers? (ii) what is the charge

state of the impurity ion after the completion of the annealing experiments? (iii) what is the mechanism by which the pre-irradiation state of the crystal is achieved? Annealing of radiation induced defects in pure and doped halides has been studied by several investigators. Kleeman (43) investigated the dissociation of Ag^--centers by optical and thermal excitation in alkali halides. He concluded that the thermal or optical excitation causes the Ag^-- centers to dissociate into neutral silver (Ag°) atoms and F-centers. The Ag° centers are bound to interstitial positions at low temperatures. At high temperatures interstitial Ag°- centers combine to form colloidal centers. The mechanism of $Ag^- \rightarrow Ag^+$ conversion by which the full thermal recovery of Ag^+ ions could be achieved was, however, not investigated.

In investigating the annealing processes leading to the recovery of the preirradiation state of irradiated alkali halide crystals, thermoluminescence (TL) has been proved to be a useful experimental technique from which some conclusions about the nature of the defects induced by irradiation can be drawn. Since the sample used in this study contained F-centers in addition to Cu^-- centers, it was necessary to know how TL glow peaks observed in alkali halides irradiated at room temperature are related to the annealing of F centers at the temperature maxima (T_m) of the glow peaks. The investigations of thermoluminescence phenomena in irradiated alkali halides were aimed to establish in a few cases a correlation between the thermoluminescent processes and the thermal stability of the radiation induced color centers, mainly F-centers. There are differing points of view about the role of the F-centers in the thermoluminescent process. According to Jain and Mahendru (44,45), F-centers play the role of electron traps in

the thermoluminescent process. It has also been suggested that F-centers act as a recombination centers for holes which are thermally released from traps (46,47). Holes which are trapped at different impurity sites during x-irradiation are emitted from the traps corresponding to the temperature maxima of the TL peak and radiatively recombine with the F-centers as evidenced from the spectral dependence of the emitted light. This model has been commonly used to explain the thermoluminescence observed in irradiated LiF. A quite different model has been recently proposed by Ausin and Alvarez Rivas (48,49). In this model the mobile entity in the thermoluminescent process is neither an electron nor a hole as in the previous models but halogen atoms which are stabilzed at interstitial positions after irradiation. They are thermally released and migrate until they recombine with F-centers. At this stage there is an electron hole recombination and light is emitted. Mariani et al.(50) perfomed thermoluminescence experiments in KI, KBr, NaCl and NaF crystals irradiated at room temperature to gain support for this model. The main support for F + H recombination hypothesis came from the experimental observation of the variation in the thermoluminescence spectrum in each material with the irradiation dose. Also, in the earlier models where F-centers are either electron traps or recombination centers, the existence of thermally stimulated currents associated with the thermoluminescence spectrum would be expected. These currents have not been observed in the investigation of thermoluminescence of irradiated halides either at room temperature or at liquid nitrogen temperature (48,49). Regarding the evolution of TL spectra with increasing F-center concentration, it was noted that in both the earlier models either each type of F-center or type of hole

trap might saturate but never is expected to vanish as the irradiation dose increases. The experimental observation of the removal of low temperature TL glow peaks with increasing F center concentrations can not be fit into earlier models for the reasons just stated. However the observed features (49,50) fit well into the model proposed by Ausin and Alvarez Rivas (49) in which the mobile entities for the thermoluminescence process are interstitial halogen atoms. The variation in the thermoluminescence spectrum is caused by the formation of large interstitial aggregates (51). The situation is different regarding the thermoluminescence of alkali halides doped with impurities whose valence states vary by irradiation. In this case, thermoluminescence in which the mobile entities are either electrons or holes has been observed. This view has also been invoked to explain the thermoluminescence of NaCl:Cu^{+} samples irradiated at room temperature (52,53). Recent work on the thermoluminescence of NaCl:Mn samples irradiated at room temperature has shown that the glow peaks are simultaneous with the recovery of Mn^{2+} ions and annealing stages of F-centers (54). This result has been ascribed to the simultaneous release of holes and interstitials (Cl°) trapped together somewhere in the lattice. From these considerations it is apparent that during the thermoluminescent processes in pure or impurity doped alkali halides irradiated at room temperature, the annealing of F- centers and the recovery of the initial charge state of the impurity ion can be explained by either the release of interstitials or by electron hole recombination. Both these possiblities will be important in interpreting our data on thermoluminescence and isothermal annealing experiments performed on NaCl:Cu^{-} samples.

Thermal annealing of Cu^- ions in electrolytically colored NaCl:Cu^- crystals has been observed by Tsuboi (2). He briefly examined the thermal stability of Cu^--centers by warming the crystal to a temperature more than 200°C. It was observed that when the colored crystal was warmed up to 500°C the Cu^- bands were completely annihilated whereas a band at 4.88 eV assigned to Cu^+-center was detected. The experimental results indicated that Cu^- ions were converted to the Cu^+ ions by warming the crystal up to a very high temperature near the melting point. Our work will show that Cu^+ ions can be recovered completely at a much lower temperature in x-irradiated crystals.

After presenting the required background to interpret the experimental results of the present work, the next section will describe the results of several experimentations done on NaCl:Cu^- systems aimed at understanding the process of $Cu^- \rightarrow Cu^+$ conversion.

Experimental Results

Optical Absorption

The optical absorption spectrum of NaCl:Cu^+ (0.05 mole percent of CuCl in the melt) as measured by a Perkin Elmer model 330 spectrophotometer is shown in Figure 17. The spectrum shows a broad band formed at 4.88 eV (254 nm) due to the presence of substitutional Cu^+ ions in the crystal. When the photon energy exceeds 5.20 eV, the spectrum shows monotonic increase in the optical density till 185 nm. The thickness of the sample was ~ 0.03 cm and taking the oscillator strength of the absorption as 0.020 at room temperature, it was estimated using Smakula's equation that the concentration of Cu^+ ions was about 10^{16} per cm^3.

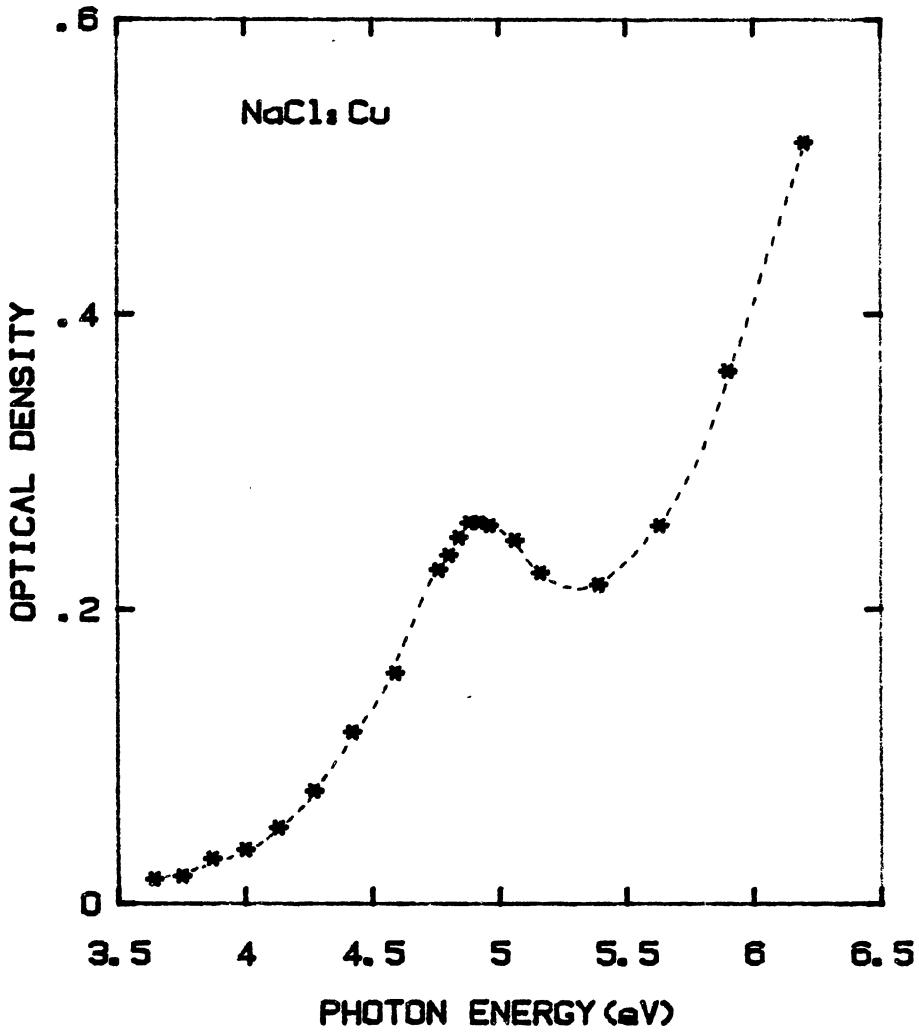

Figure 17. Optical Absorption Spectrum of NaCl:Cu^{+} at 295K

The NaCl:Cu^+ samples were x-irradiated in the VDG set up (discussed in Chapter III, Section VII) for 10 minutes at room temperature. An estimate for radiation dose received by the sample at room temparture was obtained by comparing the absorption coefficients at the peak of the F-band (460 nm) of two samples of pure NaCl in which one sample was irradiated in the VDG set up for one minute and the other was exposed to ^{60}Co γ cell (γ cell dose ~ 21 x 10^3 Rad/hour) for one hour. Figure 18 shows the absorption spectrum of these samples of NaCl. The absorption coefficient at 460 nm of the sample x-irradiated in VDG set up was 26.02 cm^{-1} while the absorption coefficient (at 460 nm) was found to 5.30 cm^{-1} for the other sample exposed to the γ cell for one hour. From this information the dose received by the sample in VDG set-up for 10 minutes irradiation at room temperature was calcualted to be ~ 6 M Rad. The growth curve of x-irradiated NaCl:Cu is shown in Figure 19 where it is shown that the optical density of 5.3 eV band due to Cu^- centers does not show appreciable change after 10 minutes of irradiation and this was the time chosen for subsequent irradiation of NaCl:Cu crystals.

Figure 20 shows the absorption spectrum of NaCl:Cu, x-irradiated at room temperature which shows bands at 4.24 (292 nm), 4.246 (278 nm), 4.80 (258 nm) and 5.30 (234 nm) eV all of which have been assigned due to Cu^--centers formed in the crystal after irradiation. An off scale F-band (F-band in NaCl:Cu peaks at 460 nm as observed during irradiation for less time) and a smaller M-band (peaking at 725 nm) were also detected. The 4.88 eV band present in the "as received" sample can no longer be detected in x-irradiated samples, showing that Cu^+ ions have been converted into Cu^- centers during the irradiation. Among the Cu^- bands detected, the band at 5.34 eV had the maximum intensity. In all

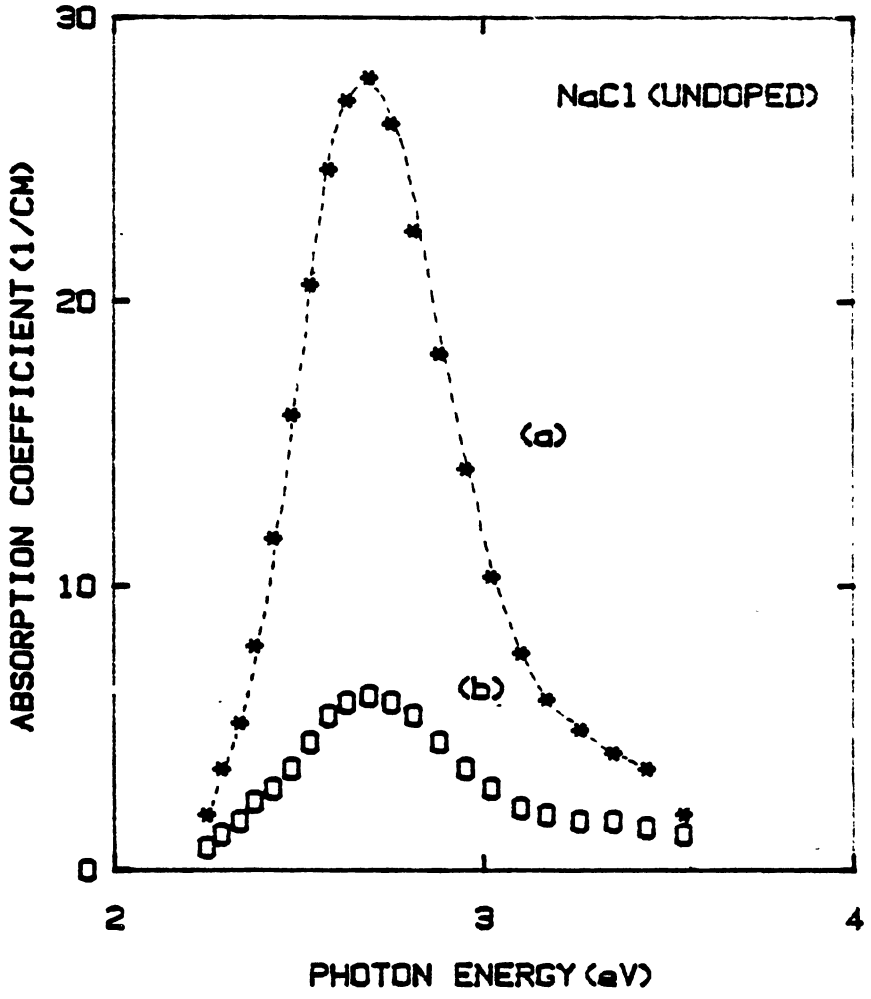

Figure 18. Optical Absorption Spectrum (RT) of (a) an Updoped NaCl Crystal Irradiated in the VDG Set-up for 1 minute (b) an Updoped NaCl Crystal Irradiated in the γ Cell for 1 Hour

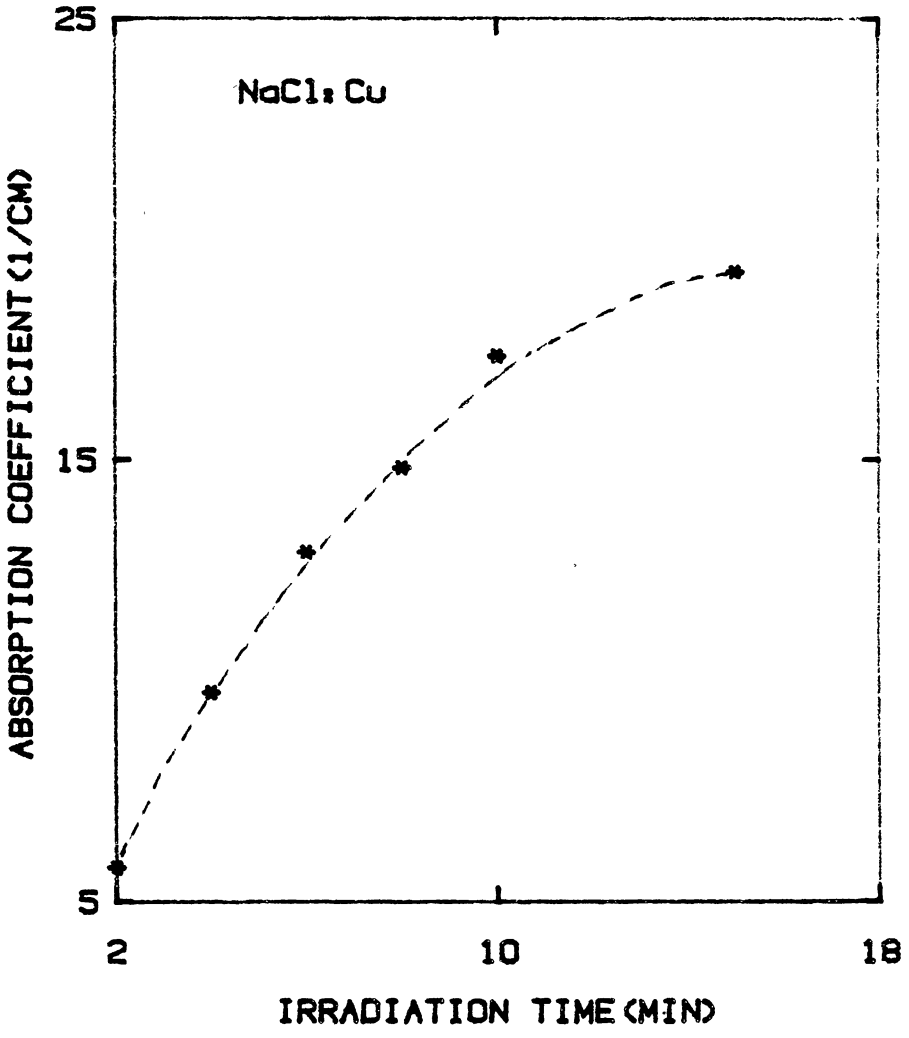

Figure 19. Growth Curve of Cu^- Centers in x-Irradiated NaCl:Cu

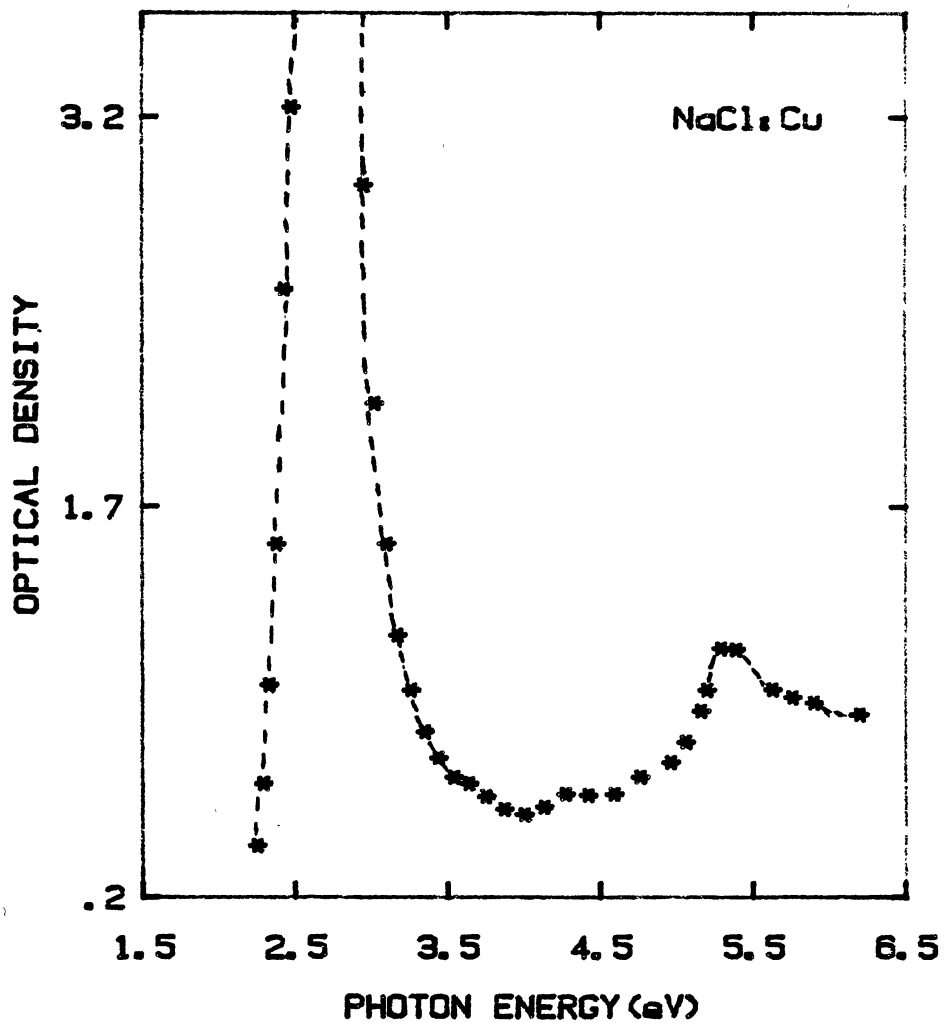

Figure 20. Absorption Spectrum of NaCl:Cu x-irradiated at Room Temperature with a Dose of ∿ 6 MRad

the subsequent experiments regarding the absorption of Cu^- ions, the optical density of the band at 5.30 eV was used as a measure of Cu^- ion concentration in the crystal. In order to find the correlation between Cu^- and F-centers, optical bleaching experiments were perfomed. Figure 21 shows the absorption spectrum of an x-irradiated sample which has been bleached by F-light (λ = 460 nm) for one hour. The F-band peaking at 460 nm is not present in the bleached sample indicating that most of the F centers produced during irradiation have been destroyed. Figure 21 also shows that the intensities of the 5.30 and 2.92 eV bands (due to Cu^- centers) have increased by about 20% due to the optical bleaching.

The thermal stability of Cu^- centers was investigated by isochronal anneal experiments. In this experiment the sample was heated to the desired temperature for ten minutes, quickly quenched back to room temperature and absorption spectra were taken. Two sets of samples were used. In both cases the samples were x-irradiated, but for one set only, the samples were subsequently bleached with F-light for one hour to remove the F-centers. The concentration of Cu^- centers in the sample without any F-centers showed a decrease as the temperature was increased, Figure 22. Till 80°C the decrease was slow and after 100°C Cu^- centers were destroyed at a much faster rate and at 160°C all the Cu^- centers were annealed completely. The growth of Cu^+ bands as monitored from the absorption coefficient at 4.88 eV is also shown in Figure 22, where it is seen that Cu^+ band reappeared at 180°C. By 220°C full recovery of the Cu^+ ions was achieved. Heating the sample at temperatures greater than 220°C did not produce any change in the Cu^+ band. Annealing of Cu^- centers in the sample containing F-centers is also shown in Figure 22. In this case the concentration of Cu^- centers

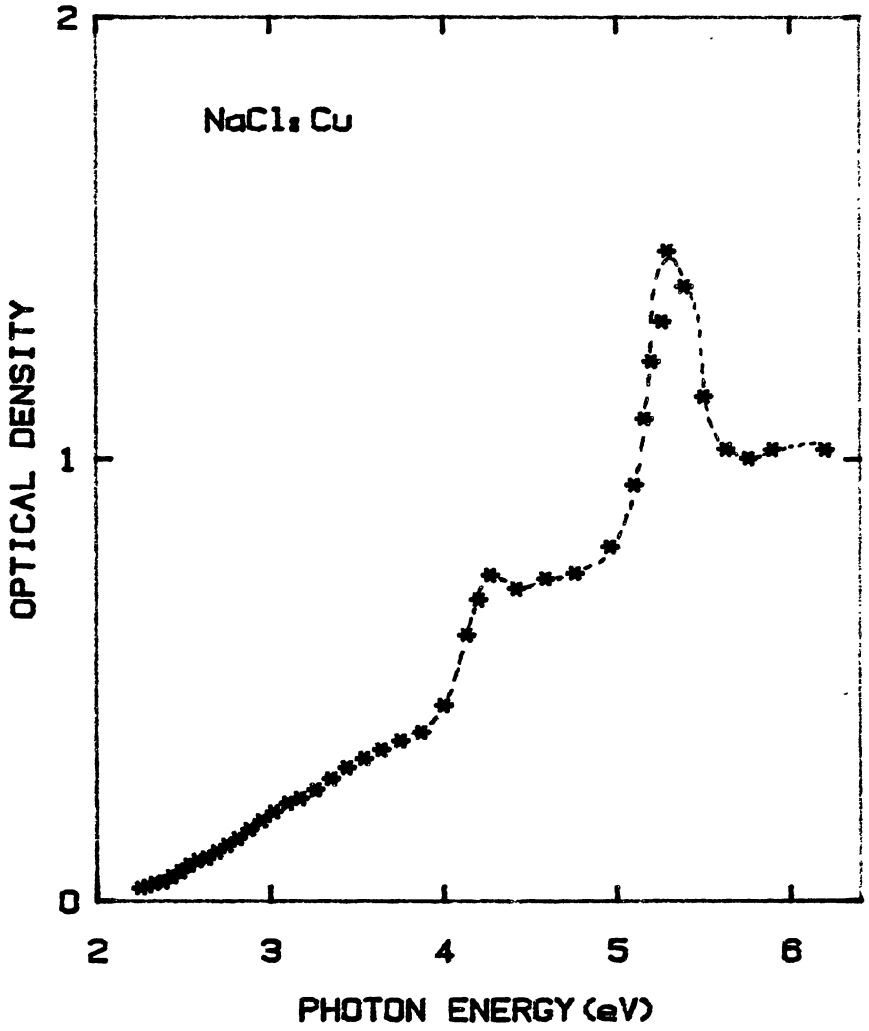

Figure 21. Absorption Spectrum of NaCl:Cu x-irradiated for 10 Minutes and Bleached with F-light (λ=460 nm) for One Hour at Room Temperature

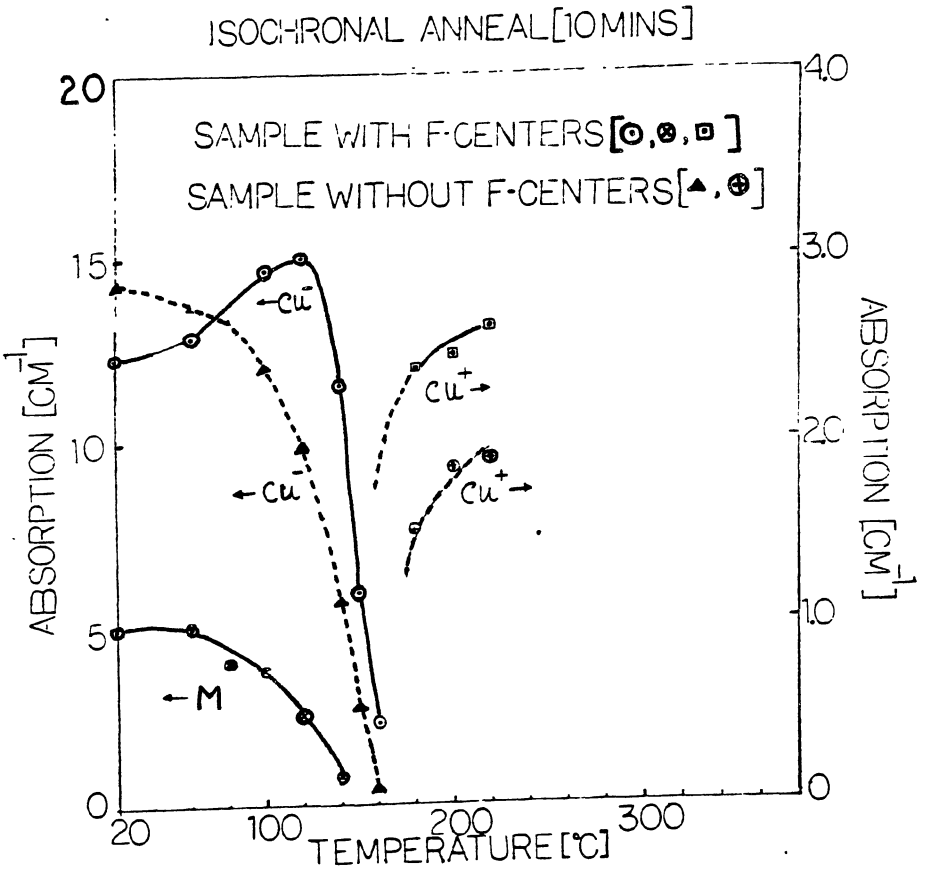

Figure 22. Isochronal Anneal Curves of Irradiated and F-Bleached NaCl:Cu Crsytals. Decay of Cu^- and M Bands are Shown in the Left Hand Side of the Diagram While the Growth of Cu^+ Bands are Shown in the Right Hand Side

increased until 120°C after which it showed a rapid decrease in Cu^- concentration so that by 160° C almost all the Cu^- centers were destroyed. Thermal annealing of M-centers (aggregate of two F-centers produced by prolonged irradiation) is also shown in Figure 22. After 60°C the concentration of M-centers showed a rapid decrease and by 120°C, were fully destroyed. F-centers were observed to be annealed completely near 150°C. An interesting point to note is that in the temperature range between 80° and 120°C where the F-and M-center concentrations showed a rapid decrease, a corresponding increase in the Cu^- centers was observed.

Isothermal anneal experiments were performed to investigate the kinetics of the thermal decay of Cu^- ions. As can be seen from Figure 22, the concentration of Cu^- ions decreases sharply between 140° and 150°C. Temperatures selected for isothermal anneal experiments were 138, 140, 142 and 146°C which fall near this temperature range. Much attention was paid to the measurement of the sample temperature during these experiments. The sample was placed on the base plate of the cryostat finger and the top cover plate was bolted down to the base plate so that the sample was tightly secured between these two plates during thermal annealing. A copper versus constantan thermocouple which measured the crystal temperature was attached to the back of the sample holder. To ensure that the temperature indicated by the thermocouple was close to the temperature of the crystal, in a special experiment, the readings of two thermocouples, one attached to the back of the base plate and the other attached directly to the crystal surface, were compared. The difference between the two readings was observed to be less than ±0.02°C. In a typical experiment the sample was heated to the

desired temperatureand the absorption of Cu^- ions was observed as a function of time. The decrease in Cu^- ion concentration was observed (by noting the absorption coefficient at 5.3 eV Cu^- band) during each scan and the scans were continued till the Cu^- ions were annealed completely. It took more than one hour for the Cu^- ions to be annealed completely for the anneal temperatures at 138°, 140°C and 142°C while at 146°C the Cu^- ions were destroyed by 20 minutes. Figure 23 shows the absorption spectrum of NaCl:Cu^- (F-bleached) sample at t = 0 minute and Figure 24 shows the spectrum of the same sample at t = 90 minutes, the anneal temperature being 142°C. In Figure 23, Cu^- band at 5.30 eV can be clearly seen while in Figure 24 this Cu^- band is not present. The later spectrum shows an increasing background. Cu^+ band at 254 nm does not appear in the spectrum at t = 90 minutes (T = 142°C) and no other absorption bands were observed to grow during the anneal process. Figure 25 shows the absorption spectrum of the same sample which has been heated at 142°C for 90 minutes and then reheated to 200°C. The presence of 4.88 eV band shows the preirradiation state of the crystal (compare with Figure 17). The absorption spectra of the samples annealed at 130°, 140°, and 146°C show similar behavior in the sense that after the complete annealing of Cu^- centers, the Cu^+ band did not reappear and subsequent heating at higher temperatures was needed for the recovery of Cu^+ ions.

In order to analyse the thermal decay of Cu^- ions it was necessary to plot the intensity of 5.30 eV Cu^- band as a function of anneal time for each of the anneal temperatures. Due to the presence of a sloping background and an accompanying shoulder near 4.84 eV the optical density of 5.30 eV band was subtracted from the sloping background and the data

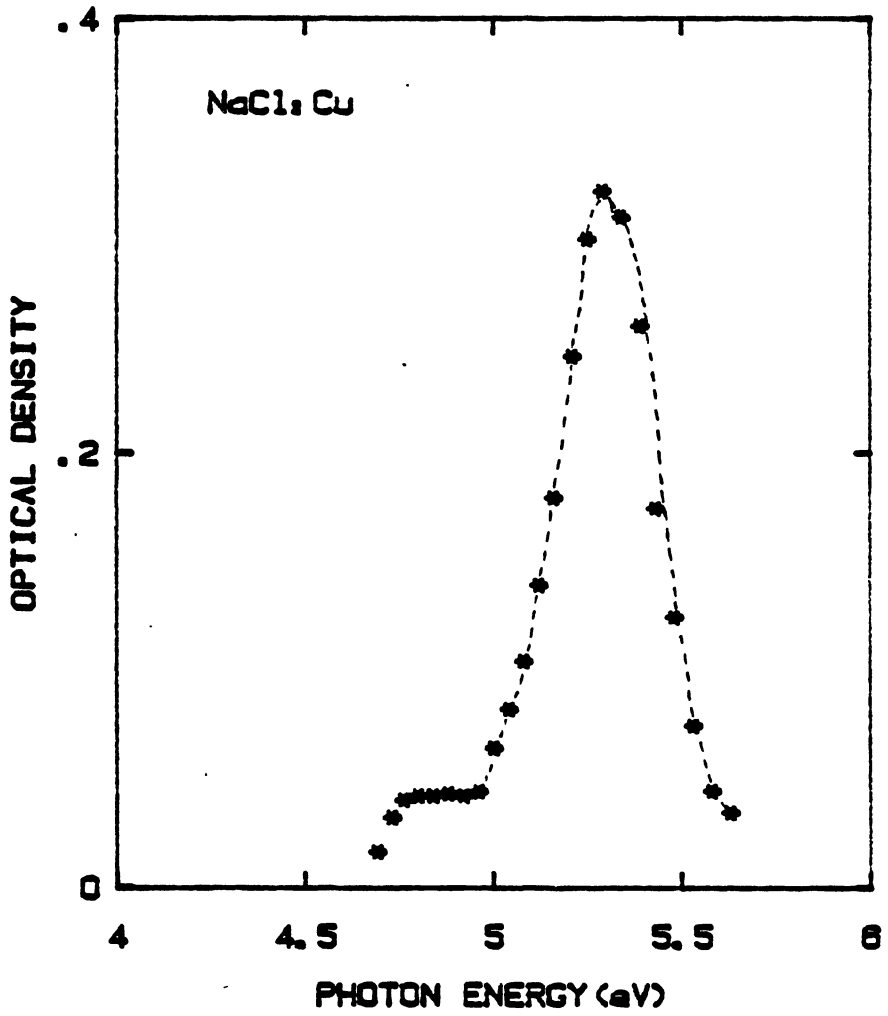

Figure 23. Absorption Spectrum of Irradiated NaCl:Cu at the Beginning of Isothermal Anneal at 142°C, (T = 142°C, t = 0 Minute)

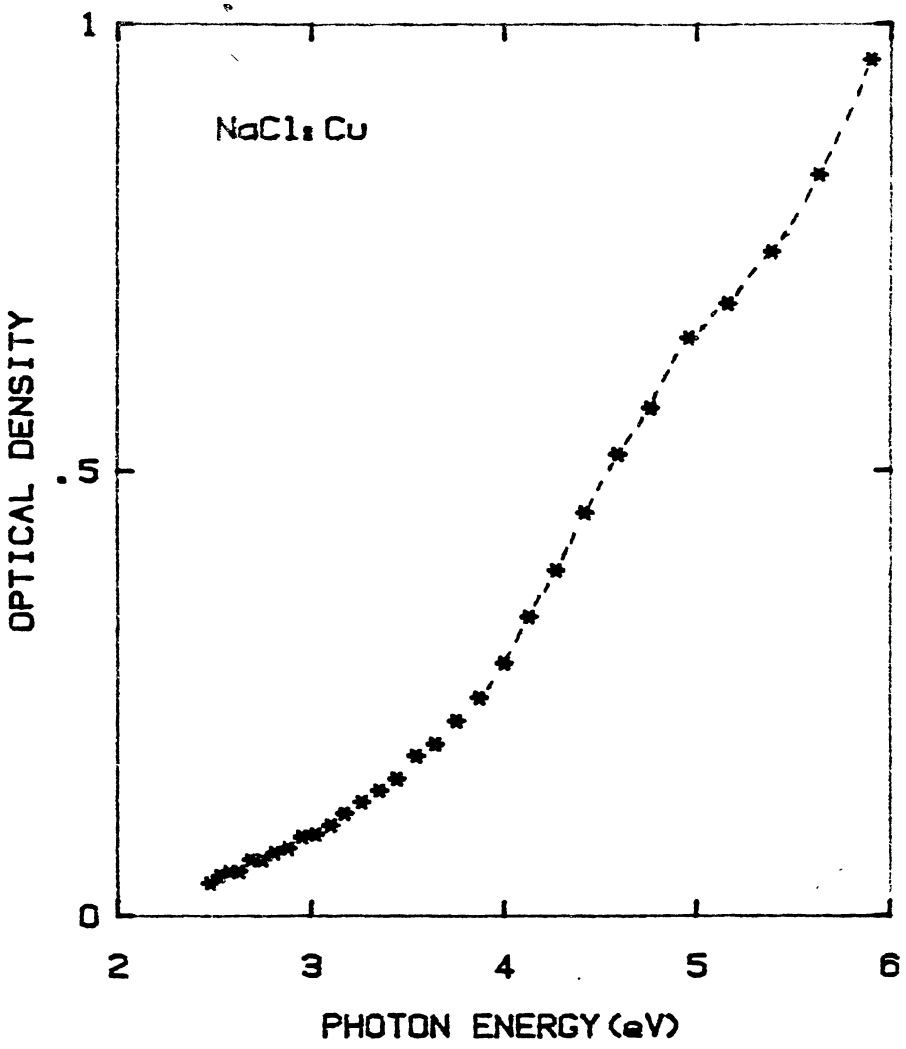

Figure 24. Absorption Spectrum of Irradiated NaCl:Cu Annealed at 142°C for 90 Minutes (T=142°C, t=90 Minutes) During Isothermal Anneal Experiments

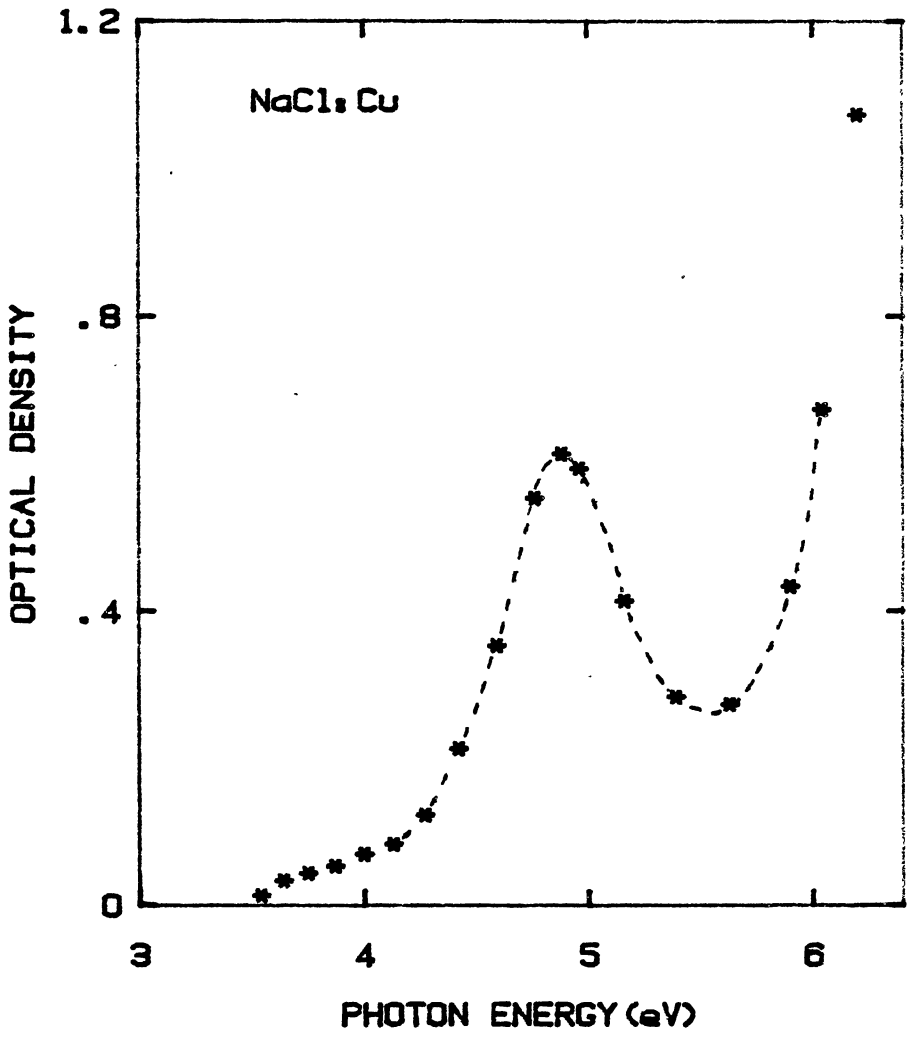

Figure 25. Absorption Spectrum of NaCl:Cu Annealed at 142°C for 90 Minutes, Quenched to Room Temperature and Annealed at 200°C for 10 Minutes

points obtained from the resulting curve (between 300-200 nm) showed two Gaussian shaped bands at 5.30 eV and ~ 4.84 eV, the intensity of the 5.3 eV peak being much larger than that at ~ 4.84 eV. The experimental data points were then fitted to a double gaussian curve in obtaining the "true" intensity of the Cu^- band at 5.30 eV. A PDP 11/10 minicomputer was used for the fitting of the data points. The function used to do this was,

$$I = K_1 \exp\{-2.772 \left(\frac{E_1 - E}{H_1}\right)^2\} + K_2 \exp\{-2.772 \left(\frac{E_2 - E}{H_2}\right)^2\}, \qquad (52)$$

where K_1 and K_2 are the heights at the band peaks, H_1 and H_2 the half widths, and E_1 and E_2 the photon energies at the peak heights for the 5.3 and 4.84 eV bands respectively. E is the energy parameter and I is the absorption intensity. The program used is a Fortran library program on the University's IBM-370 computer. It uses their Patrn (OSU computer center classification) search routine and does a linear least squares fit. Figure 26 shows such a fit to the data points at t = 140°C, t = 36 minutes, where the solid line is the computer fit and the circles are the data points. Since the band-width of the 5.3 eV Cu^- band did not change appreciably with the anneal times at a particular anneal temperature, the peak height (computer fitted) at 5.3 eV band was taken as a measure of Cu^- concentration. Isothermal anneal curves for the four temperatures are shown in Figure 27. The rate of decay for T = 146°C is shown to be fastest as expected. In all the curves it is seen that there is an early transient decay which is approximately exponential. This is followed by a non-exponential decay at longer times.

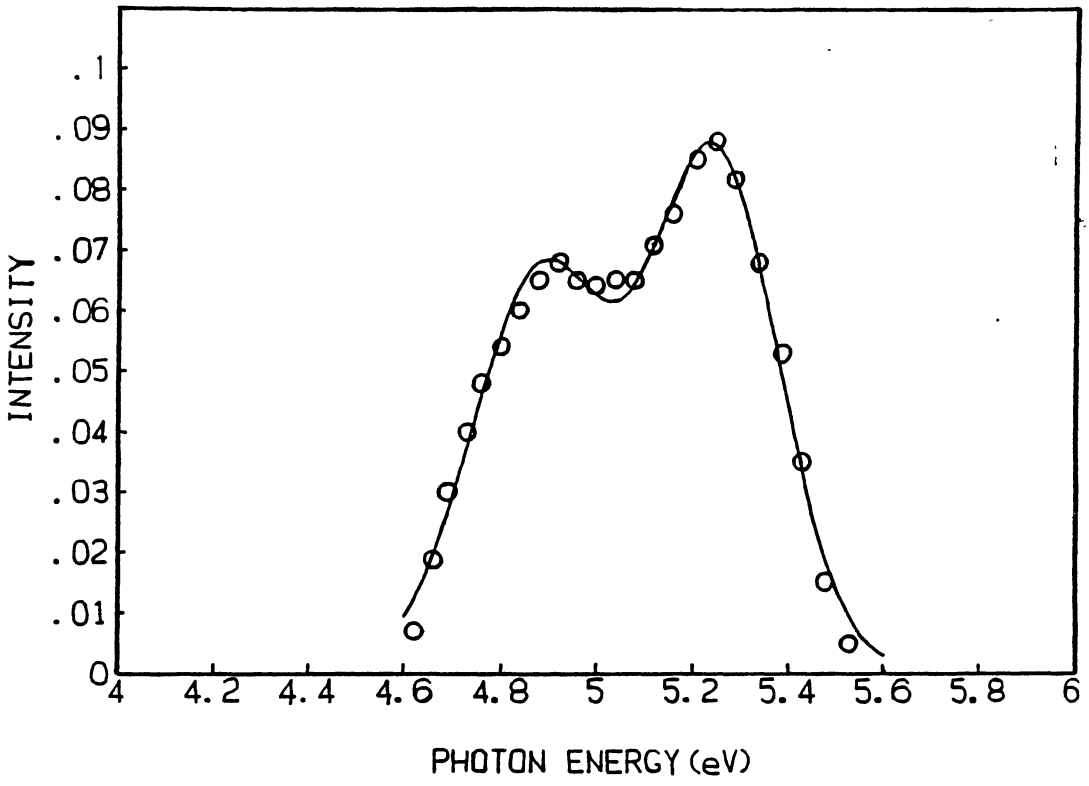

Figure 26. Gaussian Fit to the Data Points of NaCl:Cu^- Absorption at T = 140°C, t = 36 Minutes

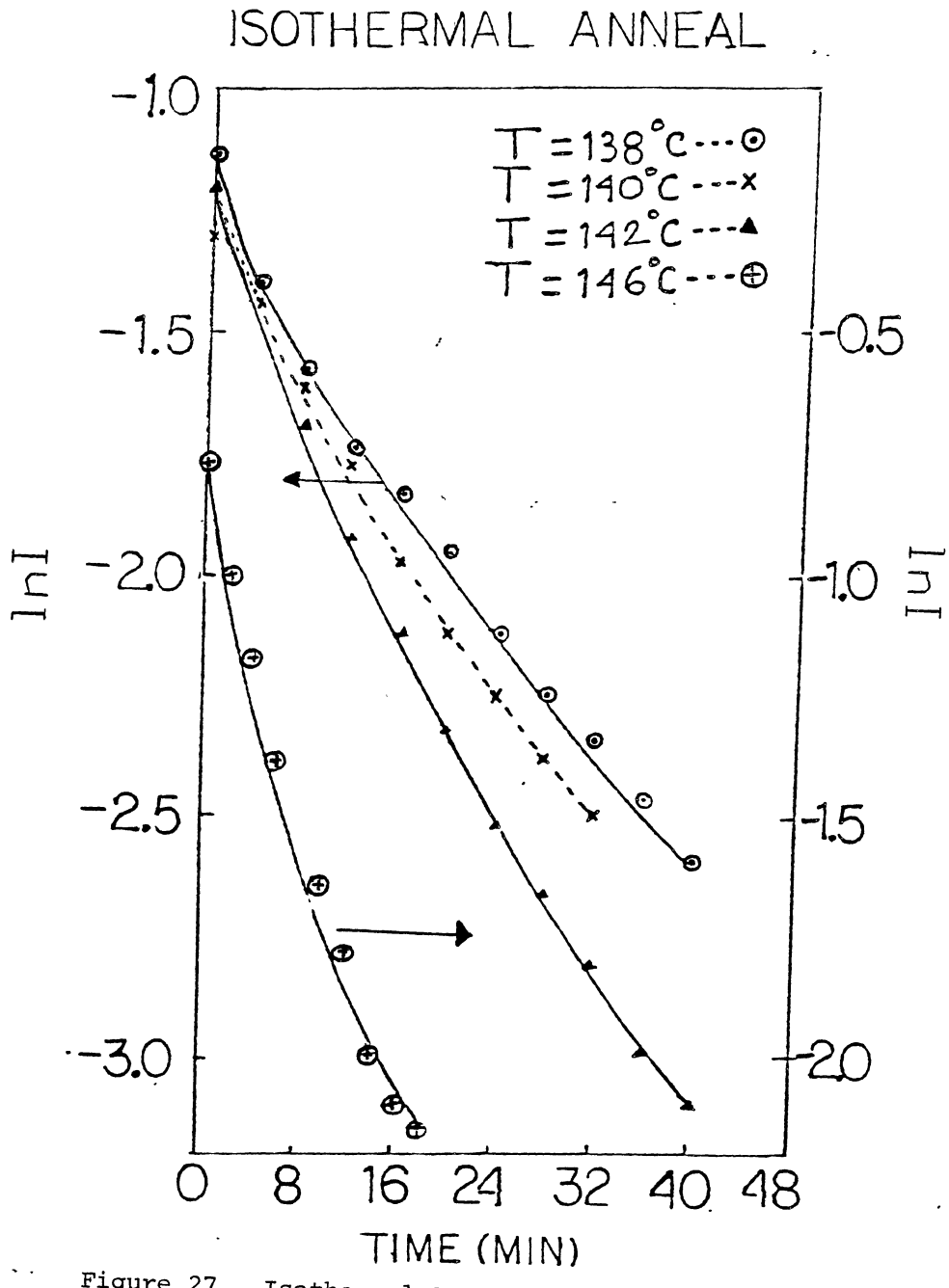

Figure 27. Isothermal Anneal Curves of NaCl:Cu⁻

Analysis of the Isothermal Decay Curves

The isothermal decay curves for Cu^- ions were analysed to gain information about the nature of the decay kinetics (i.e.whether first, second order, etc.).

For a first order process, the rate equation for Cu^- ion decay can be written,

$$-\frac{d[N]}{dt} = K_1[N], \tag{53}$$

where [N] = cencentration of Cu^- ions and K_1 = constant. Integrating Equation (51) yields

$$[N] = [N_o]e^{-K_1 t}$$

or

$$\ln[N] = \ln[N_o] - K_1 t, \tag{54}$$

where $[N_o]$ is the concentration of Cu^- ions at t=0. From Equation (54), plot of ln[N] versus anneal time should yield a straight line. Figure 27 shows such a plot from which it is seen that the thermal decay of Cu^- ions does not obey a first order kinetics.

For a second order process, the rate equation governing the decay of Cu^- centers can be written as (56),

$$-\frac{d[N]}{dt} = K_2[N]^2 \tag{55}$$

(55) gives after integration

$$\frac{1}{[N]} - \frac{1}{[N]_o} = K_2 t. \tag{56}$$

The temperature dependence of K_2 is given by

$$K_2 = K_2^{\circ} \exp\left(-\frac{\Delta E}{k_B T}\right), \tag{57}$$

where ΔE = thermal activation energy for the process.

K_2° = constant,

k_B = Boltzmann's constant.

Graphs of A^{-1} (A = absorption coefficient at 5.3 eV Cu^- band) against time of anneal 't' were found to be linear (Figures 28,29 and 30). Since A = C[N], where C is a constant of proportionality, the decay of the Cu^- ions is shown to be second order (bimolecular) over the measured temperature region.

A plot of $\ln K_2$ against $\frac{10^3}{T}$ was also found to be linear (Figure 31) giving the thermal activation energy for the process. From the slope of $\ln K_2$ against $\frac{10^3}{T}$ graph, the activation energy was calculated to be 0.80 ± 0.05 eV.

Thermoluminescence

The role of thermoluminescence experiments in obtaining information regarding the annealing of radiation induced defects has been described in the Introduction . In an attempt to clarify the mechanism which governs the process by which NaCl:Cu^- crystals are brought back to the preirradiation state, TL experiments were perfomed on x-irradiated

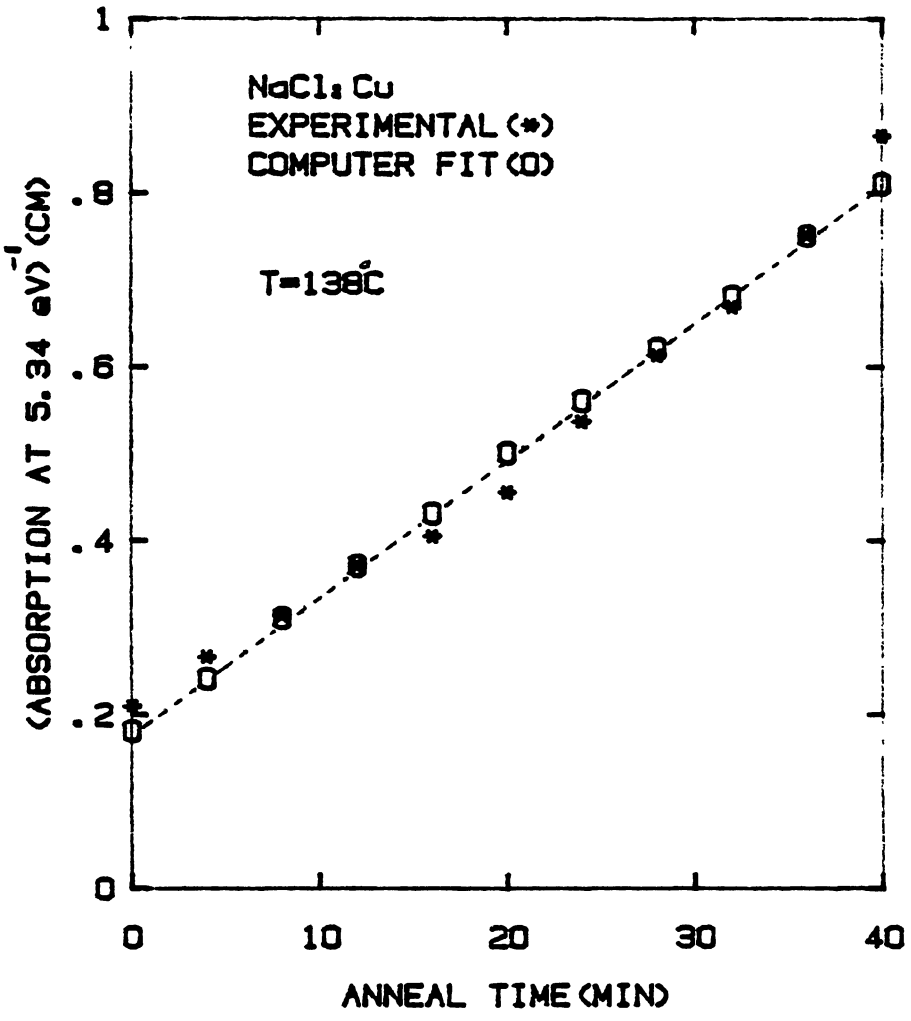

Figure 28. Plot of A^{-1} Versus Anneal Time, t. The Sample was Annealed at 138°C

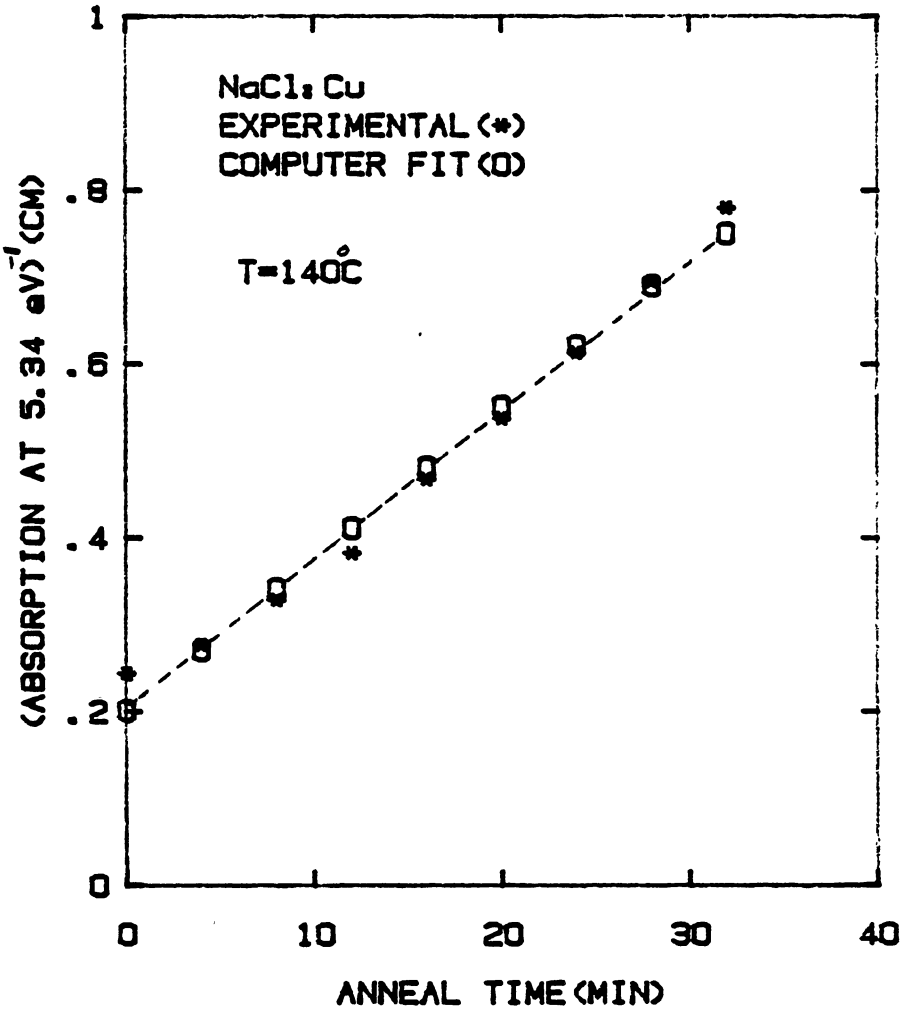

Figure 29. Plot of A^{-1} Versus Anneal Time, t. The Sample was Annealed at 140°C

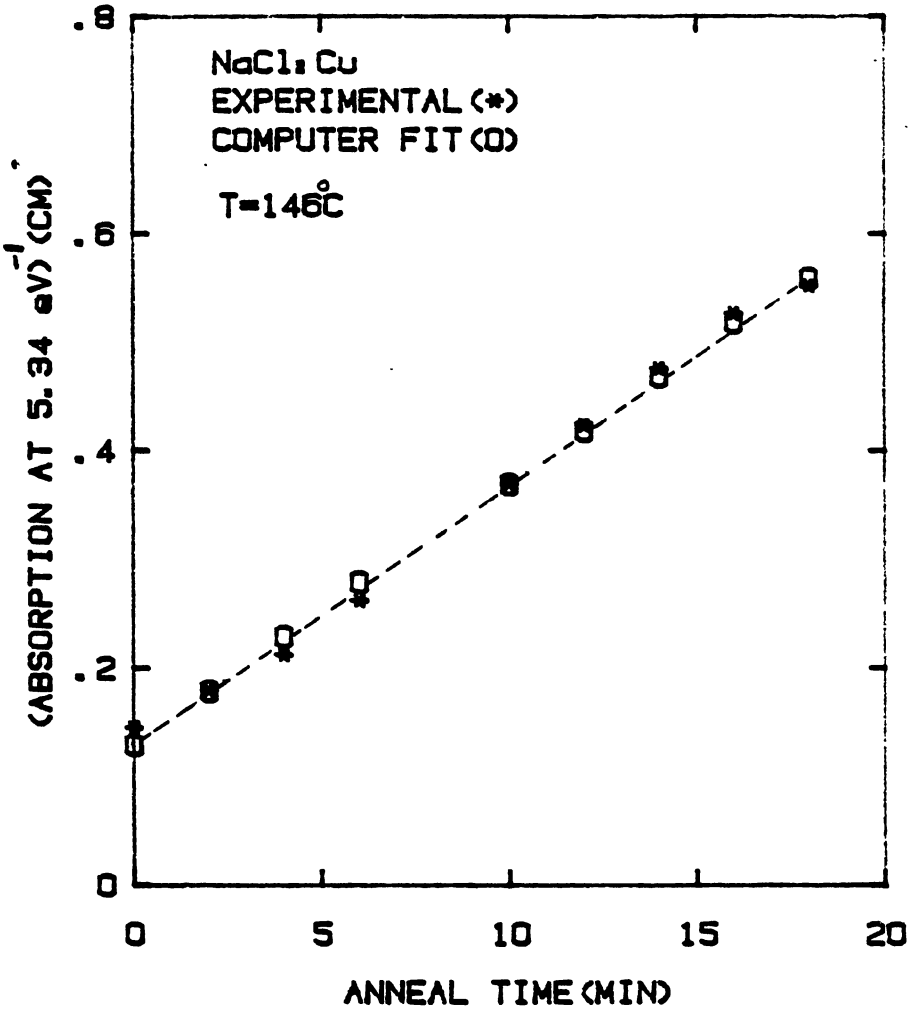

Figure 30. Plot of A^{-1} Versus Anneal Time, t. The Sample was Annealed at 146°C

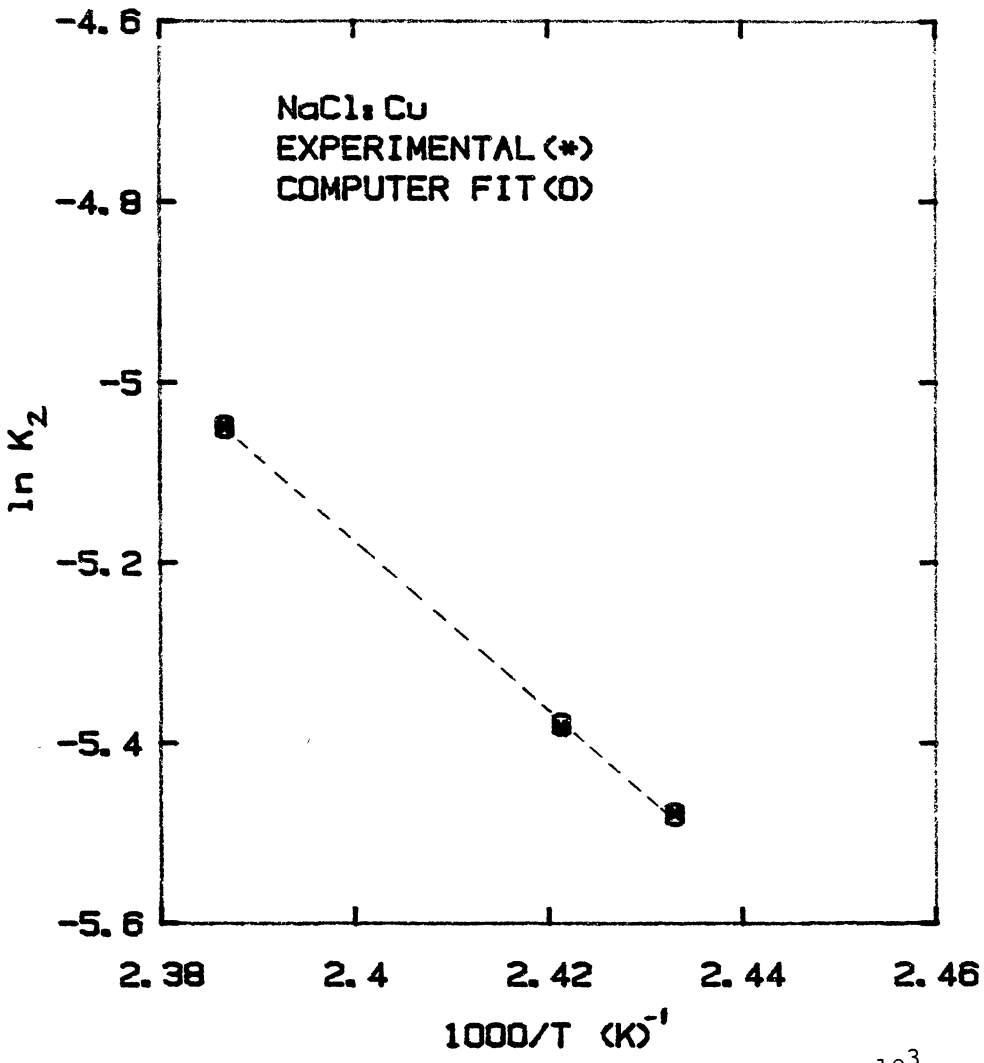

Figure 31. Plot of $\ln K_2$ Versus Inverse Temperature, $\frac{10^3}{T}$

NaCl:Cu^- crystals with and without (F-bleached) F-centers. TL experiments were performed in the temperature range 25° - 500°C with a linear heating rate of the sample. The TL glow curve of NaCl:Cu sample containing F-centers is shown in Figure 32. A small peak at 80°C is present but the main TL peak is at ~ 165°C. Figure 33 shows the TL glow curve of NaCl:Cu^- after irradiation and F-bleaching. Intensities of the TL peaks observed are about an order of magnitude smaller than those observed in samples containing F-centers. Figure 33 shows the main TL peak at 162°C, with a shoulder near 125°C which is not present in TL spectrum of the sample containing F-centers (Figure 32). A small peak near 250°C is also detected in the F-bleached sample.

The spectral dependence of the light emitted at each TL glow peak plays an important role in knowing the nature of the defect being annealed. The spectral dependence of the 165°C peak in samples containing F-centers was measured for this purpose. The temperature corre-sponding to the TL peak was obtained quickly by rapid heating of the sample and once the desired temperature was obtained, the light given off by the sample was scanned quickly, the temperature being kept constant at the temperature of the peak. Figure 34 shows the spectral dependence of 165°C TL peak in the sample containing F-centers. The spectrum consisted of a single gaussian shaped peak at 360 nm with no other bands observed in the range 300-500 nm. An attempt was made to investigate the spectral dependence of 162 and 125°C peaks in F-bleached samples, but due to the extremely small intensity of the light emitted from the sample (compare the vertical scales in Figure 32 and Figure 33) no bands could be detected at 125°C glow peak. TL peak at 162°C showed a very weak band peaking at 360 nm.

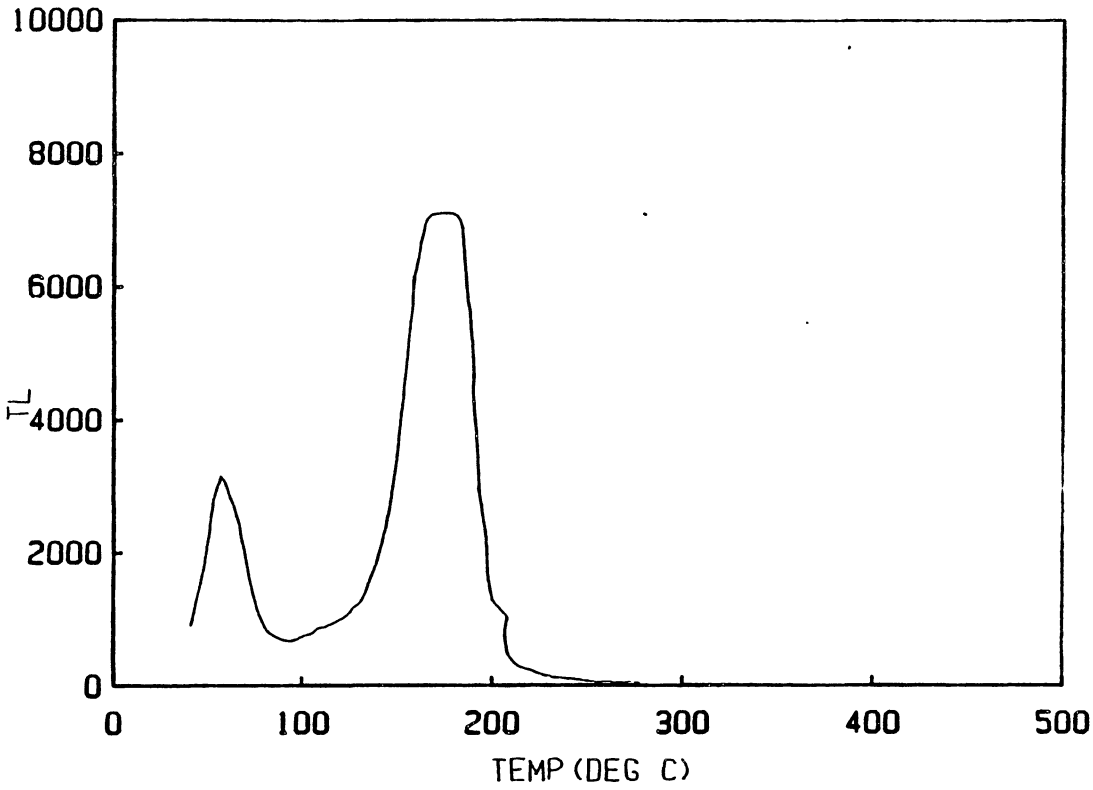

Figure 32. Thermoluminescence Spectrum (50°C - 500°C) of NaCl:Cu^- x-irradiated at Room Temerature for 10 minutes

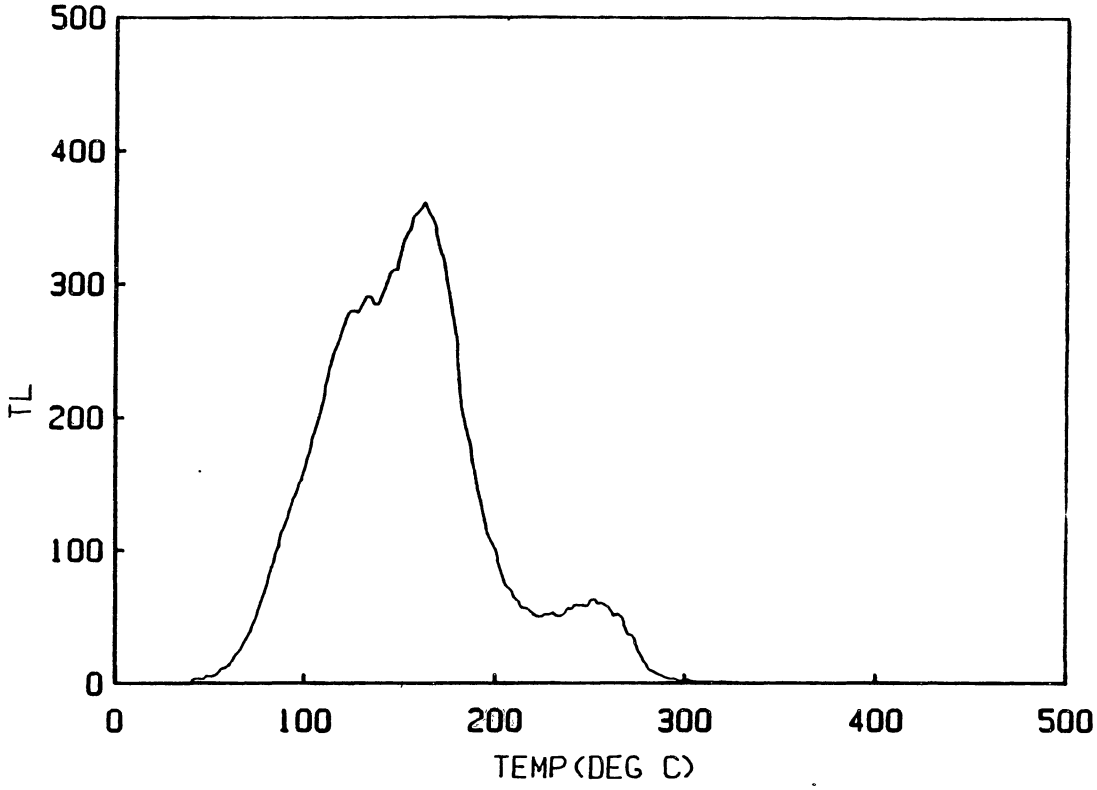

Figure 33. Thermoluminescence Spectrum (50°C-500°C) of NaCl:Cu^- x-irradiated at Room Temperature and Bleached with F-light for One Hour

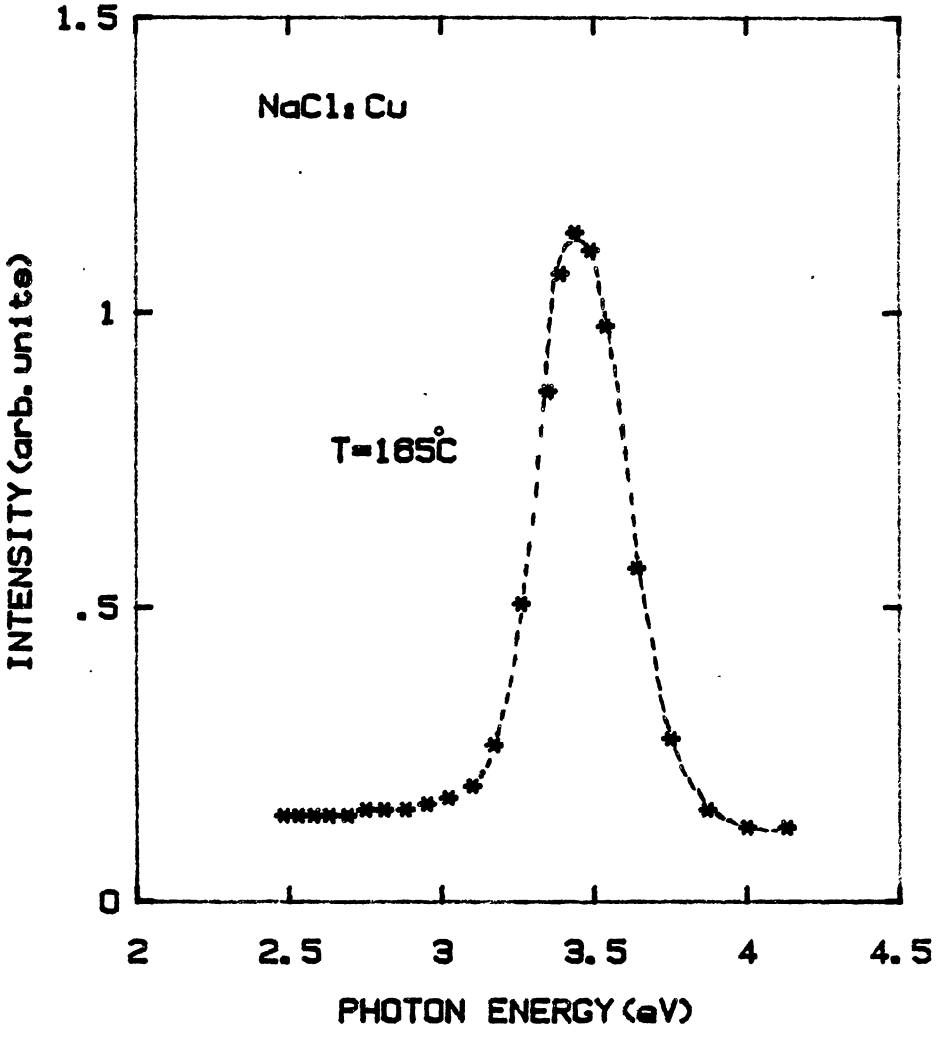

Figure 34. Spectral Dependence of 165°C TL Peak in x-Irradiated NaCl:Cu

Discussion

From the experimental results presented in Section II, it is seen that prior to thermal anneal and optical bleaching experiments, the sample contains Cu^-- and F-centers. When the irradiated sample is bleached with F-light, most of the F-centers are destroyed and an increase in the intensity of the Cu^- absorption bands is observed. This observation can be interpreted as follows: although during the irradiation most of the Cu^+- centers are converted to Cu^--centers, the interconversion process is not complete, i.e, after irradiation, in addition to the Cu^-- centers at anion sites, the crystal also contains Cu^o atoms [Cu^o_F-center according to Melinkov et al. (25)] located at cation sites close to an anion vacancy. When the sample is bleached with F - light, electrons released from F-centers are trapped by Cu^o_F- centers forming Cu^--centers, and accordingly, increase in intensity of the Cu^- absorption band is detected. This process also produces anion vacancies in the crystal. Similar correlation between the Cu^- and F bands is also observed during isochronal anneal experiments. It is seen that when the irradiated and bleached NaCl:Cu crystal is heated above room temperature, an increase in the Cu^- absorption bands is detected until 120°C, after which the absorption due to Cu^- centers decreases sharply, with the major annealing step occuring around 150°C. In unbleached irradiated samples, Cu^--centers are stable up to 120°C, but in this temperature range quick thermal decay of F-centers has been observed. Like F-centers, M-centers also decayed rapidly in this temperature range. These observations suggest that electrons from thermally excited F-(and M) centers are captured by Cu^o,

thereby increasing the Cu^- absorption. As the temperature exceeds 120°C, Cu^-- centers become thermally unstable and a corresponding decrease in the Cu^- absorption intensity is observed. During isochronal experiments on NaCl:Cu samples which have been x-irradiated and bleached with F-light, such an increase is not observed. This indicates that electrons released from F-centers due to thermal excitation are probably responsible for the initial increase in Cu^- absorption in irradiated samples seen near 120°C. Similar effects have been observed by Tsuboi (55) in electrolytically colored NaCl:Cu samples. In colored crystals, Tsuboi (55) observed that after F-bleaching, or warming the crystals to 200°C, there was an increase in the Cu^- absorption. However in electrolytically colored samples, the release of electrons from F-centers and its subsequent trapping by Cu° occurs at a much higher temperature (200°C) indicating that Cu^-- and F-centers are more stable in electrolytically colored samples than in x-irradiated crystals. Though the end products in both electrolytically colored and x-irradiated NaCl:Cu^+ crystals are the same, namely Cu^- and F- centers, the mechanisms of production differ. In x-irradiated sample large concentration of chlorine interstitials are present which seem to play an important role in the less thermal stability of these defects.

Thermoluminescnece experiments show the presence of a peak at 160°C. In irradiated crystals, a TL peak very close to this is observed in samples which have been bleached with F-light. The TL peak in bleached samples has much less intensity than that is observed in samples containing F-centers. Isochronal and isothermal anneal experiments have shown that the main annealing steps of Cu^-- and F-centers occur close to the temperature of the glow peak. This result

suggests that the glow peak near 160°C detected in irradiated and F-bleached samples corresponds to the annealing of Cu^- and F-centers. Isochronal anneal experiments show that at or above 160°C, Cu^- centers are thermally destroyed in samples with and without F-centers. F-centers are also observed to be annealed completely near 150°C. The detected glow peak occurs near 160°C thereby suggesting its origin to the recombination processes which are triggered by the same initial thermally activated process. The spectral dependence of the 165°C glow peak in samples containing F-centers is peaked at 365 nm. Delgado et al. (3) in their detailed investigation of thermoluminescent processes involved in NaCl:Cu^- crystals irradiated at different doses at room temperature have also observed the same 365 nm band in all the Tl glow peaks below 200°C. The 365 nm band has been assigned by a recent model (48,49) to be due to recombination of chlorine interstitials with F-centers. An alternative model (45,46) also exists where the annealing of F-centers has been described by the release of trapped holes at the temperature of the glow peak and its subsequent reombination with F-centers. Delgado et al. (3) have also detected an emission at 445 nm in the glow peak near 147°C where 365 nm band is also present. The 445 nm band was assigned by them to be due to the recombination of V_K centers with Cu^- ions. In samples used in this present study, a 445 nm band at the temperature of Tl glow peak was not detected. In F-bleached samples the 365 nm band could be barely detected. This result strongly suggests that 365 nm band is caused by the annealing of F-centers. The greatly reduced intensity of the 365 nm band in the F-bleached sample is explained by the substantial decrease in F-center concentration. If the 365 nm band is due to the recombination of interstitial chlorine atoms

with the F- centers then the same release of chlorine interstitials should also account for the recovery of Cu^+ ions since, at this temperature of the glow peak, Cu^- ions are also annealed and Cu^+ band observed to grow at this temperature. The role played by interstitial chlorine ions in the recovery of Cu^- ions seems uncertain at this point. We suggest that the annealing of F- and Cu^-- centers and the recovery of Cu^+ ions are due to the release of trapped holes at the temperature of the glow peak. The recombination of the trapped hole with the F-centers induces the 365 nm band while the appearance of Cu^+ band can be explained by the capture of these holes by Cu° and Cu^- ions. An interesting feature of this result is that the hole center captured by Cu° or Cu^- ions should be the same recombining with F-centers in order to explain satisfactorily the same TL peak responsible for the annealing of both the Cu^-- and F-centers.

It is observed that during isothermal anneal experiments carried out for extended times, the absorption due to Cu^+ ion does not occur even if all the Cu^- centers are destroyed. Absorption due to Cu^+ ions starts growing near 160°C as discussed in the earlier paragraph. At temperatures below 160°C, $Cu^- \rightarrow Cu^+$ conversion is not observed. Thus the recovery of Cu^+ ion seems to be at least a two stage process, these two stages being characterized by temperatures above and below 160°C. At and above 160°C, Cu^--centers are annihilated and converted back to Cu^+. Below 160°C where the thermal decay of Cu^-- centers could be measured, no growth in the Cu^+ ion concentration could be observed. Conversion of Cu^- to Cu° seems to be a likely mechanism in this stage. Cu° atoms in NaCl are known to give rise to two absorption bands in the vicinities of 3.76 and 3.26 eV (53). These bands in thermally annealed

samples used in the present work were not detected, but could have been masked by the background absorption.

The decay kinetics of Cu^- decay is shown to be approximately bimolecular (non first order). Thus there is no correlation between the trapping (due to impurities) and the recombining centers. The bimolecular decay kinetics indicates that during the heating of the samples, holes are randomly released from the impurity sites and combine with Cu^--centers elsewhere in the sample.

Thus it is shown in the present work that: (i) correlation between F- and Cu^-- centers exists in the sense that transfer of electrons between these two centers can occur by thermal and optical excitations; (ii) annealing of F-and Cu^- centers occurs at the same glow peak; (iii) recovery of Cu^+ ions after heating the irradiated crystals is a two-stage process; (iv) annealing of Cu^-- and F-centers may be due to the release of trapped holes; (v) radiation induced defects (Cu^- and F-centers) are thermally more stable in x-irradiated samples than in electrolytically colored samples; (vi) The decay kinetics of Cu^- centers is a non-first order (bimolecular) process with an estimated activation energy of 0.80 ± 0.05 eV.

CHAPTER V

$MgAl_2O_4$

Introduction

This chapter is concerned with the study of luminescence and photoconductivity in thermochemically reduced spinel ($MgAl_2O_4$). $MgAl_2O_4$ is an oxide with complicated crystal structure, its parent oxides being MgO and Al_2O_3. Broad band emissions from simple oxides such as MgO and CaO have been detected and attributed due to the luminescence of F-type centers (oxygen vacancies each of which has trapped two electrons). Such broad band emissions originating from anion vacancies in these oxides, have made them potential candidates for color center lasers. Thermochemically reduced oxides are of particular interest due to the large thermal stability of these defect centers. The purpose of the present work is to investigate whether emissions due to F-type centers are also present in complex oxides such as $MgAl_2O_4$.

With a melting point of 2135°C, $MgAl_2O_4$ is in many respects quite similar to alkaline earth oxides. However, its structure is more complicated giving rise to a greater variety of possible point defects. $MgAl_2O_4$ is a compound of MgO and Al_2O_3 and Table V shows some of the physical characteristics of the crystal.

The crystal structure of $MgAl_2O_4$ is shown in Figure 35, and Figure 36 shows the symmetry of the individual crystal elements. The magnesium ions are divalent with tetrahedral symmetry while the aluminum ions are trivalent with octahedral symmetry. The oxygen ions are divalent and

TABLE V

PHYSICAL CHARACTERISTICS OF $MgAl_2O_4$

	Al_2O_3	$MgAl_2O_4$	MgO
Resistivity (OHM CM)	10^{16}	10^{15}	10^{14}
T_{melt} (°C)	2045	2135	2800
Symmetry	HEX.	CUB.	CUB.
Band Edge (eV)	8.3	7.7	7.8
Index of Refraction	1.76	1.72	1.73
Hardness	9	7.5 - 8.0	6

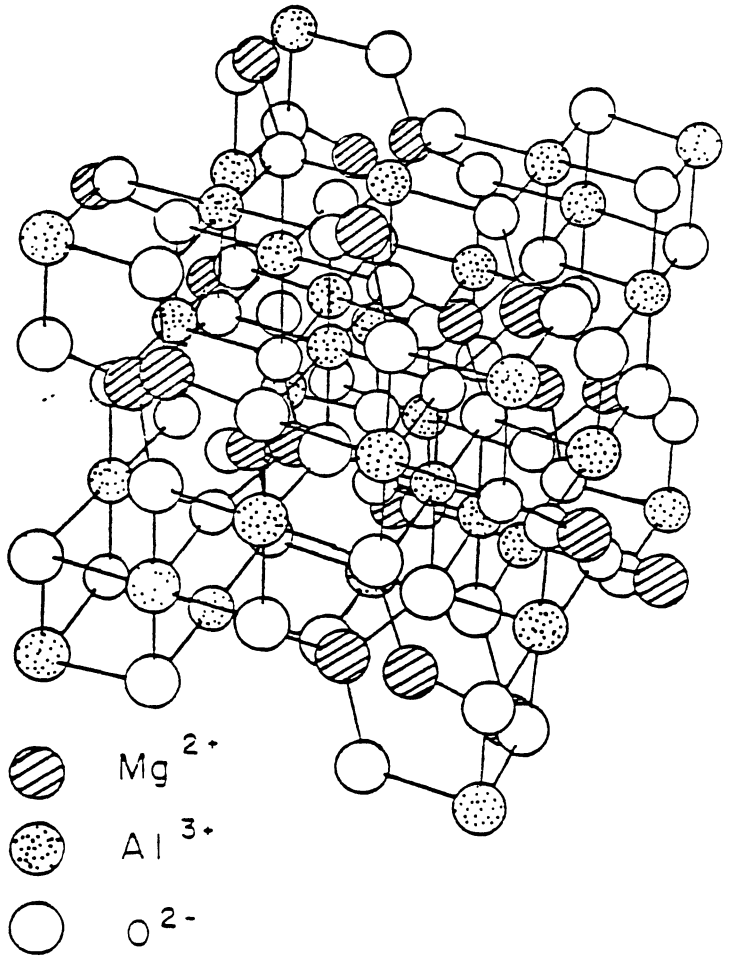

Figure 35. Crystal Structure of $MgAl_2O_4$

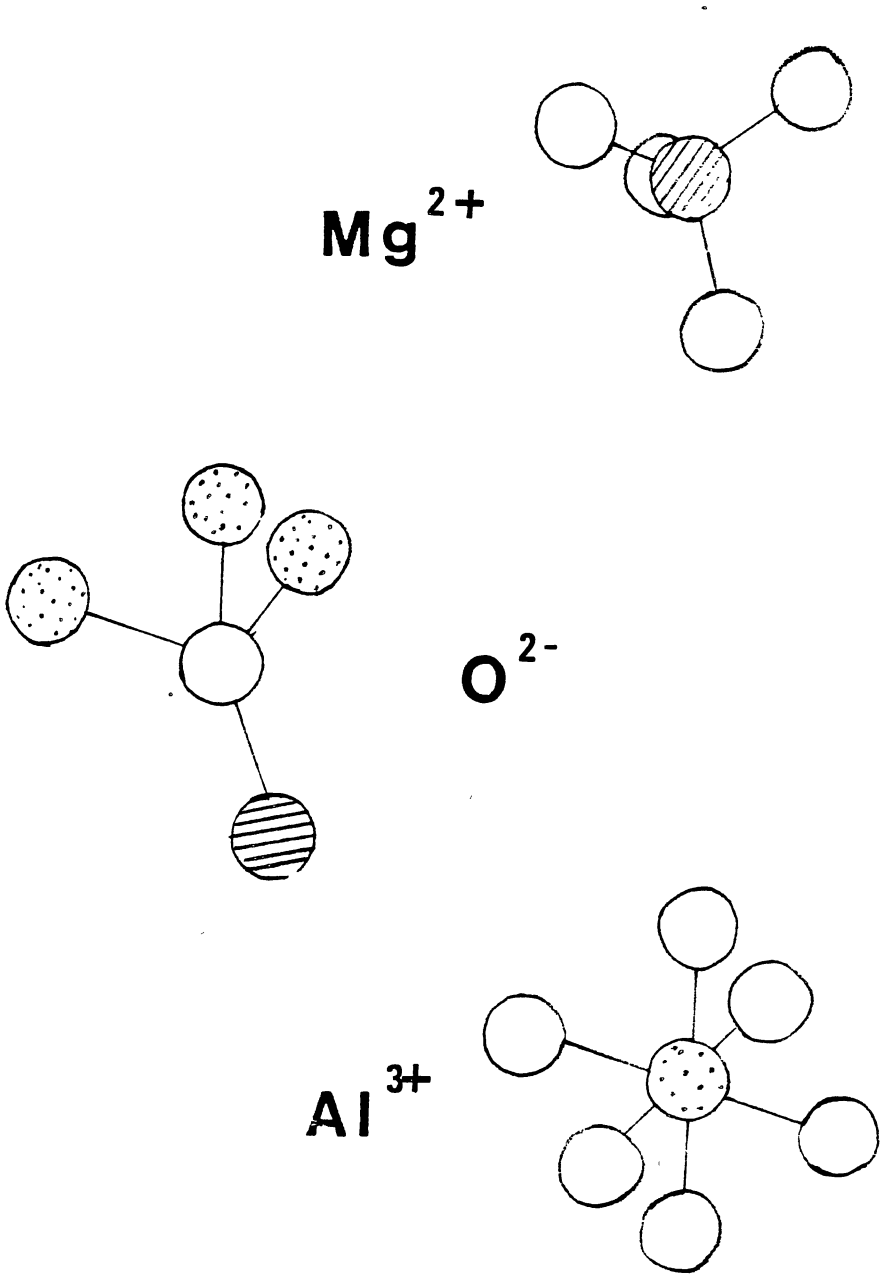

Figure 36. Symmetry of Individual Crystal Elements in $MgAl_2O_4$

are shared by one Mg^{2+} and three Al^{3+} ions occupying 1/8 of the tetrahedral sites and Al^{3+} ions occupy $\frac{1}{2}$ of the available octahedral sites (58). This structure allows a much greater assortment of defects, both intrinsic and extrinsic, than does the structure of MgO or α- Al_2O_3. Spinel's relatively complex crystal structure makes the study of defects considerably more difficult than for either α-Al_2O_3 or MgO. Consequently, although much is now known about anion vacancy (F-type) centers and cation vacancy (V-type) centers in both MgO and α-Al_2O_3, relatively little is known about these centers in $MgAl_2O_4$. Part of the problem is that synthetic crystals of spinel are usually non stoichiometric and the existence of two kinds of cations with different charge states allows for many possible defect configurations, especially antisite defects. Another problem has been that the usual experimental techniques such as photoluminescence, electron spin resonance and photoconductivity have so far not proved very productive.

Defect Creation in $MgAl_2O_4$

Defects in spinel can be created by: i) irradiation with electrons having energies greater than 0.35 MeV (57); ii) irradiation with 14-MeV neutrons (4); iii) thermochemical reduction (58). Thermochemical reduction consists of heating a crystal in the vapor of its metal constituent. This process is familiar in the alkali halides in which nonstoichiometry is produced by an excess of cations. Among the alkaline earth oxides, thermochemically reduced materials are less studied, due to the high temperatures required. In this case it appears that nonstoichiometry is caused by oxygen ions migrating to the surface

and evaporating. In spinel, both magnesium and aluminum vapors can be used for the reduction process. The sample used in this present work was thermochemically reduced by Crawford's group (60) by heating close to 2000° C in an atmosphere of aluminum vapor. In order to obtain as high a vapor pressure as possible around the crystal, the aluminum was kept close to the center of the heating element.

Defect Identification in $MgAl_2O_4$

Figure 37 shows the optical absorption spectrum of $MgAl_2O_4$ irradiated with 14-MeV neutrons (4). An optical absorption band peakin at 5.3 eV (234 nm) has been assigned with some confidence to the F-center (an O^{2-} vacancy with two electrons) on the basis of a Mollwo-Ivey-type relationship (4). Optical bleaching at 5.3 eV band in electron irradiated $MgAl_2O_4$ (57) causes the 5.3 eV band to decrease while a band at 4.75 eV (261 nm) develops, which has been assigned due to the F^+-centers (an O^{2-} vacancy with one electron). A similar phtochromic effect is observed both in MgO (59) and α-Al_2O_3 (60,71) measurements. In the case of spinel, however, no photoconductivity or luminescence has so far been reported from F-centers even in thermochemically reduced samples.

The effect of x- and γ-rays on spinel has been studied in detail by Crawford's group (62,63). In particular, a careful analysis was made of possible charge trapping sites involved in thermally stimulated processes occuring above room temperature. Woosley et al. (64) have reported a comprehensive study of the photoelectric effect and photoconductivity in untreated, particle irradiated and x-irradiated spinel. They concluded that no photoconductivity could be attributed to

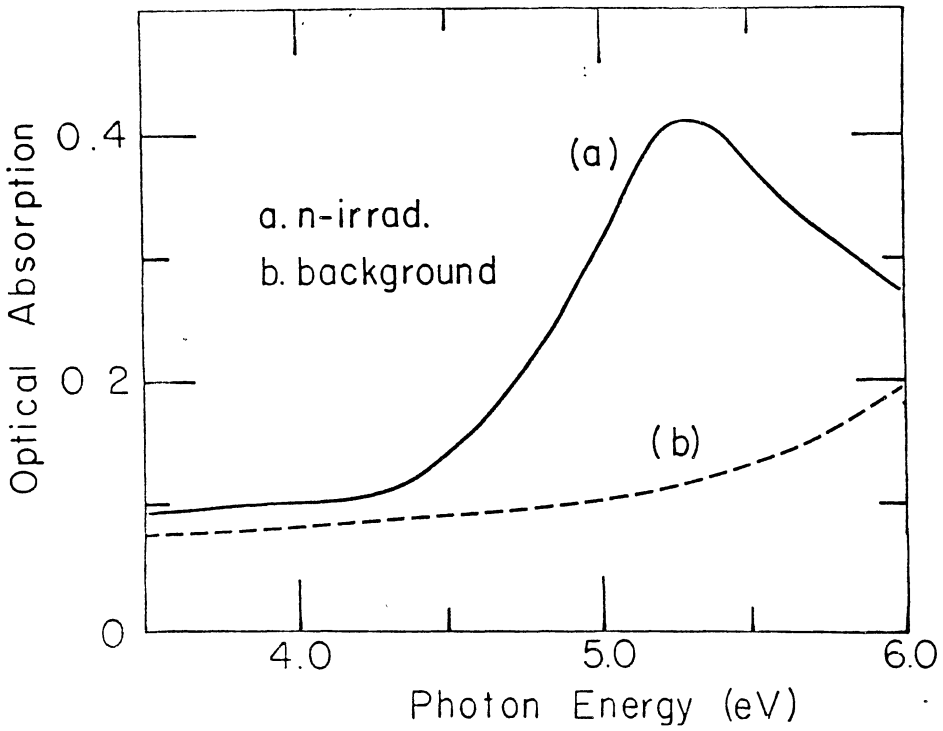

Figure 37. Optical Absorption Spectra of (a) Neutron Irradiated and (b) As Received Los Alamos Spinel. Source: G.S. White (58)

the F-center in their samples.

The anion-cation separation is comparable in spinel, α-Al_2O_3 and MgO although the F-center site symmetry is different in each material. In MgO an oxygen vacancy site has octahedral, O_h, symmetry, whereas in α-Al_2O_3 an oxygen vacancy site is surrounded by four Al^{3+} ions in C_2 symmetry. In spite of the different symmetry, F-centers in both materials have somewhat similar properties. Accordingly, there seems to be no obvious reason why the optical properties of F-centers in spinel should be significantly different from those in α-Al_2O_3 or MgO, apart from the lack of stoichiometry of the samples.

This present work investigates the photoluminescence, thermoluminescence and photoconductivity produced by optical excitation of the 5.3 eV absorption band in thermochemically reduced spinel. The measurements were made over the temperature range 80-300K. The results suggest that the F-center in spinel may luminesce and produce photoconductivity, although much less efficiently than in some other oxides.

Experimental Results

Optical Absorption

Figure 38 shows the optical absorption spectrum of thermochemically reduced spinel. An optical absorption band peaking at 5.3 eV supports Bunch's assignment (4) of this band as due to absorption by F-centers. The sample was 0.074 cm thick and had an optical density of 3.7 at 5.3 eV. Taking the oscillator strength of the F-center absorption as ~1 and the half width of the band as ~ 1 eV, the concentration of F-centers in the sample was estimated to be ~ $10^{18} cm^{-3}$ using Smakula's equation.

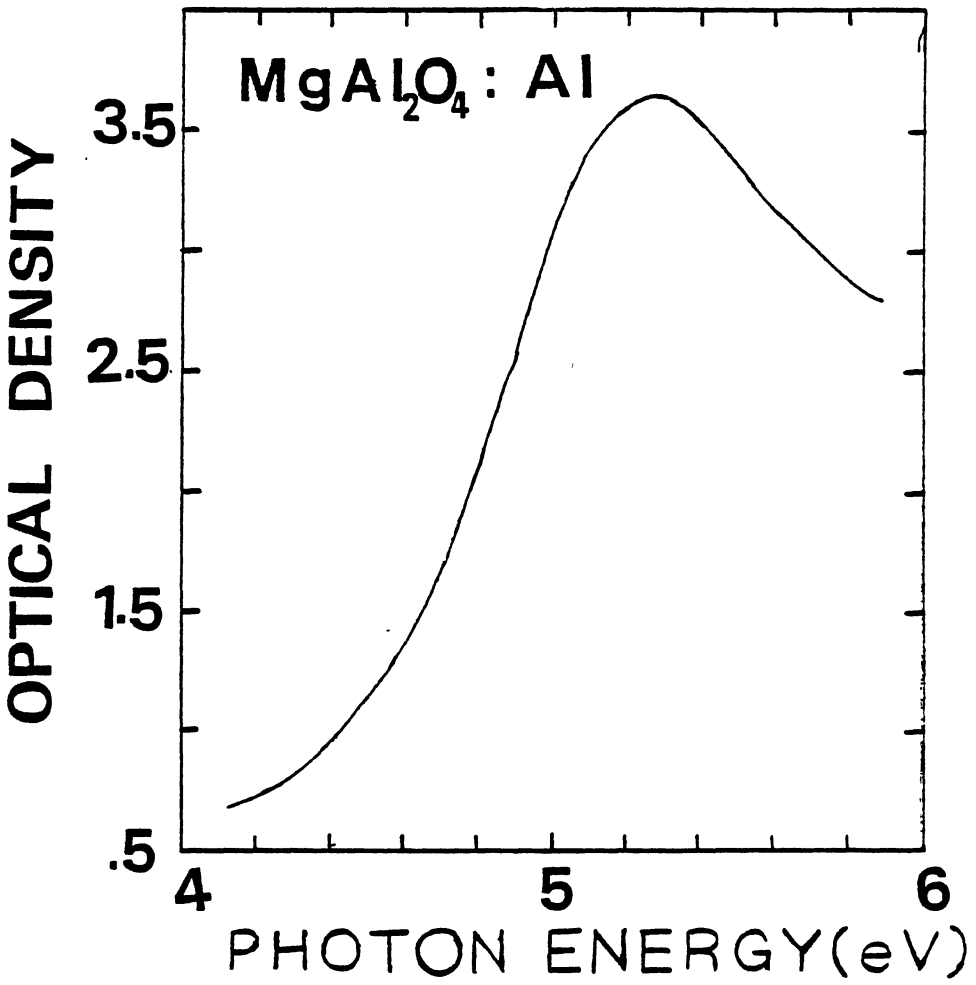

Figure 38. Optical Absorption Spectrum of Thermochemically Reduced $MgAl_2O_4$

Photoluminescence

Photoluminescence was excited using light from a 60 W Deuterium lamp used in conjunction with an interference filter with peak transmission at 225 nm. Luminescence was dispersed by a 0.8 m McPherson monochromator and detected by a thermoelectrically cooled RCA C31034 phtomultiplier tube. The luminescence band excited in thermochemically reduced $MgAl_2O_4$ is shown in Figure 39 in which the data have been corrected for the spectral dependence of the detection system. At 95K, the peak of the luminescence is at 2.69 eV (461 nm), but there is a clearly resolved shoulder at 2.95 eV (420 nm). As the temperature increased above 140K, the peak of the band shifted to lower energy and by 250K was located at 2.58 eV (480 nm). A detailed plot of the peak energy versus temperature is shown in Figure 40. The high energy side band became less clear as the temperature increased and by 250K was not resolved, Figure 39. The band became narrower as the temperature was raised, so that at 95 K the halfwidth was 0.66 eV, whereas at 250 K the half width was 0.51 eV. The relative intensity of the luminescence increased between 95 - 140 K, but then decreased again as the temperature was further raised to 300K, Figure 39.

For measuring the excitation spectra of the 2.69 eV luminescence, the light from the deuterium lamp was dispersed by the McPherson monochromator before falling on the sample. Stray light was reduced by inserting a suitable sharp cut filter before the phtomultiplier. The sample was supported in the exchange gas space of an Oxford Instruments variable temperature cryostat system. Figure 41 shows the excitation spectrum of the 2.69 eV luminescence at 160k, which is the temperature region where the luminescence intensity is maximum. Figure 41 shows

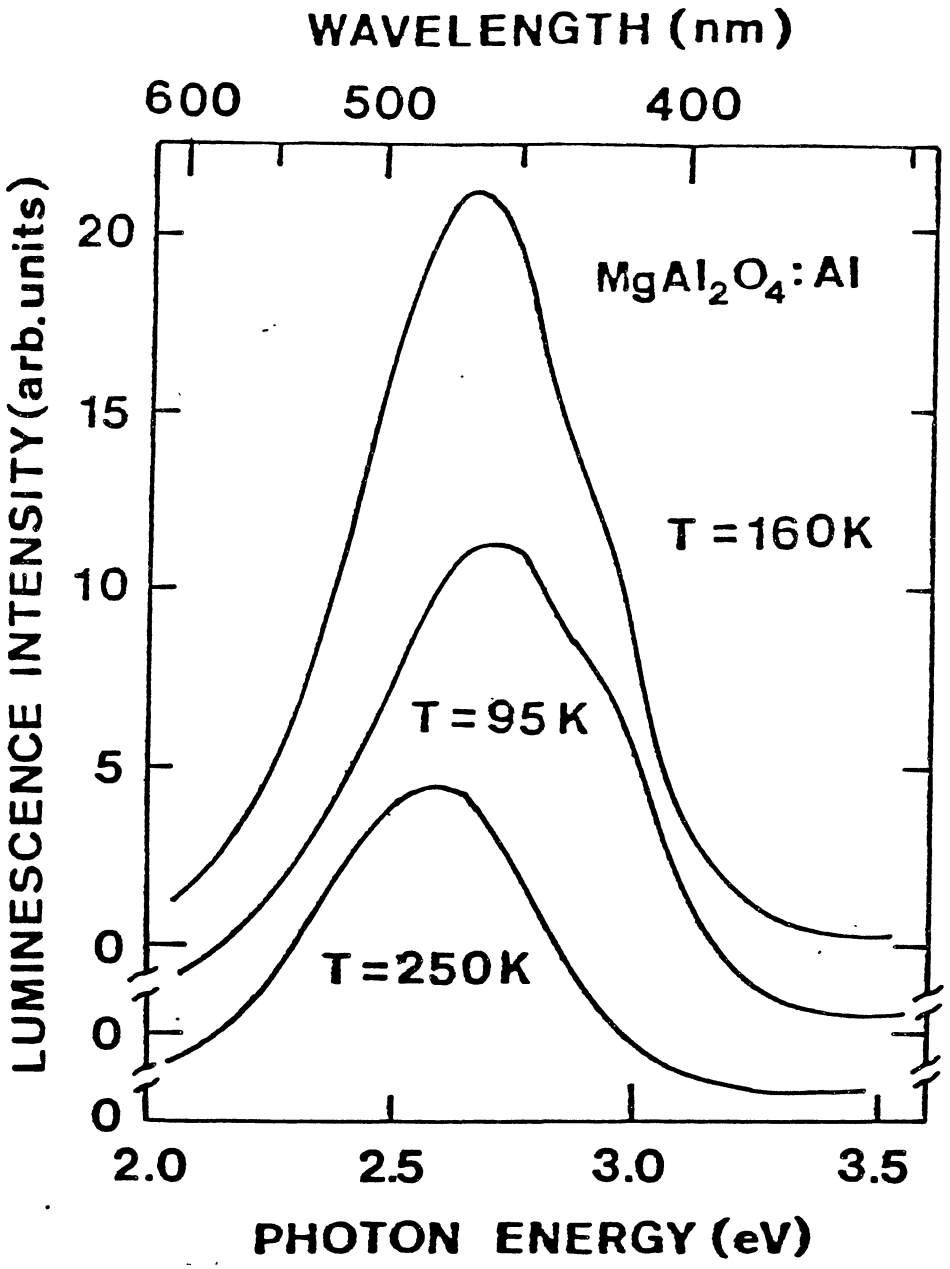

Figure 39. Photoluminescence Spectra Excited in Thermochemically Reduced $MgAl_2O_4$ by 225-nm (5.4 eV) Light

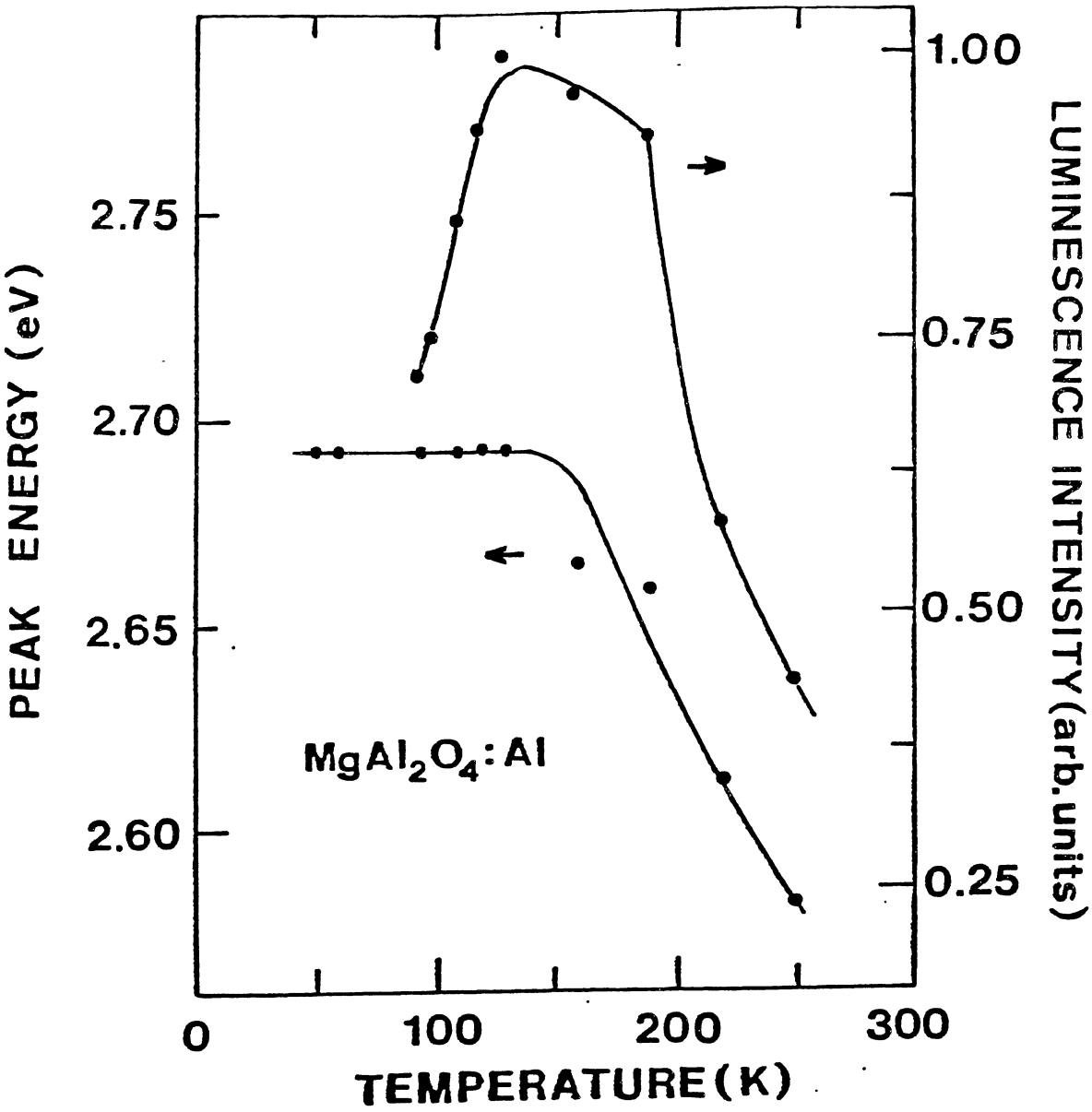

Figure 40. Peak Energy and Normalized Luminescence Intensity of the 2.69 eV Band in Thermochemically Reduced $MgAl_2O_4$ as a Function of Temperature

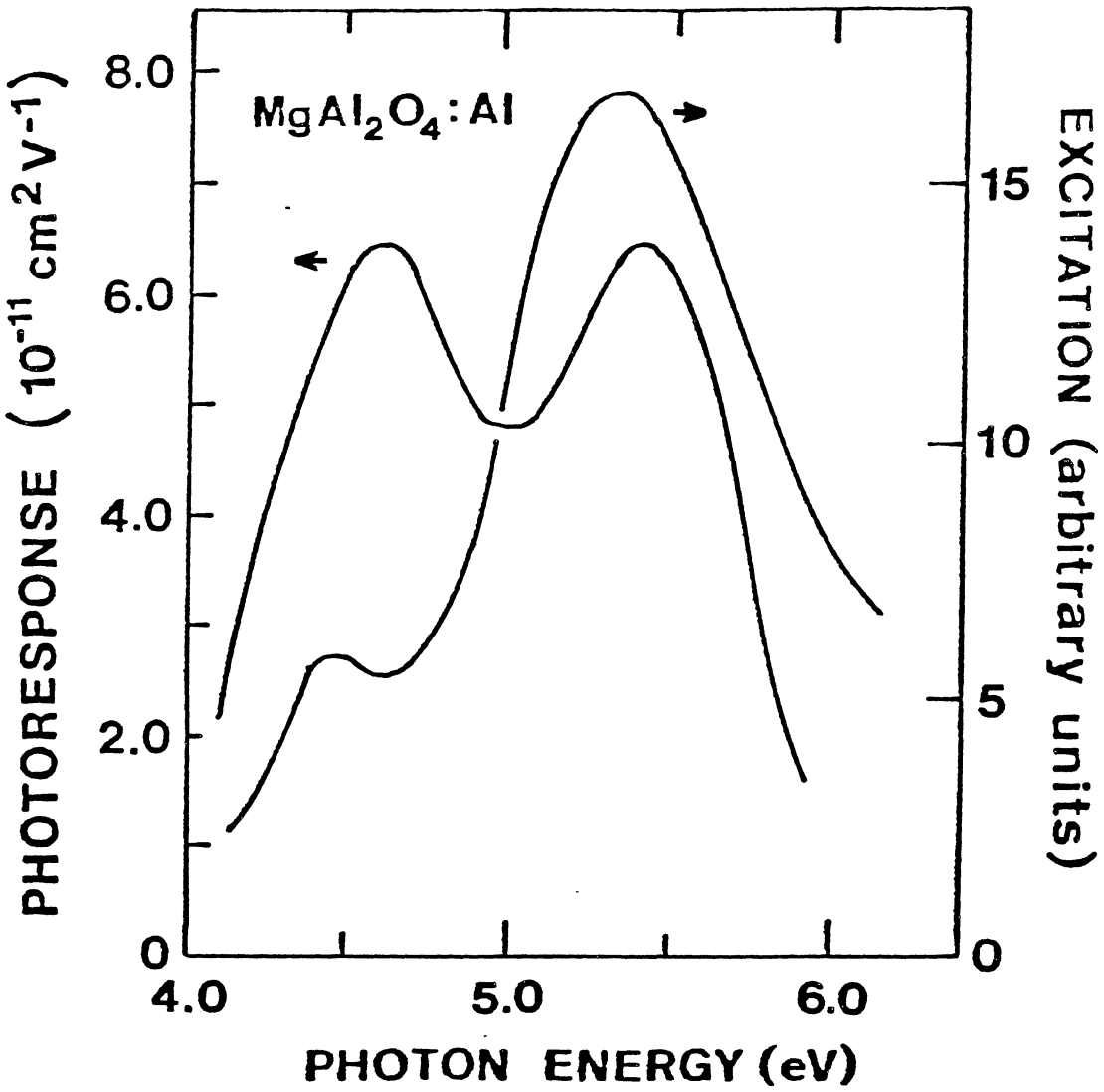

Figure 41. Excitation Spectra of the 2.69 eV Luminescence Band and the Photoresponse of Thermochemically Reduced $MgAl_2O_4$. The Photoresponse is Shown for T = 216K and the Luminescence Excitation Curve is Shown for T = 160K

that the excitation spectrum has a peak at 5.3 eV slightly skewed towards the high energy and has a halfwidth of ~ 1.0 eV. There is a small secondary secondary maximum at ~ 4.45 eV but this is only ~ 7% of the main peak. No difference was observed in the excitation spectrum for luminescence anywhere in the 2.69 eV band.

The 2.69 eV luminesence intensity decayed rapidly once the excitation was removed. The lifetime was less than ~ 1 ms, which was the time constant of the detection system. There was no evidence of the long life time observed for F-center luminescence in some samples of thermochemically reduced MgO and α-Al_2O_3 (61,65). Although the luminescence was readily detected, it was only one tenth as intense as the 2.3 eV F-center luminescence in a comparably-sized MgO sample which contained approximately the same concentration of F-centers and which was excited with the same system. The 2.69 eV band could also be excited very weakly in as-received material

Thermoluminescence

Thermoluminescence measurements were made using the same cryostat system as described earlier. In this experiment the sample was cooled to liquid nitrogen temperature, illuminated for a few minutes with unfiltered light from a deuterium lamp and then heated to room temperature at ~ 0.1 K S^{-1}. Figure 42 shows the thermoluminescence, TL, glow curve for the same sample used in the photoluminescence experiments, Figure 39. Figure 42 shows that there are TL peaks at 95K and 265K, with the latter peak considerably weaker than the first. No TL was detected from an as-received sample under similar conditions. The spectral dependence of the emission at 95K and 265K is shown in

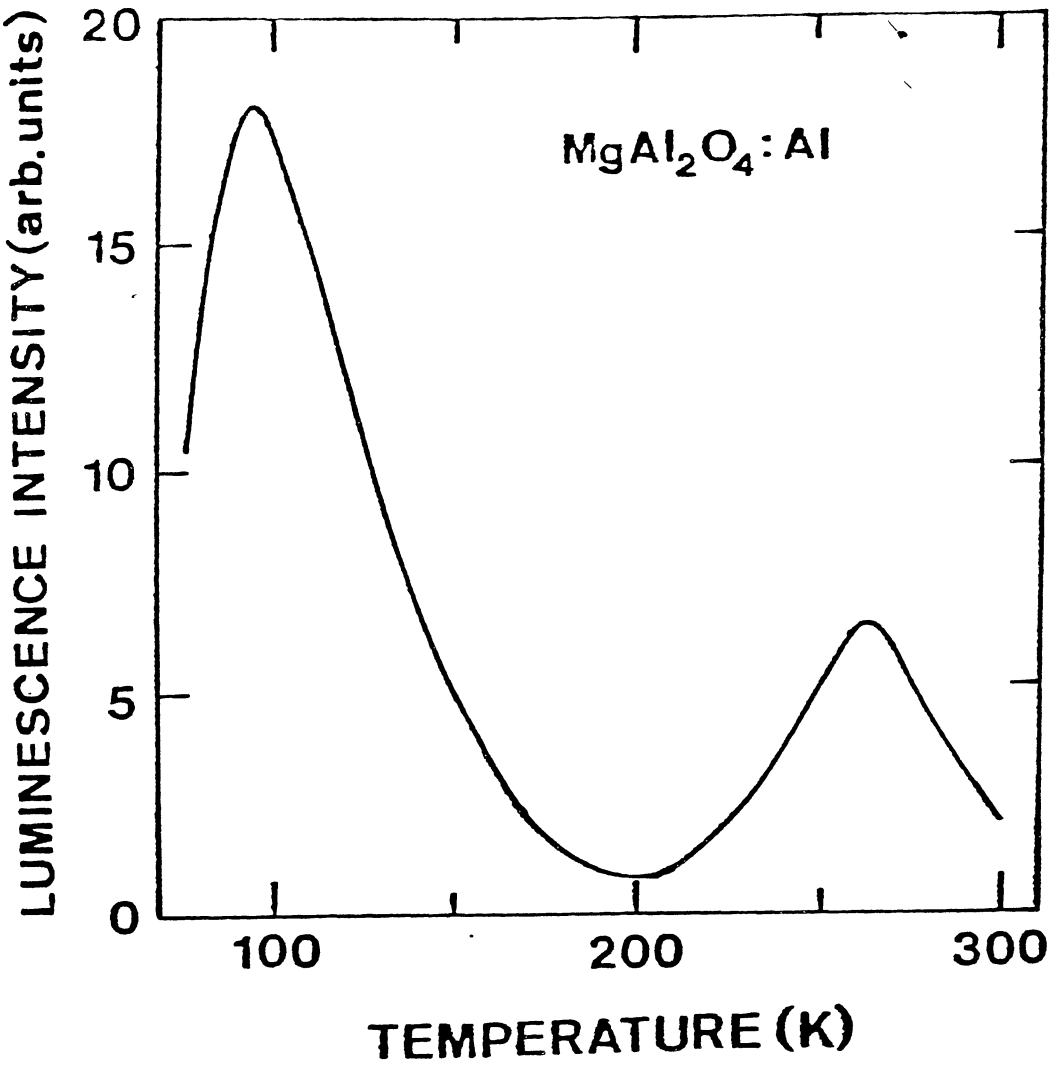

Figure 42. Thermoluminescence Glow Curve for Thermochemically Reduced $MgAl_2O_4$. The Sample was Illuminated at 80K for Several Minutes with Unfiltered Light from a Deuterium Lamp Before Heating

Figure 43. At 95K, the emission consists of a band with a main peak at 2.68 eV and with a half width of ~ 0.65 eV. A shoulder is visible at ~ 2.95 eV. At 265K the peak shifts to 2.57 eV and the half width narrows to 0.52 eV. More comments regarding the origin of the 265 K TL peak will be made later (Section V). The bands in Figure 43 are clearly similar to the photoluminescence curves shown in Figure 39.

Photoconductivity

So long as the mean charge-carrier range, ω_o v/d, in the direction of the applied field, v/d, is smaller than the thickness of the sample, d, the photoresponse of an insulating material sandwiched between two plane parallel electrodes is given by (13)

$$\eta\omega_o = (I/N)\ (d^2/|e|v), \tag{58}$$

where η is the free electron yield per incident photon, I is the photocurrent, N is the incident photon flux and $|e|$ is the magnitude of the charge on an electron. Equation (58) shows that the photoresponse at a certain wavelength depends not only on the probability of a photon producing a free charge carrier but also on the distance the charge carrier moves in the direction of the field before becoming trapped. The photocurrent is, therefore, sensitive to the distribution of effective traps in the sample and can be affected by altering this distribution, even if the quantum yield remains uncharged.

During photoconducitvity measurements the usual sample holder was replaced by one in which the sample was held between a semitransparent front electrode and a high impedance back electrode made of copper

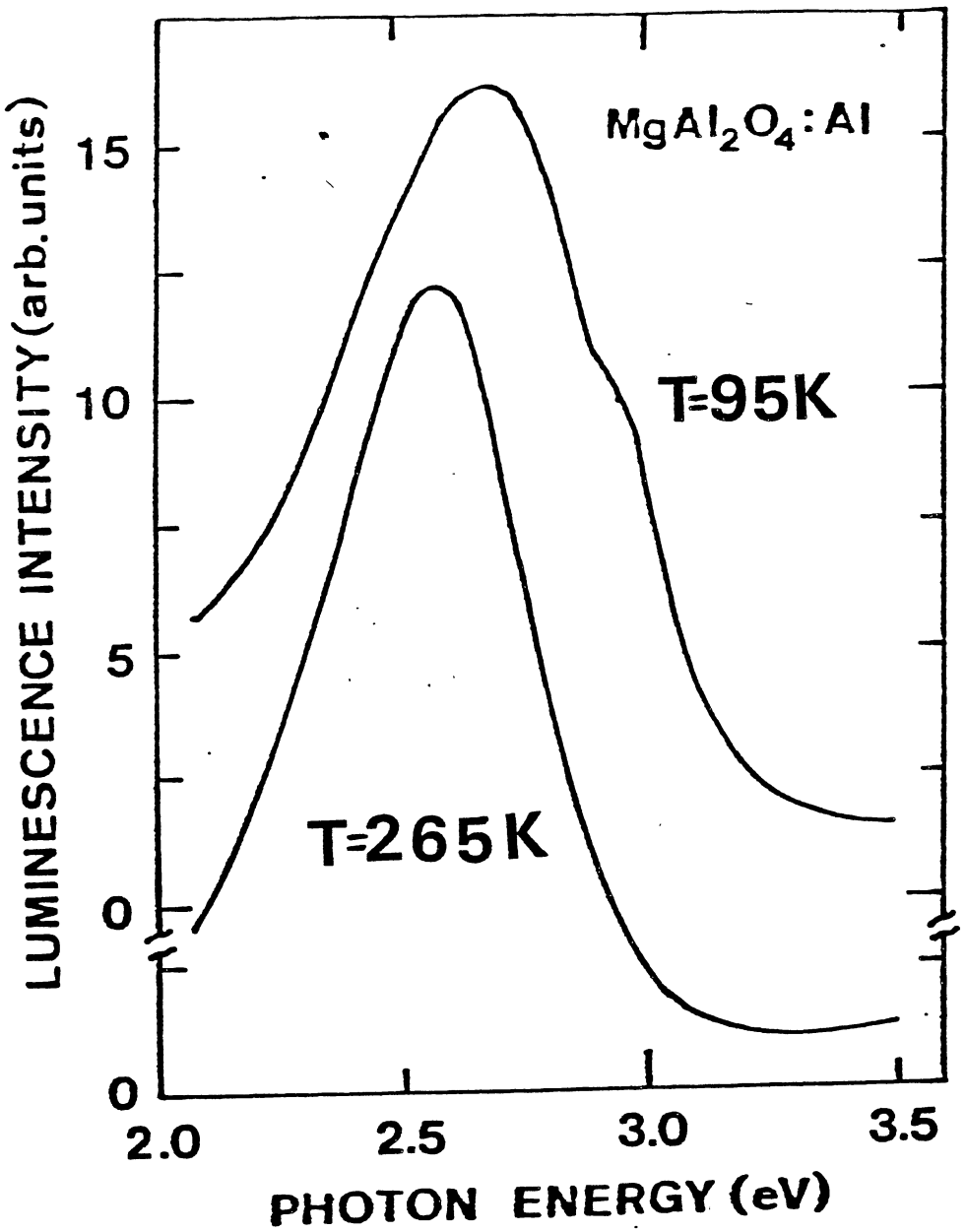

Figure 43. Thermoluminescence Emission Spectra at Each of the Glow Peaks Shown in Figure 42

foil. The front electrode consisted of a spring-mounted fine phosphor-bronze gauze, which was separated from the sample by a thin sapphire plate. This plate effectively "blocked" the front electrode. The rear electrode could be blocked in the same way. Photocurrents were excited with the same optical system used for luminescence measurements and were detected using a Cary 401 vibrating reed electrometer. Sapphire insulation was used throughout for the high impedance electrode.

Figure 41 shows the photoresponse of the same sample that was used for the luminsecence measurements. The data shown in Figure 41 was taken at 216 K. At this temperature the photoresponse consists of two peaks, one at 5.39 eV and the other at 4.59 eV. There was no measureable photoresponse over the same evergy range for an as-received sample. The intensity of the 4.59 eV peak was approximatly independent of temperature over the range 80-300K and was not affected by prolonged exposure of the crystal to the incident light. The peak at 5.39 eV, however, was only apparent between 190 - 250K and was very sensitive to bleaching by the incident light. For example when the spectrum was scanned from low to high photon energy, i.e, if the 4.59 eV band was excited first, the 5.39 eV band was not apparent. It was then necessary to reverse the direction of the applied electric field and to scan the spectrum from high to low photon energy to produce the 5.39 eV band. Although this behavior is particularly pronounced in $MgAl_2O_4$, similar bleaching effects are observed in the photoresponse of F-centers in other oxides. This will be discussed further in Section V.

Discussion

Photoluminescence, thermoluminescence and photoconductivity results

for $MgAl_2O_4$ are presented in an earlier section, which taken as a whole are similar to results for other thermochemically reduced oxides, particularly MgO. The 5.30 eV absorption band of the F-center in $MgAl_2O_4$ occurs between that for MgO (5.0 eV for MgO and 6.1 eV for α-Al_2O_3). It is tempting therefore to assign the 2.69 eV luminescence band, which falls between F-center emission bands in MgO (2.3 eV) and α-Al_2O_4 (3.0 eV) to luminescence from F-centers in $MgAl_2O_4$. This assignment is supported by the fact that the excitation spectrum of the 2.69 eV band (Figure 41) peaks at ~5.3 eV and has a half width of ~ 1.0 eV, which are characteristic of the F-center absorption band. The results indicate, however, that the quantum efficiency of the 2.69 eV band is only about one tenth that of the 2.3 eV F-center luminescence in MgO. The reason for such a low efficiency is difficult to determine without information about the local environment and electronic structure of the center. However, the large nonstoichiometry in $MgAl_2O_4$ crystals, which can be as high as 20%, suggests that some F-centers may be surrounded by four Al^{3+} ions for example, while other may be surrounded by two Al^{3+} ions and two Mg^{2+} ions. It is possible that only those F-centers in a particular configuration decay radiatively. It is noted that F-centers in other more complex crystal structures such as $KMgF_3$ do not decay radiatively or decay radiatively with a very low quantum efficiency. The resolved structure on the high energy side of the 2.69 eV band does not appear to be a phonon side band. If the 2.69 eV luminescence does indeed come from F-centers, the structure could be a result of a low site symmetry, which could raise the degeneracy of p-like excited states. The position of the structure would thus indicate a splitting of ~ 0.2 eV. Splitting of this magnitude has been deduced

for the p-like emitting state of the F-center in α-Al_2O_3 (61) in which it was suggested that the 3.0 eV emission in α-Al_2O_3 is due to transitions from the crystal field split $^3T_{1u}$ excited state of the F-center to the $^1A_{1g}$ ground state, although in this case no resolved structure was observed. The shift of the peak position of the 2.69 eV band to lower energy as the temperature is increased is observed in the luminescence of most anion vacancies. The shift is due mainly to the thermal expansion of the lattice with increasing temperature.

The increase in intensity of the 2.69 eV band as the temperature increased to 160 K, followed by a decrease in intensity as the temperature increased further is similar to the behavior of the 2.3 eV band in MgO (66). In a simple three level model in which an electron in the excited state of an F-center can either decay radiatively to the ground state or escape into the conduction band, a decrease in luminescence intensity with increasing temperature is expected to be accompanied by a corresponding increase in photoconductivity (see Equations (13) and (14), Chapter II). This behavior is apparent in spinel above 160K.. The behavior of the photoconductivity is unusual, however, and deserves further comment.

The peak of the photoconducivity band at 5.39 eV is ~ 0.1 eV higher in energy than the F-center absorption band. However, the absorption band is quite broad (~ 1.0 eV) and skewed to high energy, which suggests that it might consist of several components due to the low symmetry of the oxygen vacancy site, as discussed above. In this case photoconductivity might be found only on the high energy side of the absorption band. Because of the point-by-point measurement technique used by Wooseley et al. (64), the precise locations of the photoconductivity

peaks they reported are somewhat uncertain. Peaks were reported at 3.75, 4.0, 4.25, 4.5, 5.0 and 5.5 eV in x and electron irradiated samples, and at 4.5, 5.0, and 5.5 eV in neutron irradiated samples. None of these bands coincides with the two bands as shown in Figure 41. The 4.59 eV (276 nm) band in spinel is close in energy, however, to a band found in thermochemically reduced MgO. This band has not yet been identified (67). The magnitude of the photoresponse per absorbed photon at 5.39 eV is comparable to that of F-centers in other high resistivity materials. For F-centers in electron irradiated CaO (68) and SrO (69) the values where ~ 1.5×10^{-10} and ~ 4×10^{-10} cm^2v^{-1} respectively. The bleaching effect observed in the 5.39 eV has also been seen in MgO (67), CaO (68) and SrO (69). In each case it was necessary to irradiate the sample with x-rays or ultraviolet light to maximize the photoresponse. The usual explanation for this behavior is that the irradiation fills traps which would otherwise reduce the range of the free charge carriers. It has also been difficult to observe the photoresponse of F-centers in thermochemically reduced MgO, especially when the concentrations were high. The behavior of the 5.39 eV photoresonse band in spinel is, therfore, unusual but not atypical of behavior seen in other oxides containing F-centers.

The thermoluminescence glow curve of spinel, Figure 42, is similar to that seen in thermochemically reduced MgO (66) and CaO (70). In all cases there is a peak near room temperature and peak below 100 K. The higher temperature peak in MgO and CaO is due to release of electrons from substitutional H^- ions and their subsequent capture into the excited states of F-centers. The hydrogen originates as dampness in the starting materials from which the crystals are grown. A TL peak at 260K

is also seen in some samples of α-Al_2O_3 (71) and this has also been tentatively assigned to release of electrons from $H^=$ ions. Accordingly one expects thermochemical reduction of $MgAl_2O_4$ to produce substitutional H^- ions as well as F-centers, just as in the case of MgO. By analogy to the behavior of both MgO and α-Al_2O_3 it is therfore suggested that the 260K TL peak in spinel is due to release of electrons from H^- ions. The whole sequence can be represented as follows: during UV irradiation at 77K, electrons from F-centers in $MgAl_2O_4$ are raised to the conduction band and eventually get trapped at substitutional H^- ions. H^- center in spinel would represent a region of local positive charge and therefore can act as a electron trap. As the crystal is now heated, at 260 K the electrons released from H^- ions escape to the conduction band and recombine with the F^+ centers. The 2.58 eV lminescence as seen in 260 K TL peak in $MgAl_2O_4$ is due to the transition from excited state of an F-center to the ground state. The lower temperature peaks in MgO and CaO have not been identified. Just as in the case of spinel, however, these peaks are introduced by thermochemical reduction and are not present in the original material.

Conclusions

In Section V it has been shown that the optical behavior of thermochemically reduced $MgAl_2O_4$ is generally similar to that of other oxides. This discussion suggests that the 2.69 eV photoluminsecence band is possibly due to a low quantum efficiency process involving F-centers and that the 5.39 eV photoresponse band is due to electrons which are thermally excited into the conduction band from an excited state of the F-center. The charge trapping mechanism seems very

efficient, however, so that the photoresponse is easily bleached. It is noted that the fact that the 2.69 eV band was excited in some as-received samples does not rule out the possibility of it being due to F-centers, because crystals of oxides are often partially reduced during growth. ALternatively it could be argued that the 2.69 eV band is due to emission from a chemical impurity which has an excitation spectrum similar to the F-center absorption spectrum. Iron group ions would seem to be the most likely candidates but Cr^{3+} and V^{3+} can be ruled out which emit at 1.8 eV (72) and 2.38 eV (73) respectively. Mn^{2+} on tetrahedral sites emits at 2.38 eV (74). Fe^{2+} is unlikely to be found in the sample for the reasons discussed by White et al. (63) but Fe^{3+} on tetrahedral sites could be involved, although White et al suggested that these ions are also not observed in the as received samples. Fe^{3+} on octahedral sites absorbs at 4.8 eV, but no absorption band is observed at this energy in our samples. Finally the 2.69 eV could be an emission from Cu ions, which as far as we can tell has not been reported in the literature for an $MgAl_2O_4$ host. It is noted, however, that in MgO, substitutional Cu ions produce optical-absorption bands of about equal intensity at 5.5 and 4.5 eV, with half widths of ~ 0.6 eV at room temperature. Excitation of these crystals with ultraviolet light produces a weak luminescence band at 3.0 eV with a half width of ~ 1.3 eV. In untreated samples of the $MgAl_2O_4$ used here, the only absorption bands visible occurred at 4.8 and 6.4 eV and these have been assigned to Fe^{3+} (58). Thus it is concluded that the evidence available strongly suggests that F-centers in thermochemically reduced $MgAl_2O_4$ are more likely to be producing the photoluminescence and other effects rather than a chemical impurity.

CHAPTER VI

α-Al_2O_3

Introduction

This chapter describes the experimental results obtained from unirradiated single crystals of α-Al_2O_3 which have been subsequently annealed at high temperatures in air. Optical absorption, thermoluminescence, photoluminescence and photoconductivity experiments were performed to gain information about the possible nature of the defect responsible for the observed results. "As-received" samples of α-Al_2O_3 show the presence of anion vacancy (F-type) defects detected through the characteristic absorption and luminescence. The samples used in this present work can be classified into two categories: i) as grown α-Al_2O_3 crystals not subjected to heat treatment; ii) as grown samples of α-Al_2O_3 which were annealed in air for 12 hours at 1250 and 1500°C respectively. Much is now known about the luminescing centers present in Al_2O_3 samples which fall in the first category whereas the thermally annealed samples have not been investigated in detail so far. The present work is concerned with the study of those crystals of α-Al_2O_3 which fall into the later category. In order to understand the observed effects detected in these crsytals, it is necessary to describe the crystalline structure of α-Al_2O_3, the conditions under which the crystals are grown prior to the heat treatments and how luminescing centers are formed in "as received" samples.

Figure 44 shows the structure of α-Al_2O_3 . The structure is hexagonal consisting of an equilateral triangle of O^{2-} ions above and below an Al^{3+} ion. The apexes of the top triangle are rotated through 60° relative to those at the bottom triangle. Al^{3+} ion is situated along the line joining the centers of the triangles but is slightly displaced toward one of the triangles. The shorter Al^{3+} - O^{2-} distance is 1.86 A° and the longer Al^{3+}-O^{2-} distance is 1.97A°. The symmetry of the unit cell is C_{3v} whereas the symmetry of the crystal is C_3 due to large interstitial spaces formed in the crystal by the process of combining the cells. Figure 44 also shows that an O^{2-} ion is located at a site of C_2 symmetry with two pairs of surrounding Al^{3+} ions situtated at slightly distorted octahedral (O_h) site.

Several kinds of defect configurations may be present in the crystal structure of α-Al_2O_3. Removal of O^{2-} ions results in the formation of bare anion vacancies. F- and F^+-centers would result if the anion vacancy traps two electrons or one electron respectively. V-type centers are produced when Al^{3+} ions are removed from the cation site. Anion-cation vacancy pairs would result in the formation of P centers. P^- centers are formed when an electron gets trapped in the vacancy pair.

F-type centers in α-Al_2O_3 can be produced by: i) particle irradiation; ii) thermochemical reduction. Upon bombardment of Al_2O_3 crystals with electrons (75), neutrons (76,77) or energetic ions, several new absorption bands including a prominent band at 6.1 eV and a smaller absorption band at 4.80 eV appeared. Since no satisfactory esr signal from irradiated α- Al_2O_3 has been reported, the indentifications of the absorption bands at 6.1 and 4.80 eV had to be made by indirect

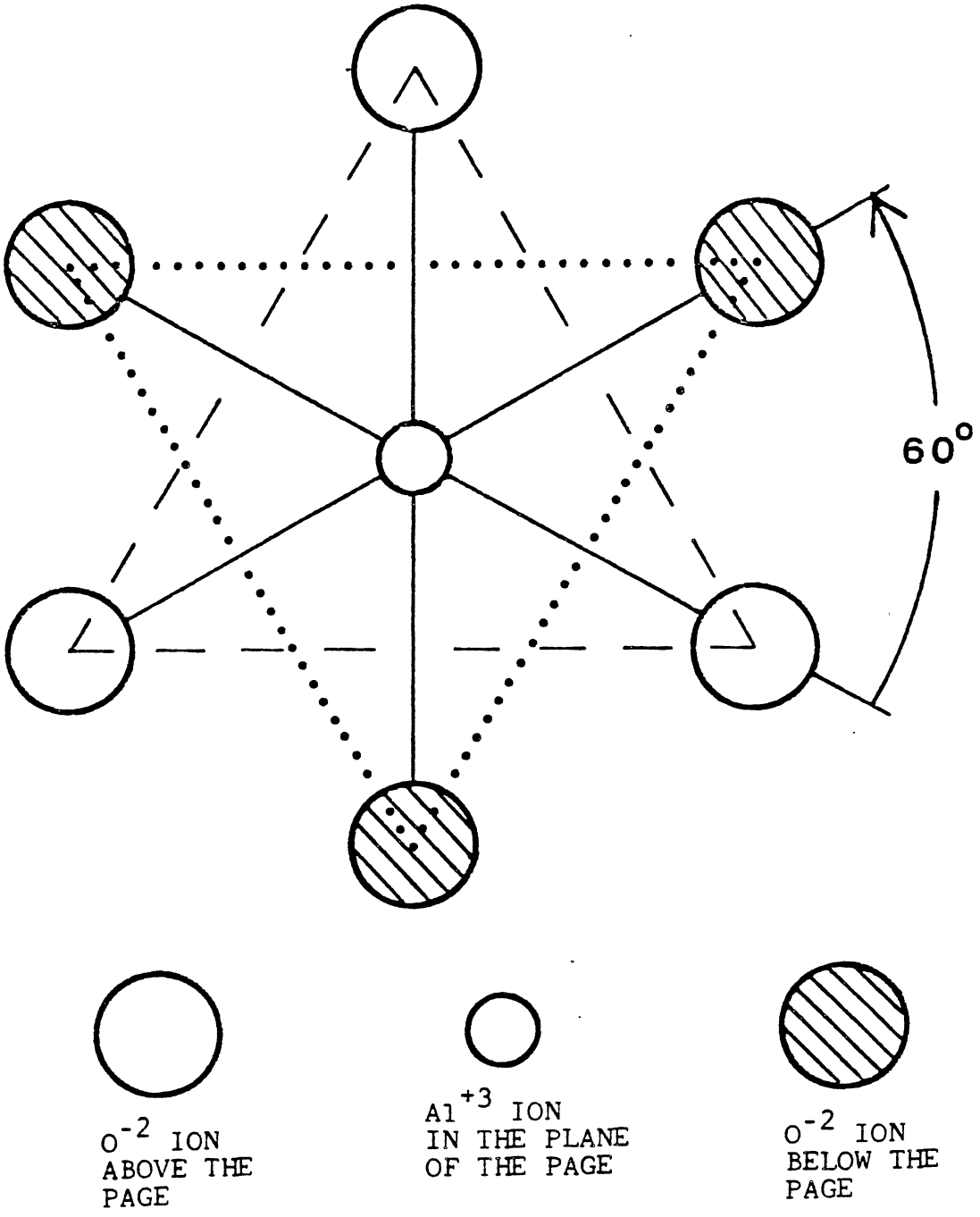

Figure 44. Crystal Structure of α-Al_2O_3

means and by analogy with known properties of F-type centers in the alkaline earth oxides. In particle irradiated Al_2O_3 the radiation damage is in the form of intrinsic, structural damage as in alkaline earth oxides (75). The identification of the 6.1 eV absorption band with the F-type defects came from the bleaching experiments in x-irradiated sapphire (78). An absorption band at 410 nm after γ-irradiation was assigned to be due to V^-_{OH} centers (trapped hole). Upon bleaching the γ-irradiated sample with 410 nm light, Turner and Crawford (78) observed that the 6.1 eV band was reduced in intensity indicating that the absorption band at 6.1 eV is due to a trapped electron center. They also observed that bleaching the neutron irradiated sample with 6.1 eV light caused the intensities of 4.80 and 5.40 eV bands to increase. These results were interpreted by assigning the 6.1 eV absorption band to be due to F-centers (two electrons trapped at an O^{2-} vacancy) while the absorption bands at 4.8 and 5.4 eV were assigned to be due to F^+-(single electron trapped at an O^{2-} vacancy) centers. The explanation of these results was that upon bleaching the irradiated crystal with F-light (6.1 eV) caused an electron to be removed from an F-center and consequently the F^+ center concentrations were increased.

Apart from particle irradiation, F-centers in α-Al_2O_3 can also be produced by thermochemical treatment (subtractive coloration). Some of the as grown samples exhibit the presence of the 6.1 eV absorption band due to F-centers also. In subtractive coloration the sample is heated in an atmosphere of aluminum vapor or in an atmosphere with low partial pressures of oxygen. This process involves removal of oxygen ions from the sample and the charge compensation of the vacancies, thereby producing F-centers. The presence of 6.1 eV absorption band in as grown

samples of α- Al_2O_3 can be explained by the same reduction process which is likely to occur during the growth of a sample, so long as the oxygen partial pressure is less than 10^{-6} atmosphere (80). The 6.1 eV absorption band in growth colored samples behave in a similar way as in particle irradiated sample (79) thereby providing additional evidence for the assignment of the 6.1 eV absorption band in particle irradiated, thermochemically reduced and as-grown samples of α-Al_2O_3 to be due to F-centers.

An F-center's nearest neighbors are shown in Figure 45. The bond lengths indicate the shortest Al-O and longest Al-O distances in the unit cell discussed earlier. As seen in Figure 45, the F (also F^+) -center has C_2 symmetry compared to the crystal symmetry of C_3. One suprising fact is that only one F-center absorption band is observed over the range 2-9 eV (80). A possible explanation for this result is that the p-like excited state is widely extended and that the local symmetry close to the center is therfore relatively unimportant. No theoretical calcualtions have been reported for the electronic structure of the F-center in α-Al_2O_3 . However, La et al. (81) calculated the energy level scheme of F^+ center in α-Al_2O_3 . Their predicted energy level scheme is shown in Figure 46 where the energies indicated are from the experiments conducted by Evans and Stapelbroek (82). The 1A state is equivalent to a 1s state in a case with spherical symmetry. The upper three levels are derived from the triple degeneracy of a 2p state. The 2p state is split into components of A_2, B_1, and B_2 characters by the C_2 symmetry of the center. The model predicts three absorption bands which have been detected experimentally at 4.8 eV, 5.4 eV and 6.3 eV.

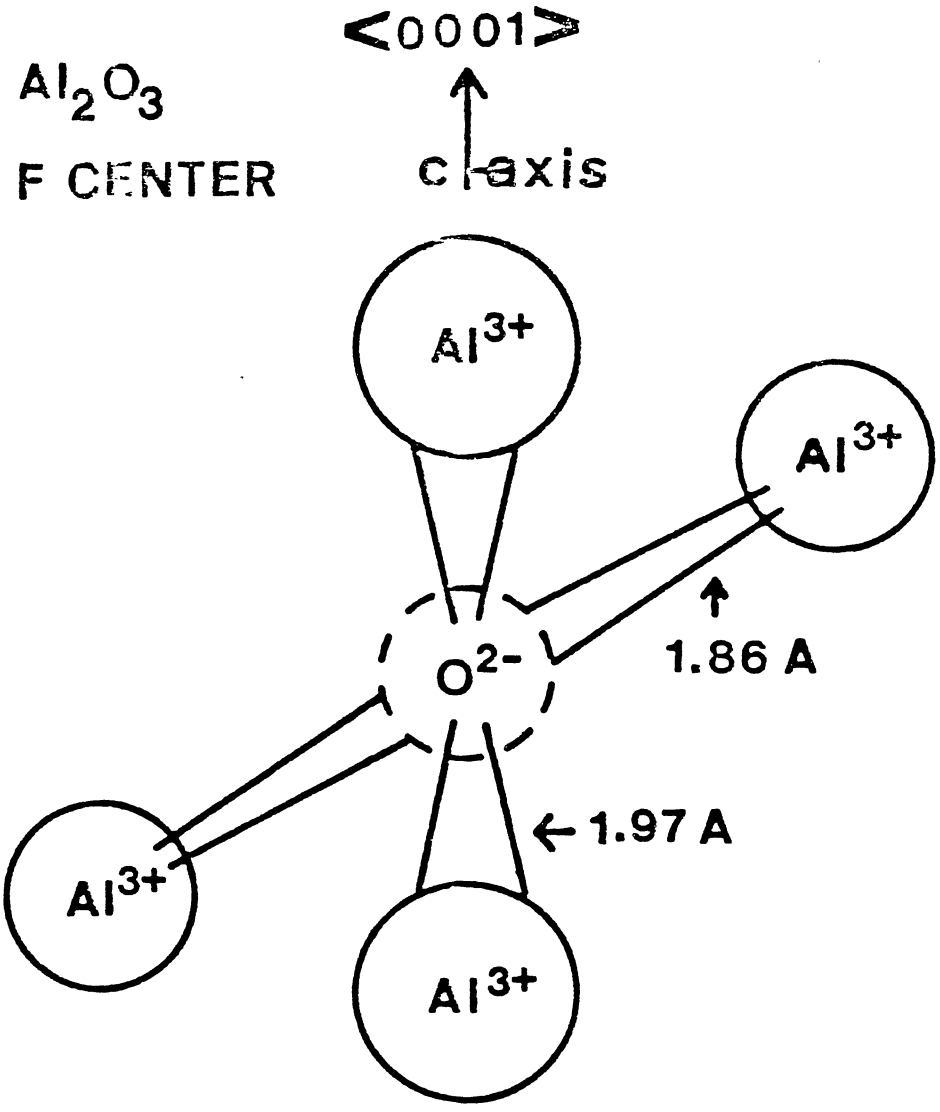

Figure 45. Symmetry of the F-center in α-Al_2O_3

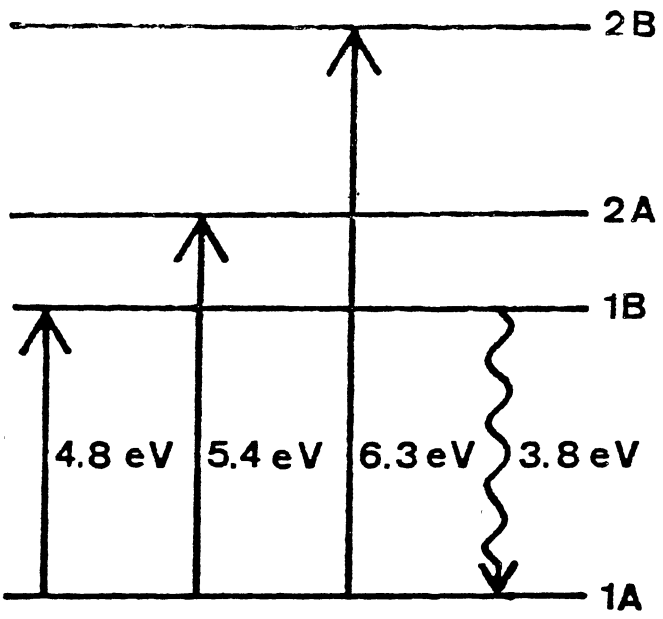

Figure 46. Energy Level Scheme for the F^+-Center in α-Al_2O_3

α-Al_2O_3 samples used in this work were grown under reduced atmoshpere. Unannealed α-Al_2O_3 sample from Insaco (#9) was thermochemically reduced during growth. The effects observed in the annealed samples were somewhat different but related to those observed in the unannealed sample as concluded from optical absorption, thermoluminescence, photoluminescence, excitation, and photoconductivity experiments. Thus it is necessary to understand the properties of F-type defects in the unannealed sample of α-Al_2O_3 .

Figure 47 shows the optical absorption spectrum of Insaco # 9 (unannealed) sample where a band peaking at 6.1 eV with FWHM of 0.68 eV is the most prominent band and is due to $^1A_{1g} \rightarrow {}^1T_{1u}$ transition of the F-centers present in the crystal. Since the crystal was grown under vacuum, F-centers were incorporated during the growth process. Draeger and Summers (79) have shown that photoconductivity results when 6.1 eV light is absorbed by F-centers in reduced samples at temperatures down to 10K, which implies that the optically accessible excited state of the center is in or very close to the conduction band and the electrons can be removed from F-centers by UV light. In the Insaco sample, the conversion of F to F^+ center is found to be efficient. Absorption of 6.1 eV light by F-centers produces a blue luminescence with a maximum at 410 nm (3.0 eV). The emission is partially polarized so that the intensity with the electric vector parallel to the C-axis of the crystal is less than the intensity with the electric vector perpendicular to it. Although the life time of the 3.0 eV luminescence is complicated below a temperature of 50K, above ~70K a single lifetime of 34 ms is observed (61). From a consideration of these results in unannealed and irradiated samples, Brewer et al. (61) suggested that the 3.0 eV

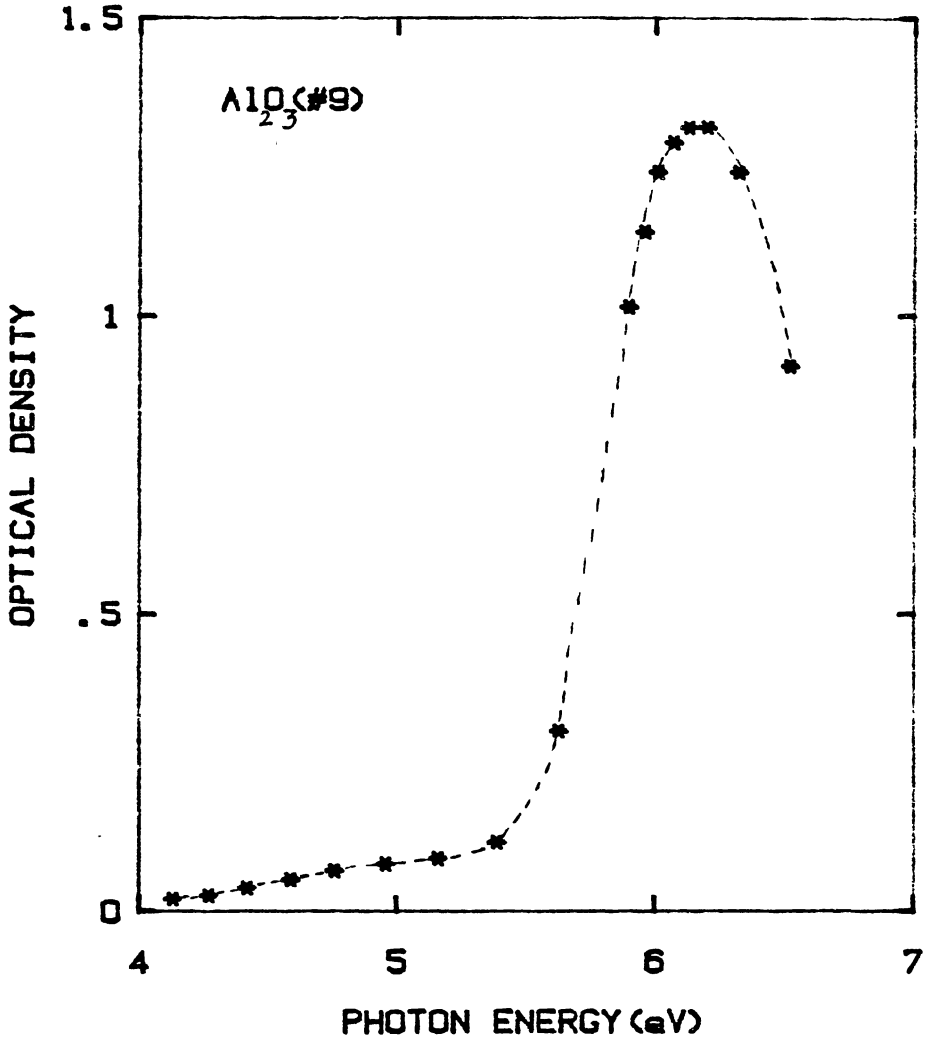

Figure 47. Optical Absorption Spectrum (RT) of the Unannelaed (#9) Insaco Sample

emission is due to transition from the crystal field split $^3T_{1u}$ excited state of the F-center to the $^1A_{1g}$ ground state. They concluded that the emitting state of the F-center is a spin triplet. The transition is thus "forbidden" which accounts for the much longer lived lifetime components present in the emission at lowest temperatures.

Jeffries et al. (71) have also investigated the presence of an electron trap which strongly affects the photoconductivity of unannealed samples of α-Al_2O_3 . This trap causes the 260K thermoluminescence peak observed in as received samples grown under reducing atmosphere and also makes possible the interconversion of F and F^+ centers by optical means. The origin of the 265K TL peak comes as follows: UV light optically excites F-centers which are present in the sample when grown. At ~ 260K the trapped electrons are thermally excited back into the conduction band from the traps and become recaptured by F^+ centers. $F^+ - e^-$ recombination at 260K forms the excited state of an F-center which decays radiatvely by emitting a 410 nm photon. The TL excitation spectrum is therfore expected to peak at ~ 6.1 eV which is observed to be the case (83). Jeffries et al. (71) discussed the possibile identify of the trap as H^- ions. Such a center would represent a region of local positive charge in an oxide and could act as an electron trap. Summers et al. (66) have also shown that TL peak near 260K in thermochemically reduced MgO is caused by substitutional H^- ions. α-Al_2O_3 powder contains OH^- ions like powdered MgO and since several growth techniques employ reducing conditions, the formation of H^- ions may be expected. H^- trap in α-Al_2O_3 causes the $F \rightarrow F^+$ conversion efficient. Upon bleaching the sample with 6.1 eV light (F absorption energy), electrons are removed from the F-centers and get

trapped at H^- ions. Such a process increases F^+-center concentration in the crystal and 4.8 eV absorption band due to F^+ centers is observed to grow in intensity. H^- trap present in the sample also causes the photoconductivity to be observed even at temperatures as low as 10K.

From the above considerations it is apparent that in the unannealed sample of α-Al_2O_3 (#9), F centers are present indicated by: i) the absorption band at 6.1 eV; ii) blue luminescence from the sample peaking at 410 nm under 6.1 eV excitation; iii) TL peak at 265K; iv) the similarity of excitation spectrum of the 3.9 eV luminescence with F-center absorption at 6.1 eV; v) the photoresponse maxima at 6.1 eV.

Existing literature on the luminescing defects in annealed α-Al_2O_3 crystals is meagre. Even in simple oxides such as MgO and CaO, not much work has been done so far. In neutron or electron irradiated MgO, F- and F^+- centers disappear near 500°C whereas in thermochemically reduced crystals, annealing of these centers takes place at about 900 - 1000°C (84). The kinetics of the annealing process have not been examined in detail, but it has been suggested that in irradiated crystals, the anion interstitials become mobile at 500°C and annihilate the vacancies. Alternatively, in neutron irradiated samples, the F^+- centers could be converted to P^-- centers as cation vacancies become mobile (85). In neutron irradiated samples of MgO, F^+ - P^- conversion was observed after heating the neutron irradiated crystals above 300°C. The presence of P^- centers was detected from esr signals which showed that the complex hyperfine interaction is roughly four times that for the F^+ centers showing the extent to which the cation vacancy affects the charge distribution. In thermochemically reduced samples, the annealing temperature must represent that of the diffusion of vacancies

themselves, although which charge state is involved is not known. No similar data appear to be available in CaO, SrO or BaO. Sibley et al. (86) have shown that anion-cation vacancy pairs are formed after the plastic deformation of MgO crystals. They observed no changes in EPR spectra of impurity ions even after deforming up to 14% in compression but a new absorption band at 216.5 nm after the treatment was observed. Turner et al (87) also found deformation-induced absorption bands in CaO and SrO at 268.0 and 304.0 nm respectively. They have attributed these deformation-induced bands in MgO, CaO and SrO to the transition of a bound exciton formed in the neighborhood of a cation-anion vacancy pair. Arguments in favor of the assignment were the similar modes of production in the three oxides and the linear dependence of the absorption intensity on deformation. In the case of α-Al_2O_3 , however, the formation of vacancy pairs has not been positively indentified. Effect of thermal annealing on the 6.1 eV absorption band in thermochemically reduced samples of Al_2O_3 has been studied briefly by Summers et al. (79). Like CaO and MgO, it was found that 6.1 eV absorption band in the reduced samples was comparatively stable against thermal decay compared to the same band in particle irradiated material. They suggested that thermal decay of F- centers in reduced samples was not exclusively an electronic process since it was not possible to restore the 6.1 eV band in the unannealed Insaco sample by γ-irradiation once the band had decayed thermally. This present work focuses on these samples of α-Al_2O_3 which have been annealed at 1250°C and 1500°C in air for 12 hours. Recently Puzats et al. (88) have investigated the nature of violet luminescence from quenched single crystals of α-Al_2O_3 . Before the heat treatment the crystals did not

contain appreciable F-centers. They suggested that vacancy pairs in α-Al_2O_3 have been formed after heat treatment which luminesce in the violet region. More comments on their assignment will be made in Section III. Insaco Crystals (#9a, #9b) studied in this work contained F-centers before heat treatment. Optical absorption, thermoluminescence, photoluminescence and photoconductivity experiments done on these samples suggest that the observed effects are due to perturbed F centers, the perturbation being caused by heat treatment. Section II presents the experimental results and in Section III the results of different experimentations will be interpreted.

Experimental Results

Absorption

Absorption spectra of unannealed (#9) and annealed (#9a, #9b) samples of Al_2O_3 were measured with a Perkin Elmer Model 330 spectrphotometer at room temperature. Figure 47 shows the absorption spectrum of #9 and the absorption spectra of #9a and #9b crystals are shown in Figure 48. Unannealed sample shows a band peaking at 6.1 eV (204 nm) with the presence of no other bands at other photon energies. Absorption spectrum of #9a which has been heated to 1250°C shows the hint of a shoulder near 5.6 eV and near 6.1 eV. The sharp absorption band found in unannealed sample has become much broader in #9a. Absorption spectrum of #9b shows the disappearence of the 6.1 eV band and the shoulder near 5.6 eV can be clearly seen. Figure 49 shows the difference curve of absorption of #9a and #9b which shows that a broad band near 5.6 eV is clearly formed.

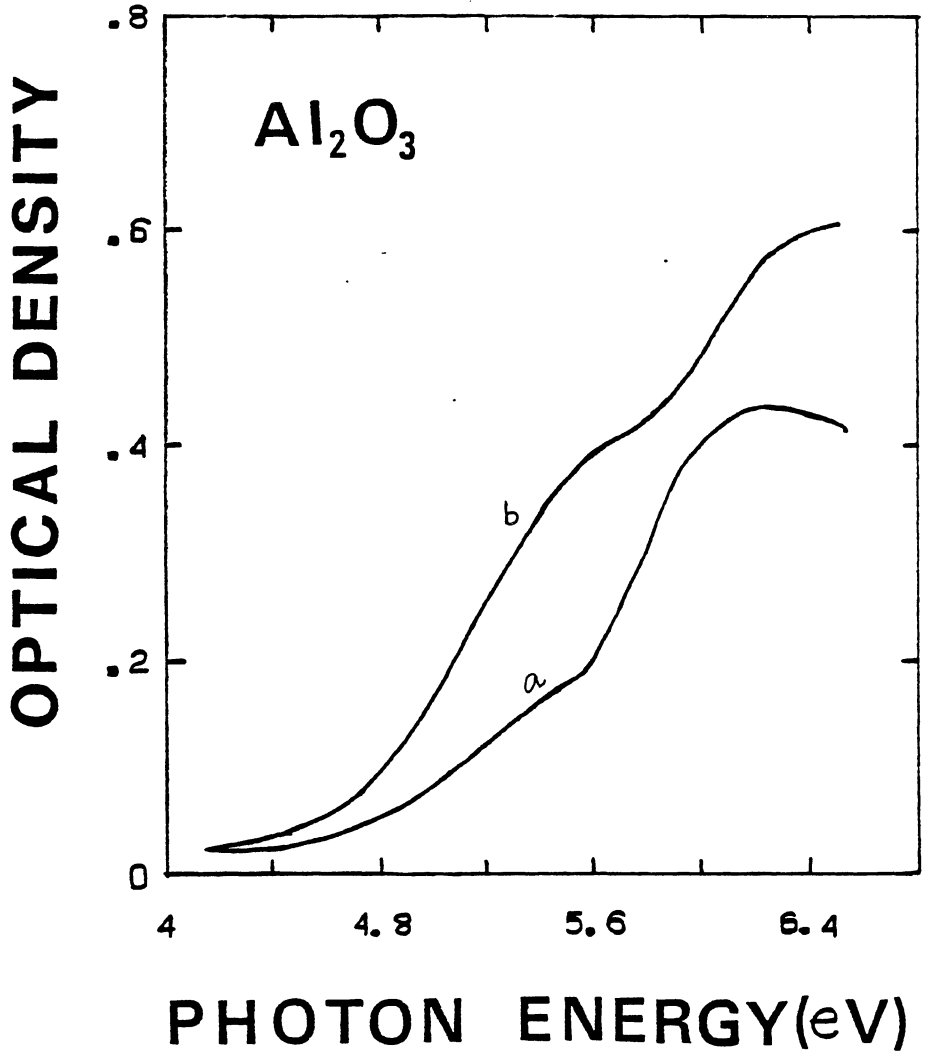

Figure 48. Optical Absorption Spectra of (a) the Insaco Sample (#9a) Annealed at 1250°C (b) the Insaco Sample (#9b) Annealed at 1500°C

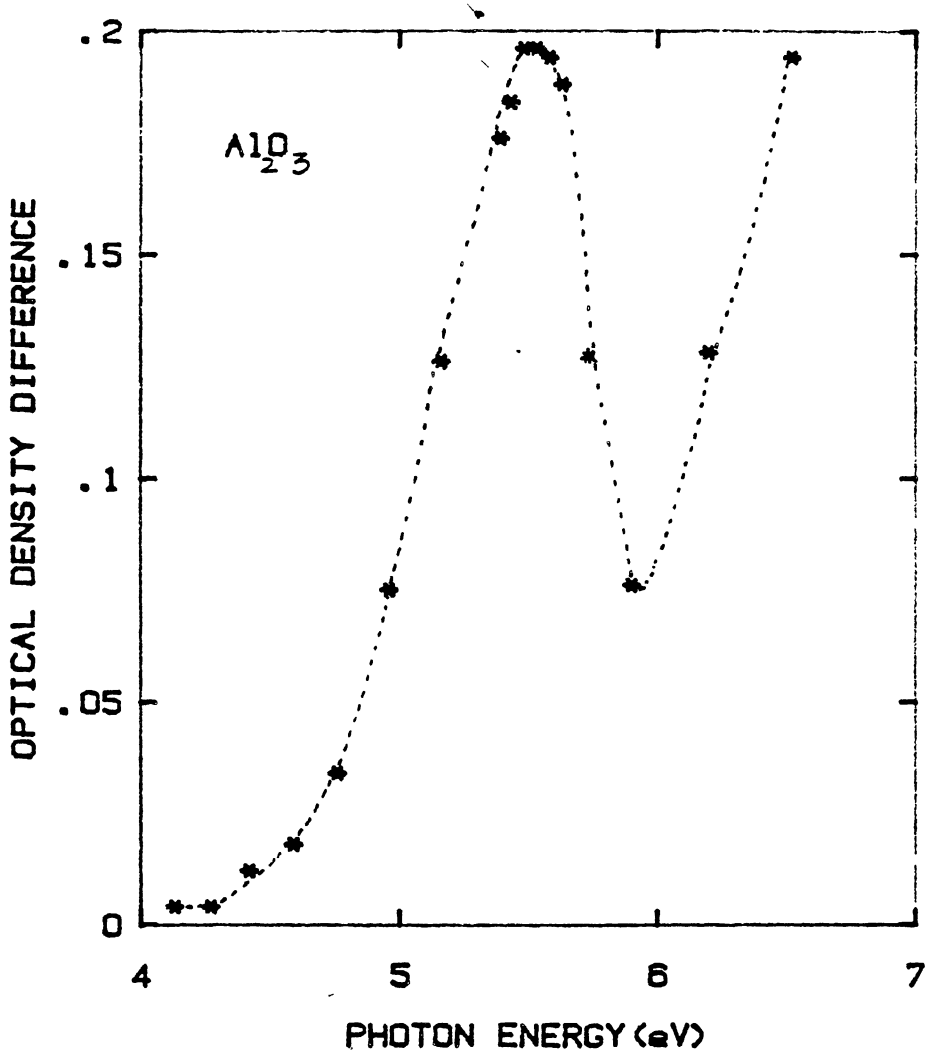

Figure 49. Difference (Δ OD) in Absorption Between the Insaco Samples (#9a, #9b)

Photoluminescence

Photoluminescence was excited with light from a deuterium lamp, used in conjunction with interference filters with peak transmissions at 200 and 225 nm. The luminescence band excited by 200 nm in unannealed Al_2O_3 (#9) sample is shown in Figure 50 in which the data have been corrected for the spectral dependence of the detection system. At room temperature the luminescence is at 3.0 eV and 4.8 eV respectively. When the luminescence peak is excited by 225 nm, the 3.9 eV luminescence peak is much reduced in intensity and that at 4.80 eV is observed to increase considerably. The luminescence spectrum at room temperature of #9a sample (heated to 1250°C) is shown in Figure 51, the excitation being at 225 nm. The peak of the luminescence is at 2.95 eV with a shoulder near 3.1 eV. The experimental set-up in the detection of luminescence from #9b sample (heated to 1500°C) was slightly different than the usual set up, in the sense, that a polariser was inserted between the sample and the entrance slit of the monochromator to investigate any possible polarization properties of the luminescence. The C-axis of #9b was found to be in the plane of the crystal. This allowed the C axis to be horizontally oriented on the sample holder. The crystal was then put in the cryostat and oriented so that the angle of incidence of the exciting light was less than 45° with a line perpendicular to the crystal face. The polariser was then rotated and the emission from the crystal due to continuous excitation was recorded. The luminescence band excited in the sample #9b with the polariser transmission axis perpendicular to the C-axis of the crystal is shown in Figure 52. At 95K the peak of the luminescence is at 2.75 eV with a shoulder at 2.95 eV. As the temperature was increased above 160K, the peak of the band shifted to

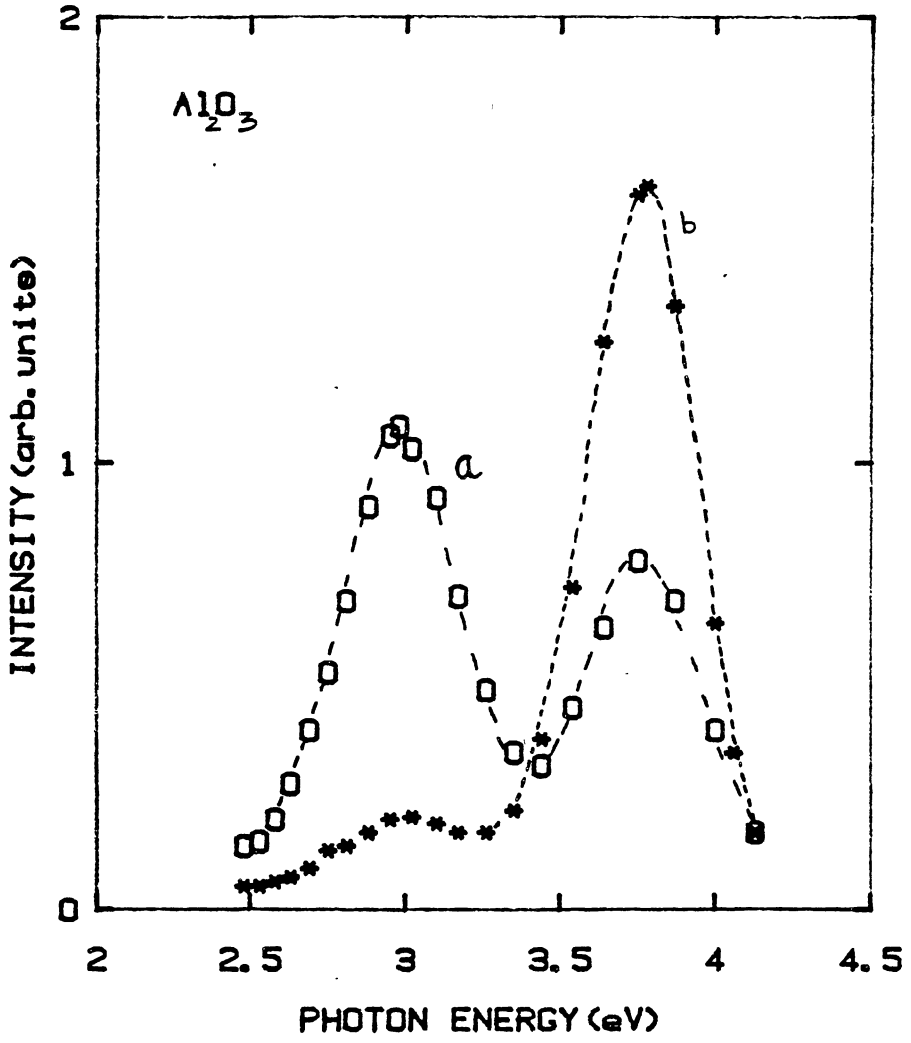

Figure 50. Photoluminescence Spectra of the Unannealed Insaco (#9) Sample Excited by (a) 200 nm Light (b) 225 nm Light

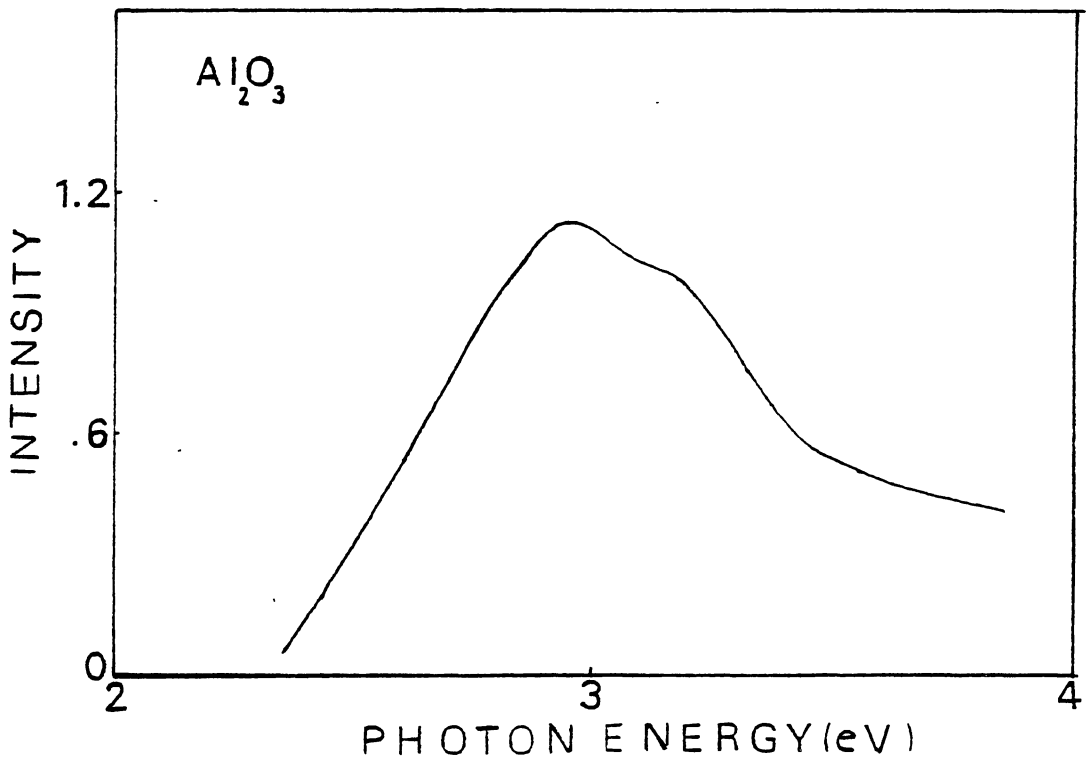

Figure 51. Photoluminescence Spectrum of the Insaco (#9a) Sample with 225 nm Excitation

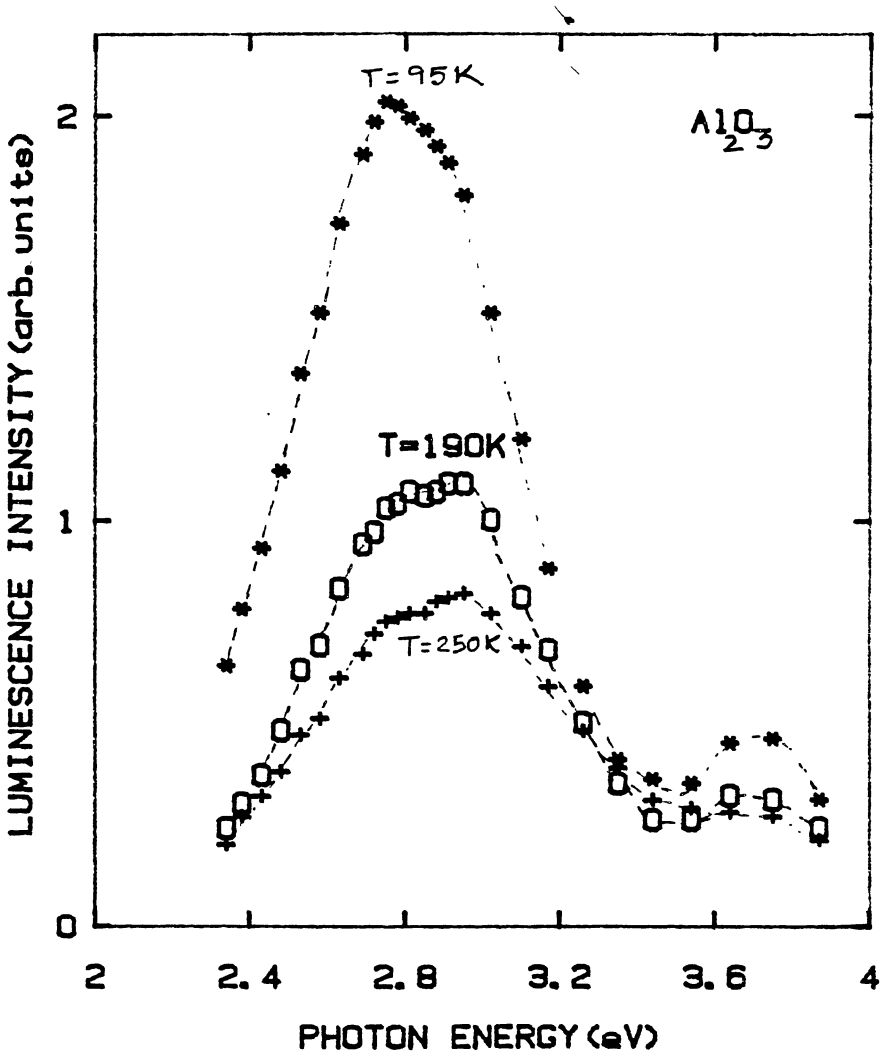

Figure 52. Polarized Photoluminescence Spectra of the Annealed Insaco Sample (#9b) with 225 Excitation. Polarizer Transmission Axis was Perpendicular to the C-axis of the Crystal

higher energy and by 250K was located at 2.95 eV with a shoulder near 2.75 eV. When the poalriser transmission axis was parallel to the C axis of the crystal, the relative intensity of the composite luminescence band decreased as shown in Figure 53 where the data have been corrected for the inherent polarization of the detection system. At 95 K the peak of the luminescence is at 2.75 eV with the appearence of a shoulder near 2.95 eV. As the temperature was increased above 160 K, the peak shifted to 2.91 eV with a shoulder near 2.89 eV and by 250 K, the peak intensity of the luminescence was observed to be at 2.95 eV. The relative intensity of the luminescence decreased between 95 and 250K so that at 250K the intensity of the band was about three 3 times weaker than that at 95K.

The excitation spectrum of the composite luminescence in sample #9a at room temperature is shown in Figure 54. The spectrum has a peak at 5.53 eV and at photon energies greater than 5.9 eV, the excitation intensity shows a steady increasing trend. Excitation spectrum of the same luminescence for sample #9b is shown in Figure 55 and as seen from the figure, the luminescence intensity at 80K is higher than that at room temperature. The peak energy is at 5.53 eV and shows the same increasing trend (as observed in #9a) with photon energies exceeding 5.9 eV.

Luminescence observed in samples #9a and #9b decayed rapidly once the excitation was removed. The lifetime was ~1.5 ms which was of the order of the time constant of the detection system. Luminescence from the unannealed sample (#9) showed the evidence of long lifetime and the relative luminescence intensity was much higher than those detected in annealed samples of Al_2O_3.

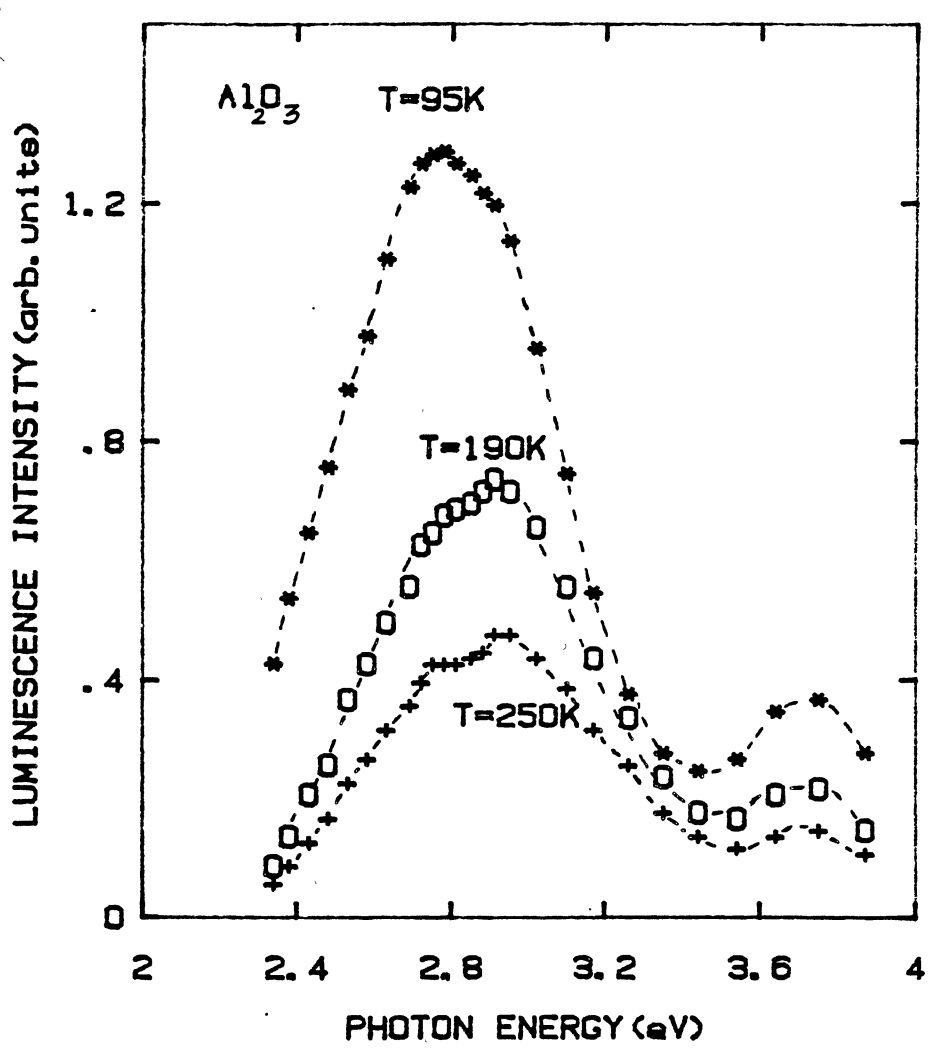

Figure 53. Polarized Photoluminescence Spectra of the Annealed Insaco Sample (#9b) with 225 nm Excitation. Polarizer Transmission Axis was Parallel to the C-axis of the Crystal

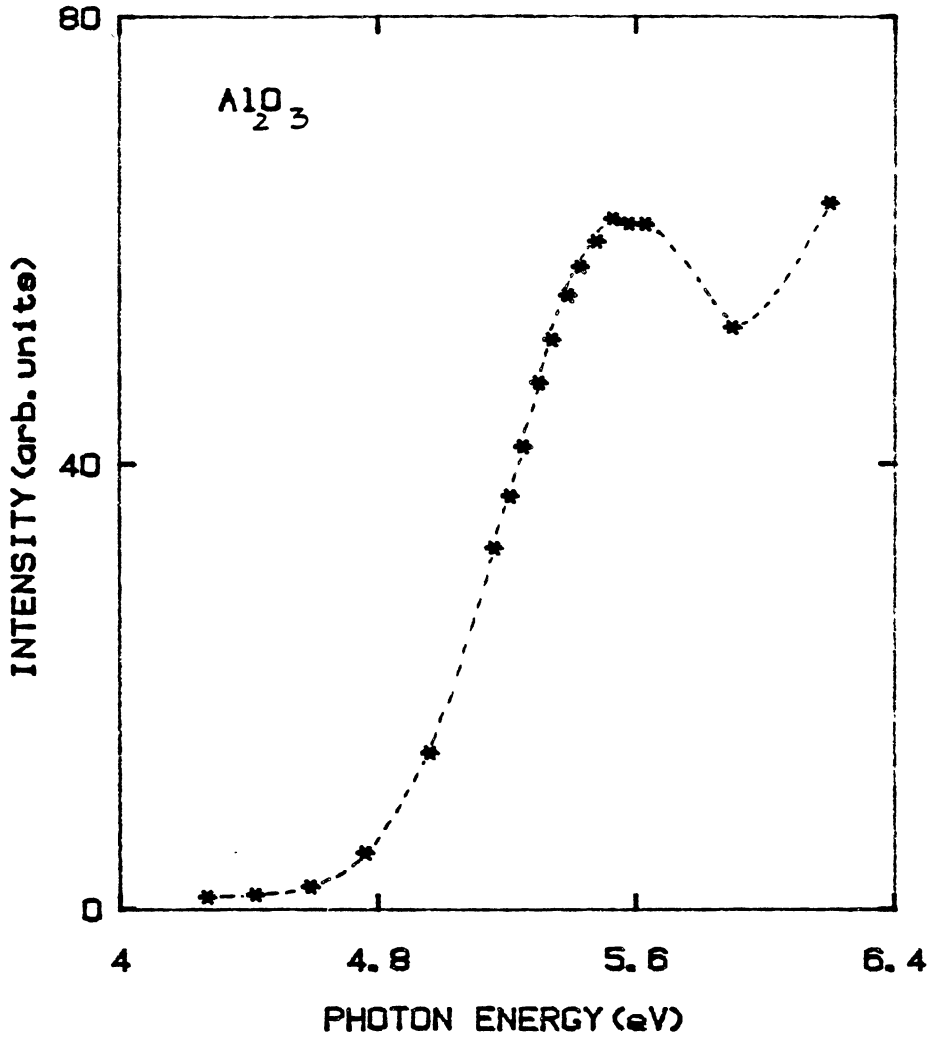

Figure 54. Excitation Spectrum (RT) of the Observed Luminescence in the Annelaed Insaco (#9a) Sample

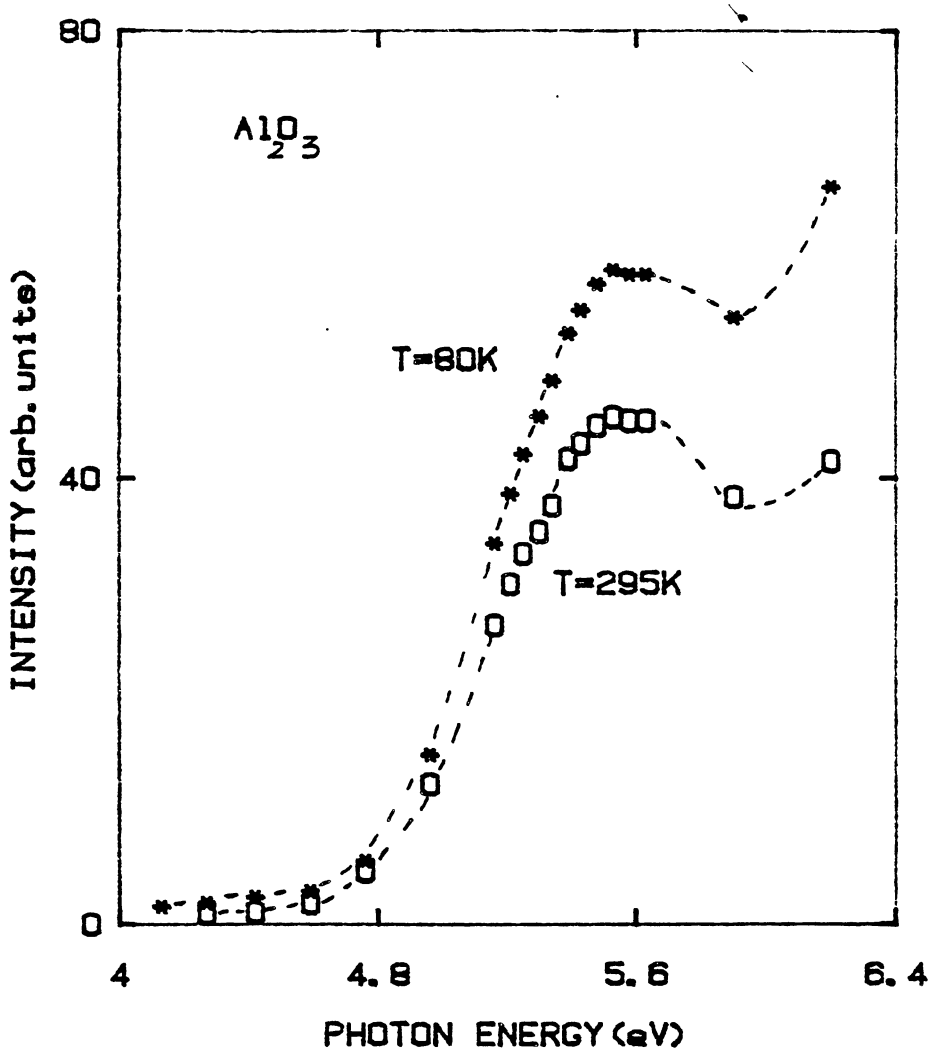

Figure 55. Excitation Spectra of the Observed Luminescence in the Insaco (#9b) Sample

Composite luminescence bands observed in annealed samples could not be decomposed into two gaussian bands. However, qualitative information regarding the temperature dependence of the luminescence detected in #9b sample was obtained by choosing two energy values in the band outside the region of overlap of the low and high energy component and noting how these two energy components present in the luminescence varied with temperature. Figure 56 shows the variation of the luminescence at 2.6 eV and 3.0 eV with temperature. The low energy component shows a rapid decrease in intensity till 190K and as the temperature was increased further the intensity did not show appreciable change. The high energy component behaved in the same way except that the rate of decrease is somewhat slower in this case.

Thermoluminescence

Figure 57 shows the theroluminescence glow curve for the sample #9b, used in the photoluminescence experiments. In TL measurements, the sample was cooled to liquid nitrogen temperature, illuminated for a few minutes with unfiltered light from a 60 W deuterium lamp and then subsequent warming up of the crystal at ~ 8K minute^{-1}. Figure 57 shows the presence of a glow peak at 265 K. It was observed that the TL spectra of samples #9 and #9a also showed a single peak at 265 K.

Photoconductivity

Photoconductivity experiments were peformed on #9a (heated to 1250°C). It has been shown (Chapter II) that the photoresponse of a crystal at a certain wavelength depends not only on the probability of a photon producing a free charge carrier but also on the distance that the

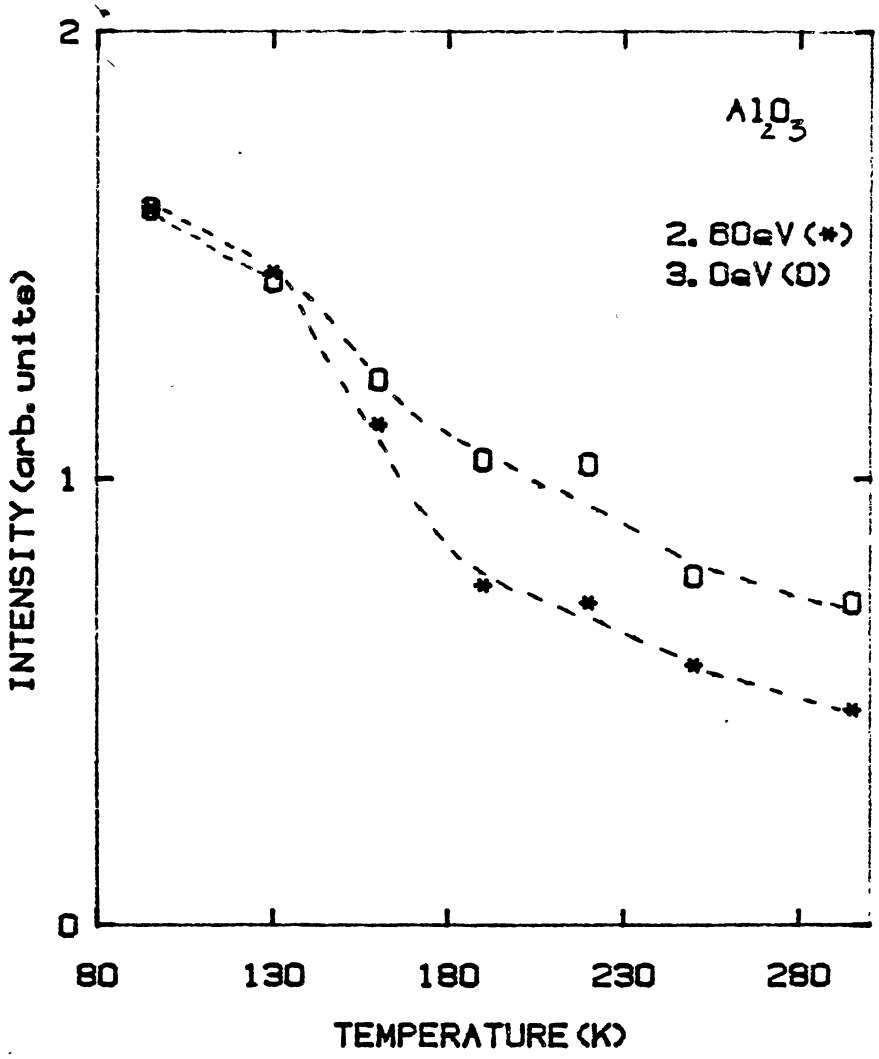

Figure 56. Temperature Dependence of the High and Low Energy Component of the Luminescence Detected in the Insaco Sample (#9b)

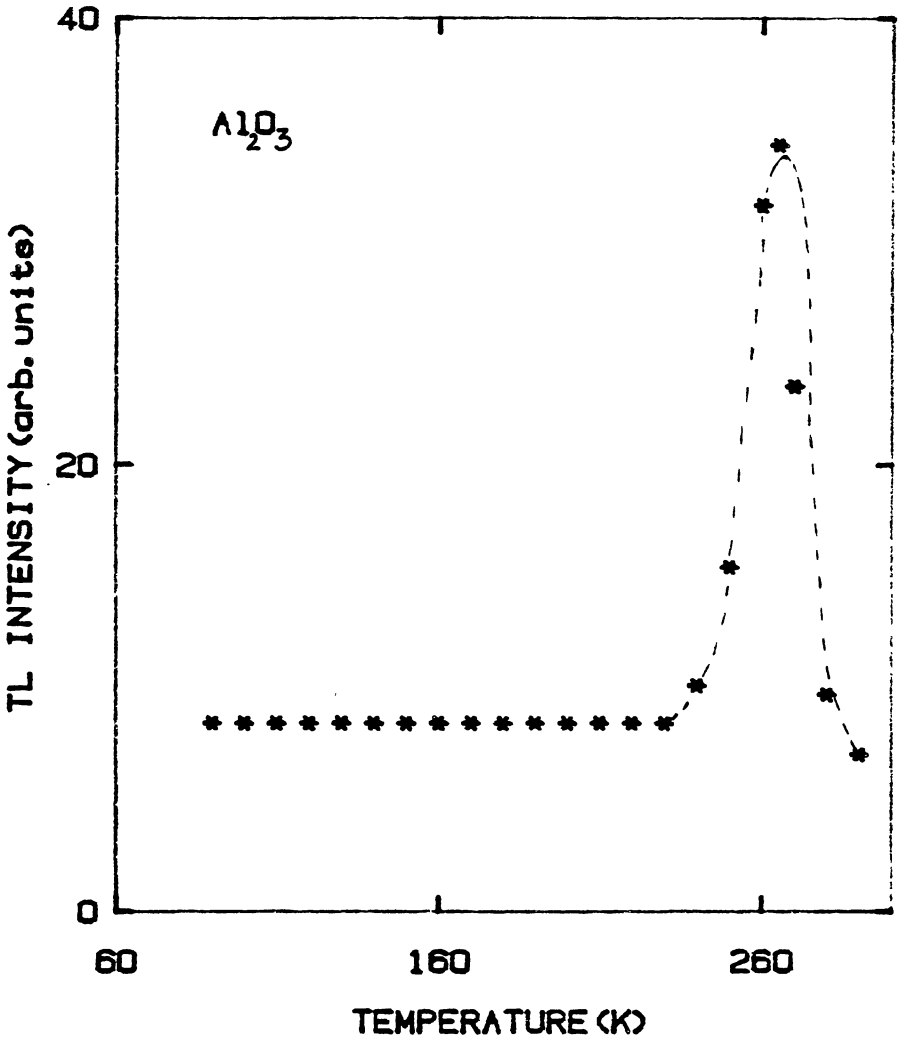

Figure 57. Thermoluminescence (80K - 300K) Spectrum of the Insaco (#9b) Sample

charge carrier moves in the direction of the field before becoming trapped. The photocurrent detected in a sample is therfore sensitive to the distribution of effective traps and can be affected by altering this distribution, even if the quantum yield remains unchanged.

Photoresponse observed in sample #9a was extremely weak. At room temperature it was not possible to detect photocurrent in the sample in the current mode of the detecting electrometer and it was necessary to use the "charge mode" of the detection system which can measure photocurrents as low as 10^{-16} amperes. At room temperature using the "charge mode", the dark current, (current detected in the sample unexposed to light) which occurs due to the thermal motion of the charge carriers due to the applied electric field, was too high (~ 10^{-13} amperes). The spectral dependence of photoresponse was obtained at 80 K where the dark current present in the sample was minimum. 'Point-by-point' measurement technique was used in obtaining the photoresponse of the sample. Figure 58 shows the photoresponse at 80K of the sample #9a where the data have been corrected for the spectral depencdence of the incident light. The spectrum shows a shoulder present near 5.0 eV and with increasing photon energies the photoresponse increases continuously. There is a hint of a peak near 6.2 eV. Data with photon energies greater than 6.2 eV would have clarified the existence of such a peak, but it was not possible to extend the measurements beyond 200 nm (6.2 eV) due to the low output of the deuterium lamp.

Figure 59 shows the temperature dependence of the photocurrent detected in sample #9a in the temperture range 80K - 180K. Above 180K the dark current became increasingly large, thus obscuring the

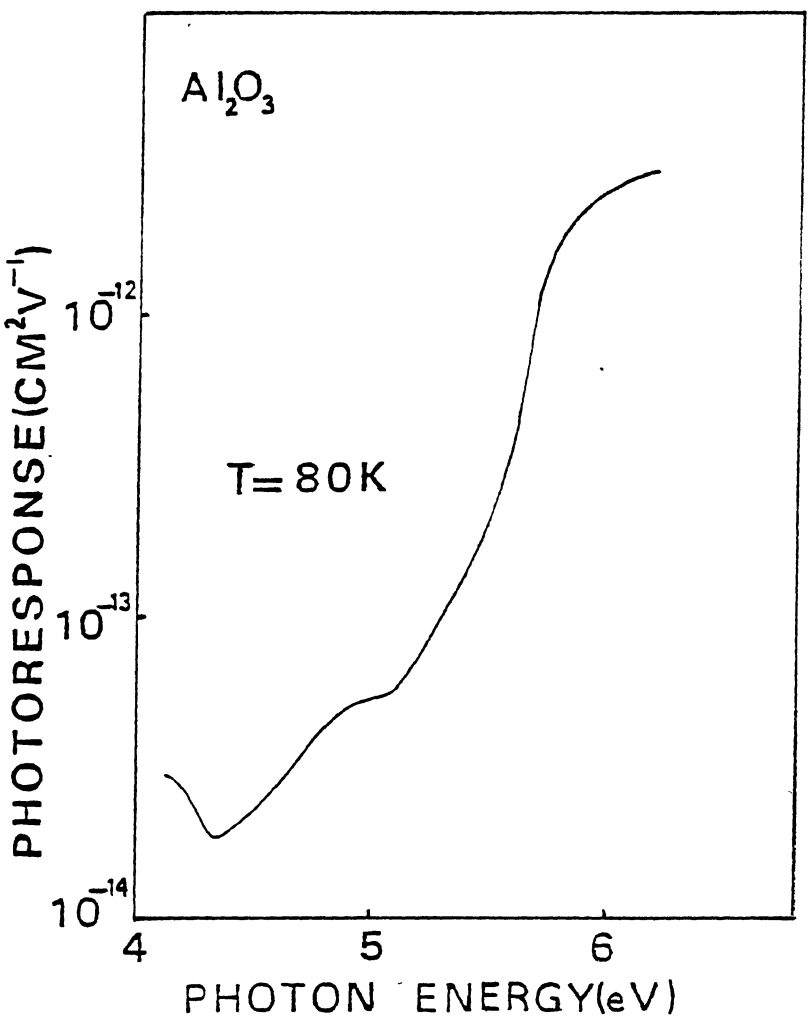

Figure 58. Spectral Dependence of the Photoresponse Observed in the Insaco (#9a) Sample

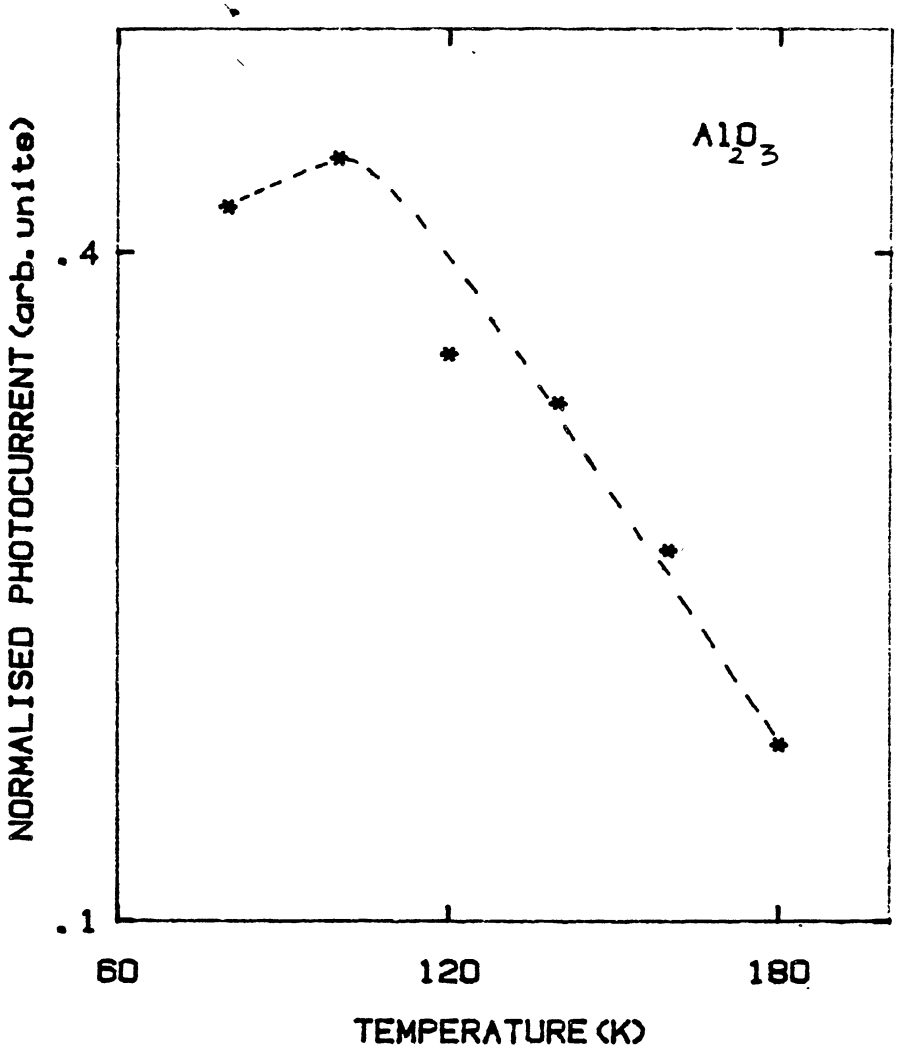

Figure 59. Temperature Dependence of the Photocurrent Excited by 200 nm Light in the Insaco (#9a) Sample

photocurrent present in the sample. Figure 59 shows that the photocurrent induced by 200 nm excitation shows a continous decrease in the temperature range studied in the present work. Similar temperature dependence has been observed in some samples of unannealed α-Al_2O_3 (71).

Experimental results obtained from unannealed and annealed samples of α-Al_2O_3 presented so far will be interpreted in the next section.

Discussion

In Section II, results of optical absorption, thermoluminescence, photoluminescence and photoconductivity experiments for annealed α-Al_2O_3 samples have been presented, which taken as a whole are different from the results for the unannealed α-Al_2O_3 sample. After the heat treatment new luminescing centers are formed whose optical properties are different from those of F - centers in α-Al_2O_3 . Excitation spectrum of the luminescence in heat treated samples has a peak at 5.6 eV which coincides with the shoulder at the same energy found in the absoprtion spectrum. The high energy component of the luminescence at ~ 2.95 eV is close in energy to the F-center luminescence (3.0 eV) in the unannealed sample which suggests that the emission in heat treated samples may be due to some center whose structure (nearest neighbor and local symmetry) does not differ markedly from that of an F- center. Two possible models to explain the luminescence in heat treated samples (#9a and #9b) are suggested: (i) formation of a cation-anion vacancy pair (P^- center); (ii) formation of a perturbed F-center. The mechanism of production of these centers is not known. However, it has been suggested that anion and cation vacancies in thermochemically reduced Al_2O_3 samples are mobile at

temperatures above 1000°C which may play an important role in the formation of P^- or perturbed F-centers in thermally annealed samples. Puzats et al. (88) have briefly investigated the luminescence observed in high purity α-Al_2O_3 crystals which have been annealed at temperatures as high as 1800°C. Before heat treatment their samples did not exhibit any considerable luminescence bands under excitation by UV light in the 200 to 400 nm region. But after starting from annealing temperatures of about 1300°C, they observed a luminescence band at 420 nm (2.95 eV) with FWHM of 105 nm. The main excitation maximum of the luminescence peaked at 230 nm (5.39 eV) with other maxima at higher energies. Puzats et al. (88) reported that the absorbing and emitting dipoles of the emitting centers were oriented at an angle of $60^\circ \pm 10^\circ$ to the C_3 axis though no experimental data were presented to support of the assigned angular orientation of the centers. In samples #9a and #9b used in this work, the luminescence consisted of a composite band with the high energy component near 2.95 eV and the main excitation maxima of the luminescence was peaked at 5.6 eV, the values being close to those reported by Puzats et al. (88). If the model of anion-cation vacancy pair is assumed for the observed effects in our crystals, then the absorption at 5.6 eV can be envisaged as a sort of charge transfer transition from the oxygen ions surrounding the cation vacancy to the state representing the electron trapped at the anion vacancy. The resulting excited state can be regarded as an exciton bound to a pair of vacancies. Life times of the luminescence (~ 1.5 ms) in annealed Al_2O_3 samples (#9a and #9b) were of the order of the time constant of the detection system which suggest that the excited state of the vacancy pair (P^-) had insignificant overlapping with the ground state. The

upper state of the center can thus be regarded as that of a perturbed F^+-center. Luminescence curs when the electron bound to the anion vacancy in the excited state of the center radiatively combines with the hole left on the oxygen ion. However the presence of structure in the luminescence cannot be explained with this model and more difficulties are encountered in explaining the TL response obtained from these samples. According to the model of the pair of vacancies as the luminescent center, the resulting excited state can be regarded as the bound state of an electron-hole pair. The excited state wave function of the center would be relatively compact and lie well below the conduction band. The observations of TL peak at 265K in thermally annealed samples of Al_2O_3 (#9a and #9b) suggests that the assignment of the anion-cation vacancy pair as the luminescent center may not be correct. The 265K Tl peak requires the removal of an electron from the luminescent center to the conduction band and subsequent trapping at some electron trapping site. In unannealed samples of Al_2O_3, luminescent centers are the F-centers whose excited states lie in or very close to the conduction band as evidenced from photoconductivity measurements. H^- ions are suggested as the possible electron trap and the TL emission at 265 K (hv = 3.0 eV) is indeed found to be the emission of an F-center. Consequently the TL response at 265 K in annealed samples would also require the presence of trapped electron centers whose excited states are close to the conduction band. Such requirements cannot be obviously met by the model of vacancy pair as the possible luminescent center. An alternative model to interpret the results of different experimentations in annealed samples is to regard the luminescent center representing an F-center in a perturbed

environment. An F-center in which one of the nearest neighbor Al^{3+} ions being replaced by an impurity ions may act as a suitable model as the possible luminescent center, i.e. an F_A- center. Arguments in favor of this model are the closeness in peak energy of the luminescence band (~ 2.95 eV) with that of the F- center observed in unannealed sample and the presence of the 265 K TL peaks in both annealed and unaanealed samples. 265K TL peak detected in annealed sample can be explained in the light of the model as follows: UV excitation of the samples prior to TL measurement causes the electron to be trapped at the neighboring impurity ion. Though the charge state of the impurity ion nearest to the F- center is not known, a change in the Madelung energy at the defect site due to the presence of impurity may be expected. Thus the trapped electron at the impurity ion site would have a less binding energy and consequently be freed to the conduction band. Once freed into the conduction band the electron may get trapped by H^- ions. At 265 K, the electron being emptied from the trap recombines with the perturbed F^+- center (since the C_2 symmetry is changed due to the presence of the impurity) causing luminescence. The spectral dependence of the TL at 265 K was similar to that observed in photo-luminescence in annealed samples.

Luminescence from annealed α-Al_2O_3 samples (#9a, #9b) was polarized, in the sense, that the intensity of the electric vector parallel to the C-axis of the crystal was less than the intensity with the electric vector perpendicular to the C-axis. Similar polarization effects have been observed in F-center luminescence in unannealed α-Al_2O_3 (61). Information obtained from the polarization measurements of the luminescence from annealed samples are not enough to determine

the angular orientation of the emitting dipole with respect to the C-axis. Composite luminescence curves with a clearly resolved structure accompanying the peak maxima at temperatures from 95 to 250 K could not be decomposed to two gaussians thereby making the detailed temperature dependence analysis of the composite band somewhat difficult. The data shows that at low temperatures the peak maxima is near 2.8 eV with a shoulder near 2.95 eV. As the temperatue is increased, luminescence intensity at 2.8 eV decreases while the intensity of the high energy component near 2.95 eV increases and at 250 K the luminescence is peaked at 2.95 eV with a resolved shoulder near 2.8 eV. This suggests that the emission is from a split excited state of the center. At low temperatures the lower energy emitting state is essentially more populated than the state at higher energy and thus at these temperatures the lunminescence band has a peak at a low energy (~ 2.85 eV) with a shoulder at 2.95 eV. As the temperature is increased, the electrons escape to the higher energy emitting level and thus the high energy component (~ 2.95eV) of the luminescence becomes more intense. Similar effects have been observed in fluoresence in unannealed α-Al_2O_3 where the transition is from the crystal field split $^3T_{1u}$ state of the excited F- center.

The photoresponse observed in #9a (heated to 1250°C) shows a shoulder near 5 eV. At incident photon energies greater than 5 eV the photoresponse spectrum shows a continuously increasing trend. The photoresponse at 200 nm was ~ 0.3 x 10^{-11} cm^2v^{-1} which is much smaller than the photoresponse (~ $10^{-8}cm^2v^{-1}$) observed in unannealed samples showing that the charge carriers in thermally annealed samples have much shorter mean range. An unannealed sample of α-Al_2O_3 shows a broad

photoresponse band near 5 eV (71). In our sample (#9a), the origin of the photoresponse shoulder near 5 eV is not unkown. The temperature dependence of photoresponse in #9a, however, behaves in a similar way to that observed in unannealed samples which have been thermochemically reduced.

In view of the above mentioned features regarding the luminescent centers in α-Al_2O_3 samples annealed at high temperatures, it is suggested that F_A- (perturbed F-centers) centers may be responsible for the observed effects. This suggestion may be verified by esr experiments in identifying the possible nature of luminescent centers in annealed samples of α-Al_2O_3.

CHAPTER VII

CONCLUSIONS AND FUTURE STUDY

$NaCl:Cu^-$

The results obtained in the present work have shown that:

(i) Definite correlation exits between Cu^- and F-centers in x-irradiated Sodium Chloride. Electron transfer between Cu^- and F centers can be achieved by thermal or optical excitations.

(ii) The isothermal decay of Cu^- ions obey a non first order (biomolecular) decay kinetics with an estimated activation energy of 0.80 ± 0.05 eV.

(iii) The same TL glow peak is responsible for the annealing of Cu^-- and F- centers. Recombination of trapped interstitials or holes with Cu^- and F-centers brings the crystal to the preirradiation state.

(iv) Thermal recovery of Cu^+ ions is a two stage process marked by temperatures above and below 160°C (89).

Future experiments such as esr will be very helpful in clarifying the intermediate stage in $Cu^- \rightarrow Cu^+$ conversion.

$MgAl_2O_4$

Results obtained in the present work suggest that F- centers may luminesce in thermochemically reduced $MgAl_2O_4$. Photoluminescence and

photoconducivity experiments show that the observed behaviors are similar to those present in its parent oxides (90). The photoresponse maxima at 4.59 eV in reduced $MgAl_2O_4$ and the origin of the 95K TL peak need to be investigated further.

α-Al_2O_3

The results of different experiments on annealed α-Al_2O_3 samples have shown that the luminescence different from F- center luminescence can be excited in as grown crystals of Al_2O_3 after heat treatment. The possible origin of the observed effects in annealed Al_2O_3 crystals seem to be due to F-centers in a perturbed environment (F_A-centers), the perturbation being casued by heat treatment.

Electron Spin Resonance and Optically Detected Magnetic Resonance experiments should be performed on annealed α-Al_2O_3 crystals to gain valuable information regarding the ground and excited states of the luminescent center responsible for the observed effects.

BIBLIOGRAPHY

1. Hughes, A.E. and B. Henderson, In Point Defects in Solids, edited by J.H. Crawford and L.M. Slifkin (Plenum, New York, 1972).

2. Tsuboi, T., Can. J. Phys. 55, 1316 (1977).

3. Delgado, L. and J.L. Alvarez Rivas, Phys. Rev. B. 23, 6699 (1981).

4. Bunch, J.M., Phys. Rev. B 16, 724 (1977).

5. Turner, T.J. and J.H. Crawford, Phys. Rev. 13, 1735 (1976).

6. Lee, K.H. and J.H. Crawford, Phys. Lett. 33, 273 (1977).

7. Schulman, J.H. and W.D. Compton, Color Centers in Solids (Pergamon, New York, 1971).

8. Knox, R.S. and A. Gold, In Symmetry in the Solid State (Benjamin, New York, 1964).

9. Fowler, W.B. and D.L. Dexter, Phys. Status Solidi. 2, 821 (1962).

10. Swank, R.K., and F.C. Brown, Phys. Rev. Letters. 8, 10 (1962).

11. Swank, R.K., and F.C. Brown, Phys. Rev. 130, 34 (1963).

12. Hecht, K., Zeits. f. Physik 77, 235 (1962).

13. Van Heyningen, R.S. and F.C. Brown, Phys. Rev. 111, 462 (1958).

14. Seitz, F., J. Chem. Phys. 6, 150 (1938).

15. Yuster, P.H., and C.J. Delbecq, J. Chem. Phys. 21, 892 (1953).

16. Knox, R.S., and D.L. Dexter, Phys. Rev. 104, 1245 (1956).

17. Condon, E.U., and G.H. Shortley, In "Theory of Atomic Spectra" (Cambridge University Press, 1935).

18. King, G.W. and J.H. Van Vleck, Phys. Rev. 56, 464 (1939).

19. Sugano, S., J. Chem. Phys. 36, 122 (1962).

20. Fukuda, A., Sci. Light (Tokyo). 13, 64 (1964).

21. Mabuchi, T., A. Fukuda and R. Onaka, Sci. Light (Tokyo). 15, 79 (1966).

22. Knox, R.S., J. Phys. Soc. Japan 18, Suppl. II, 268 (1959).

23. Sakoda, S., and T. Tsuboi, Phys. Rev. 22, 4966 (1980).

24. Zazubhovich, S.G., N.E. Lushchik, Opt. Spectry. (USSR) 15, 203 (1964).

25. Melinkov, N.I., P.G. Baranov, R.A. Zhitnikov and N.G. Romanov, Sov. Phys. Solid. State 13, 1909 (1971)

26. Baranov, P.G., Yu. P. Veschunov, R.A. Zhitnikov and N.G. Romanov, Phys. Status Solidi 79, K 27 (1977).

27. Van Sciver, W.J. and H.N. Chan, Phys. Rev. B12, 3438 (1975).

28. Tsuboi, T., Physica B 95, 397 (1978).

29. Kleeman, W., Z. Phys. 249, 145 (1971)

30. Satoko, C. and S. Sugano, J. Phys. Soc. Japan 34, 701 (1973).

31. Conway, J.M., D.A. Greenwood, J.A. Krumhansl and W. Martienssen, J. Phys. Chem. Solids 24, 239 (1963).

32. Simonetti, J. and D.S. McClure, Phys. Rev. B. 16, 3887 (1977).

33. Crawford, J.H., Private Communication

34. McKeever, S.W.S, Private Communication.

35. Fowler, W.B., In Physics of Color Centers (Academic Press, New York, 1968).

36. Inohara, K., Sci. Light (Tokyo) 14, 92 (1965).

37. Mabuchi, T., A. Yoshikawa and R. Onaka, J. Phys. Soc. Japan 23, 805 (1970).

38. Schmitt, K. and F. Fischer, Crystal Lattice Defects 6, 61 (1975).

39. Fussgaenger, K., Phys. Status Solidi 34, 157 (1969).

40. Pooley, D. and W.A. Runciman, Solid State Comm. 4, 351 (1966).

41. Muradov, S.M., M.Kh. Muradova and M.A. Elango, Fiz. Iverd. Tela. 11, 3149 (1969).

42. Zhitnikov, R.A. and N.G. Romanov, Fizika Tverdogo Tela, 13, 2275 (1971).

43. Kleeman, W., Zeitshrift fur Physik 214, 285 (1968).

44. Jain, S.C. and P. Mahendru, Phys. Rev. 140, A957 (1965).

45. Jain, S.C. and P. Mahendru, J. Phys. C: Solid St. Phys. 3, 1491 (1970).

46. Timusk, T. and W. Martienssen, Phys. Rev. 128, 1656 (1962).

47. Klick, C.C., E.N. Claffy, S.G. Gorbyes, F.H. Attin, J.H. Schulman and J.G. Allard, J. Appl. Phys. 38, 3867 (1967).

48. Ausin, V. and J.L. Alvarerz Rivas, J. Phys. C: Solid. St. Phys. 5, 82. (1972).

49. Ausin, V. and J. Alvarez Rivas, J. Phys. C: Solid. St. Phys. 7, 2255 (1974).

50. Mariani, D.F. and J.L. Alvarez Fivas, J. Phys. C: Solid St. Phys. 11, 3499 (1978).

51. Hobbs, L.W., A.E. Hughes and D. Pooley, Proc. R. Soc. A 322, 167 (1973).

52. Murti, Y.V.G.S. and K.R.N. Murthy, J. Phys. C 5, 2827 (1972).

53. Takeuchi, N., M. Adachi and K. Inabe, J. Lumin. 18/19, 897 (1979).

54. Lopez, F.J., F. Jaque, A.J. Fort and F. Agullo-Lopez, J. Phys. Chem. Solids 38, 1101 (1977).

55. Tsuboi, T. Phys. Rev. B 21, 5486 (1980).

56. Searle, T.M. and A.M. Glass, J. Phys. Chem. Solids 29, 609 (1968).

57. Summers, G.P., G.S. White, K.H. Lee and J.H. Crawford, Phys. Rev. B 21 2578 (1980).

58. White, G.S., K.H. Lee and J.H. Crawfod, Appl. Phys. Lett. 35 1 (1979).

59. Kappers, L.A., R.L. Kroes and E.B. Hensley, Phys. Rev. B 1, 4151 (1970).

60. Lee, K.H. and J.H. Crawford, Phys. Status Solidi A 42, K137 (1977).

61. Brewer, J.D., B.T. Jeffries and G.P. Summers, Phys. Rev. B 22, 4900 (1980).

62. White, G.S., K.H. Lee and J.H. Crawford, Phys. Status Solidi A 42, K137 (1977).

63. White, G.S., R.V. Jones and J.H. Crawford, J. Appl. Phys. 52, 927 (1982).

64. Woosley, J.D., C. Wood, E. Sonder and R.A. Weeks, Phys. Rev. 22, 1065 (1980).

65. Jeffries, B.T., R. Gonzalez, Y. Chen, and G.P. Summers, Phys. Rev. B 25, 2077 (1982).

66. Summers, G.P., T.M. Wilson, B.T. Jeffries, H.T. Tohver, Y. Chen and M.M. Abraham, Phys. Rev. B 27, 1283 (1983).

67. Roberts, R.W. and J.H. Crawford, J. Nonmentals 2, 133 (1979).

68. Feldott, J. and G.P. Summers, Phys. Rev. B 16 1722 (1977).

69. Feldott, J. and G.P. Summers, Phys. Rev. B 15, 2295 (1977).

70. Summers, G.P., K. Chakrabarti and Y. Chen, Phys. Rev. B 29, 5878 (1984).

71. Jeffries, B.T., J.D. Brewer and G.P. Summers, Phys. Rev. B 24, 6074 (1981).

72. Lou, F.H. and D.W.G. Ballentyne, J. Phys. C 1, 608 (1968).

73. Fraas, L.M. J.E. Moore and J.B. Salzberg, J. Chem. Phys. 58, 3585 (1973).

74. Boksha, O.N, T.M. Varian and A.A. Popova, Kristoallografiya 17, 1063 (1972) [Sov. Phys. - Crystallogr. 17, 940 (1973)].

75. Arnold, G.W. and W.D. Compton, Phys. Rev. Lett. 4, 66 (1960).

76. Levy, P.W., Phys. Rev. 123, 1226 (1961).

77. Mitchell, E.W.J., J.D. Rigden and P.D. Townsend, Philos. Mag. 5, 1013 (1965).

78. Turner, T.J. and J.H. Crawford, Phys. Rev. B 13, 1736 (1976).

79. Draeger, B.G. and G.P. Summers, Phys. Rev. 19, 1172 (1979).

80. Kulis, P.A., M.J. Springis, I.A. Tale and J.A. Valbis, Phys. Stat. Sol. (a) 53, 113 (1979).

81. La, S.Y., R.H. Bartram and R.T. Cox, J. Phys. Chem. Solids 34, 1079 (1973).

82. Evans, B.D. and M. Stapelbroek, Phys. Rev. B 18, 7089 (1978).

83. Kristianpoller, N. and A. Rehavi, J. de Physique 37 C7-212 (1976).

84. Chen, Y., R.T. Williams and W.A. Sibley, Phys. Rev. 182, 960 (1969).

85. Henderson, B. and D.H. Bowen, J. Phys. C 4, 1487 (1971).

86. Sibley, W.A., J.L. Kolopus and W.C. Mallard, Phys. Stat. Sol. 31, 223 (1969).

87. Turner, T.J., N.N. Isenhower and P.K. Tse, Solid State Comm. 7, 1661 (1969).

88. Pujats, A.V., M.J. Springis and J.A. Valbis, Phys. Stat. Solidi. a 62, K 85 (1980).

89. Bandyopadhyay, Pradip K. and G.P. Summers, Bull. Am. Phys. Soc. 31, 396 (1985).

90. Bandyopadhyay, Pradip K. and G.P. Summers, Phys. Rev. B. 31, 2422 (1985).

VITA

PRADIP KUMAR BANDYOPADHYAY

Candidate for the Degree of

Doctor of Philosophy

Thesis: AN EXPERIMENTAL INVESTIGATION OF LUMINESCENCE AND PHOTOCONDUCTIVITY IN SINGLE CRYSTALS OF SPINEL AND SAPPHIRE AND A STUDY OF IONIC MOTION IN NaCl:Cu

Major Field: Physics

Biographical:

Personal Data: Born in Calcutta, India, January 21, 1955, the son of Mr. and Mrs. Probodh Chandra Bandyopadhyay.

Education: Graduated from Jadavpur High School, Calcutta, 1970; received Bachelor of Science degree with a major in Physics from Jadavpur University, Calcutta, India, in 1973; received Master of Science degree in Physics from Jadavpur University, Calcutta, India in 1976; completed requirements for the Doctor of Philosophy degree at Oklahoma State University in December, 1985.

Professional Experience: Research Scholar, Indian Space Research Organization grant, Department of Applied Physics, Calcutta University, Calcutta, India, 1977-1979; Graduate Teaching Assistant, Boston College, Chestnut Hill, Massachusetts, 1979-1980; Awarded Certificate of Academic Merit from Residence Halls Association, Oklahoma State University, Stillwater, Oklahoma, 1982; 'STEP' (Travel Grant to attend the March Meeting of the American Physical Society) Award from the American Physical Society,1985; Graduate Teaching Assistant, Oklahoma State University, Stillwater, Oklahoma, 1980 - 85.